Wave Propagation Behaviour in Symmetric and Non-symmetric Three-dimensional Lattice Structures for Tailoring the Band Gaps

by

Jaehoon Won

A thesis submitted in conformity with the requirements
for the degree of Masters of Applied Science
Graduate Department of Aerospace Science and Engineering
University of Toronto

Abstract

Wave Propagation Behaviour in Symmetric and Non-symmetric Three-dimensional Lattice Structures for Tailoring the Band Gaps

Jaehoon Won
Masters of Applied Science
Graduate Department of Aerospace Science and Engineering
University of Toronto
2016

In this thesis, the longitudinal flexural wave propagation behaviour through symmetric and non-symmetric tetrahedral and pyramidal lattice structures is analyzed. Finite element analysis employing Floquet-Bloch theory is used to generate and plot dispersion curves. The design variables of the lattice structures are modified to analyze their impact on the dispersion curves. In symmetric lattice structures, changes in stiffness and density provide the effect of scaling the dispersion curves, whereas in non-symmetric lattice structures, based on the location of the inhomogeneities applied, asymmetric dispersion relations are obtained. For systems in which only certain directions of wave propagation are considered, non-symmetric lattice structures and the resulting asymmetric dispersion relations demonstrate great strength in terms of their flexibility when tailoring dispersion curves, as a large number of directionally different dispersion curves can be obtained, providing more options to design and optimize the lattice structure. Critically, band gaps can be designed at desirable frequencies and directions.

Acknowledgements

I would like to thank my supervisor Dr. Craig A. Steeves, for his support, trust, and guidance throughout the duration of the Master's program. It was invaluable opportunity and experience to work with him. Secondly, I wish to thank my RAC advisors, Dr. David W. Zingg, Dr. Phillippe Lavoie, Dr. Prasanth B. Nair and Dr. Alis Ekmekci for their instructions and constructive feedback throughout the Master's program. Thirdly, I wish to thank Manan Arya, former student who had worked on the topic of wave propagation in periodic lattice structure, for allowing his initial work on numerical models and his research to be used as back bone structure, being great guidance of initiating this Master's research. Special thank to my family for endless support on pursuing my goal, allowing me to be able to focus on the research without being interrupted by any obstacles. Lastly, I would like to thank Bharat Bhaga, David Platt, Nick Ewaschuk, and Qian Zhang, the colleagues in the Multifunctional Structures Lab of University of Toronto Institute for Aerospace Studies, for their support and feedback, and making studying environment to be full of enjoyment.

Jaehoon Won

University of Toronto Institute for Aerospace Studies

Contents

1 Introduction **1**

1.1 Motivation: Design for Sustainable Aviation 1

1.2 Literature Review 3

1.2.1 Nanocrystalline Metals 3

1.2.2 Electrodeposition Processing 3

1.2.3 Lattice Structure 3

1.3 Wave Propagation in Two-dimensional Periodic Lattices 4

1.4 Project Scope 6

1.5 Outline of the Thesis Structure 7

2 Periodic Lattice Structures **8**

2.1 Generating Physical Lattice Structures 8

2.2 Direct Lattice Structures in the Wave Space: Reciprocal Lattices 11

2.3 Properties and Behaviour of Wave Propagation in an Infinite Lattice Structure 13

2.3.1 Brillouin Zone in a Reciprocal Lattice 13

2.3.2 Floquet and Bloch Theorem 14

2.3.3 Coated Polymer Lattice Structure: An Ultralight Structure 14

3 Finite Element Analysis **16**

3.1 Defining the Input Parameters 16

3.2 Defining the Mesh Size and Meshed Elements 18

3.3 Defining the Nodes of the Structure 18

3.4 Defining Direct Basis Vectors and Reciprocal Basis Vectors 20

3.5 Defining the Brillouin Zone 21

3.6 Defining Eigenvalue Problems 21

3.6.1 Timoshenko Beams and Nodal Displacements 21

3.7 Setting up the Shape Functions 22

3.8 Kinetic Energy of a Timoshenko beam: Setting the Local Mass Matrix 24

3.9 Setting the Local Stiffness Matrix 29

3.10 Evaluating the Shape Functions Involved in the Mass and Stiffness Matrices 33

3.11 Construction of the Local and Global Mass and Stiffness Matrices 34

3.12 Obtaining the Equation of Motion 36

4 Wave propagation analysis **41**
4.1 Plotting Dispersion Curves . . . 41
4.2 Modifying the Design Variables to Tailor the Dispersion Curve . . . 42
4.3 Properties of Dispersion Curves . . . 44
4.3.1 Velocity of Wave Propagation . . . 44
4.3.2 Dispersion Branches, Veering Effect and Natural Frequencies . . . 44
4.3.3 Band Gap Phenomenon . . . 47
4.4 Validation Through Two-dimensional Triangular Lattices . . . 47
4.5 Gaining a Physical Understanding of the Lattice Structure . . . 49
4.6 Wave Propagation Through a Tetrahedral Lattice Structure with a Radius to Length Ratio of 0.1 . . . 50
4.6.1 Initial Symmetric Lattice Structure . . . 50
4.6.2 Impact of Changing the Design Variables E and ρ for All the Struts of the Lattice Structure . . . 53
4.6.3 Impact of Changing the Design Variables E and ρ for a Non-Symmetric Lattice Structure . . . 57
4.6.4 Impact of Modifying Different Combinations of Struts of the Lattice Structure . . . 65
4.6.5 Impact of Increasing the Number of Struts Being Modified . . . 70
4.6.6 Intuitive and Physical Understanding of the Dispersion Relations of a Non-Symmetric Lattice Structure . . . 74
4.6.7 Significance of the Asymmetric Dispersion Relations . . . 76
4.6.8 Impact of Changing the Other Design Variables . . . 76

5 Conclusion and Future Recommendations **81**
5.1 Conclusion . . . 81
5.2 Future Recommendations . . . 83
5.2.1 Multi-Tetrahedral/Pyramidal Non-Symmetric Unit Cell . . . 83
5.2.2 Shape Shifting Lattice Structure . . . 85
5.2.3 Lattice Structure as the Core of Sandwich Panel . . . 86

Bibliography **87**

Chapter 1

Introduction

1.1 Motivation: Design for Sustainable Aviation

Air transport has experienced rapid expansion as the global economy has grown and the technology of air transport has developed to its present state. However, with the expected increase in global air travel over the next 30 years, the reliability and environmental impact of aviation are becoming critical issues for the future of flight. Without significant action, large economic and environmental impacts are expected. Sustainable aviation is the initiative to prevent or reduce the expected economic and environmental impacts of aviation. The goal of designing for sustainable aviation is to develop technologies that will allow a tripling of capacity yet at the same time with a reduction in environmental impact. The following are the main areas where work is focused to achieve sustainable aviation:

1. Source noise reduction;
2. Source emissions reduction;
3. Materials and manufacturing processes;
4. Airport operations;
5. Aircraft operations;
6. Alternative fuels;
7. Product lifecycle management.

Recently, light weight structures that can be used in various engineering applications have been a focus of research and development. Metallic foams, a cellular structure consisting of a solid metal filled with gas bubbles with 75% to 95% of the volume void space, have been one of the competing ultralight materials. However, Hutchinson and Fleck[13] state that because the cell walls deform by local bending, the mechanical properties of metallic foam are poor. This led to a search for stretch-dominant open-cell microstructures, such as periodic lattices, which give much higher stiffness and strength per unit mass than foams. For example, when an octet-truss lattice structure is compared with metallic foam, the stiffness and strength of the lattice material exceeds the corresponding values for metal foams by a factor of between 3 and 10 [8]. Indeed, due to a high strength-to-weight ratio, relative ease of manufacture, and potential for multifunctional applications, lattice structures are an attractive alternative to metallic foams.

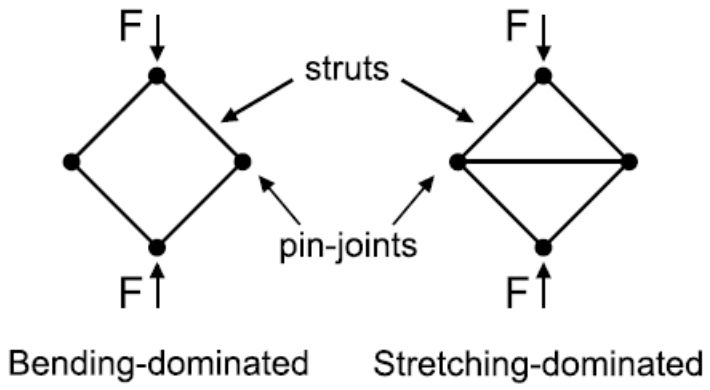

Figure 1.1: Illustration of a bending-dominant structure versus a stretch-dominant structure from Deshpande et al. [8].

When force is applied at the top and bottom corner of a bending-dominant structure, the struts can rotate around each pin-joint, potentially leading to the structure to collapse. However, when force is applied at the same location for a stretch-dominant structure, an additional strut placed in the centre can support the applied forces through tension and compression in the other struts, keeping the structure intact[6].

Previously at the University of Toronto Institute for Aerospace and Studies (UTIAS), Arya and Steeves[1] developed a numerical model of wave propagation behaviour in three-dimensional(3D) lattice structures. The goal of this thesis is to explore this numerical model and to construct new algorithms for a deeper analysis and comparison of various 3D lattice structures that have a tailorable structural stiffness and strength, together with capability to preventing vibrations at undesirable frequency ranges.

The first goal of the research therefore is to improve the performance of light-weight 3D lattice structures in terms of their tailorable structural strength, stiffness, and band gaps. Achieving this goal will contribute to sustainable aviation by improving fuel efficiency, which will be enhanced by reducing the overall weight of the plane through the use of such lightweight structures. The second goal of the research is to investigate how the band gaps can be engineered to appear in the desirable frequency range, such that there will be no vibration within the band gaps. Preventing the vibration by introducing the band gaps in a certain frequency range is another potential contribution towards sustainable aviation as this knowledge could be used in developing frequency filters in noise filters or in vibration protection materials or devices aimed at reducing aircraft noises due to sound or vibration. The final goal of the research is to apply inhomogeneities into the lattice structures, changing the lattice structures from symmetric to non-symmetric lattice structures, with the purpose of analyzing the differences in the wave propagation behaviour and the resulting dispersion curves between symmetric and non-symmetric lattice structures. This will assist exploring the advanced approaches that will allow easier and flexible tailoring of the lattice structures and band gaps.

1.2 Literature Review

1.2.1 Nanocrystalline Metals

Gleiter [11] presented a comprehensive overview of nanocrystalline materials. Nanocrystalline materials have characteristic length scales of nanometres, which endows them with unique microstructure-dependent properties. Most properties of solids depend on their microstructural features, such as their chemical composition, arrangement of the atoms, and grain size. Two solids composed of exactly the same atoms may show differences in their solid properties if there are differences in their microstructures. One example of this, for instance, is the difference in the solid properties between diamond and graphite. Diamond contains carbon atoms arranged tetrahedrally in three dimensions, while graphite contains carbon atoms arranged hexagonally in two dimensions, a planar layered structure. Due to this difference in atomic arrangement, diamond has a higher strength, hardness, and density than graphite.

Nanocrystalline materials can also attain new properties through a controlled manipulation of their microstructural parameters at the grain size level. This enables new nanocrystalline materials to gain better material properties and performances, such as ultra-high yields and fracture strengths, decreased elongation and toughness, and superior wear resistance according to Kumar et al. [14]. For example, the Hall-Petch effect [19] states that plastic deformation occurs more rapidly with larger grain sizes, and the yield strength rises as the grain size decreases, which implies that nanocrystalline materials can have an ultra-high yield strength.

1.2.2 Electrodeposition Processing

Kumar et al. [14] presented four methods of laboratory-scale processing applicable to metals or alloys in different grain size ranges: 1) mechanical alloying and compaction, 2) severe plastic deformation, 3) gas-phase condensation of the particulates, followed by consolidation and 4) electrodeposition. While the first two methods are applied to yield ultrafine but not nanocrystalline materials, the last two methods yield nanocrystalline materials. Electrodeposition, which is capable of producing material with a mean grain size in the tens of nanometres, has so far been used for two major purposes: to produce sheets of nanocrystalline metals (such as Ni, Co, Cu) and to produce binary alloys (such as Ni-Fe and Ni-W), in which the grain size can be controlled to produce nanocrystalline metal coatings on complex shapes. Electrodeposition is well-suited to depositing nanocrystalline metals with high accuracy onto complex lattice preforms of various solid materials, such as metal alloys or polymers at the micrometre length scale [28, 27].

1.2.3 Lattice Structure

Lattice structures are obtained by tessellating a unit cell along independent periodic vectors. The advantage of the lattice structures comes from their tailorability to manipulate their mechanical properties as desired for specific applications. The unit cell can be, among many other possible geometries, triangular, square, or hexagonal honeycomb, in two dimensions, and octahedral, pyramidal, or tetrahedral in three-dimensions.

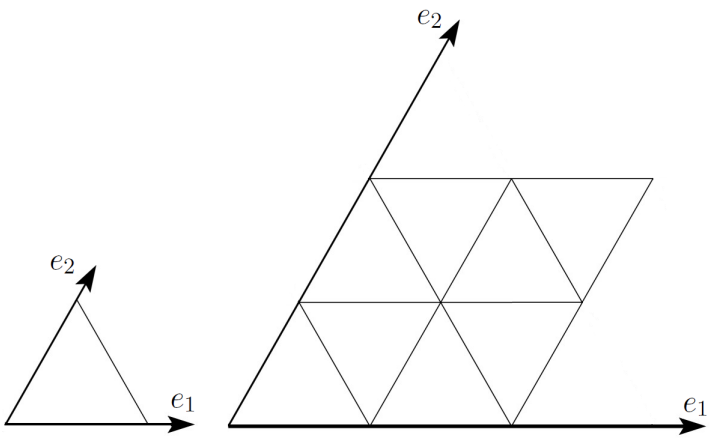

Figure 1.2: Illustration of a 2D triangular unit cell (left) and a "2 by 2" triangular lattice structure (right).

For example, a two-dimensional (2D) triangular unit cell was constructed with three struts, angled by 60 degrees at each corner. This unit cell contained two direct basis vectors, e_1 and e_2. The unit cell was tessellated along the directions of the basis vectors, creating a periodic 2D triangular lattice.

Lattice structures can be tailored to endow them with the enhanced ability to prevent vibrations at particular frequency ranges. These adjustable design variables in the lattice structure provide high flexibility when optimizing the design of the lattice structure.

1.3 Wave Propagation in Two-dimensional Periodic Lattices

There has been extensive research on wave propagation through various 2D periodic lattices. O. Sigmund and J. S. Jensen illustrated two waves propagating at different frequencies in separate 2D square domains, and reported the changes in wave propagation behaviours and the band gap phenomenon when 2D periodic circular inclusions were applied to each domain [26]. For example, Figure 1.3(a) illustrates a wave propagating at low frequency in 2D square domain, while the Figure 1.3(b) shows another wave propagating at a high frequency in a separate 2D square domain. When circular periodic inclusions are introduced to each square domain, changes in wave propagation behaviour occur, as is presented in the following figures. As illustrated in Figure 1.3(c), for a wave propagating at a lower frequency, wave propagation is still present, but is distorted due to reflections and refraction from the periodic inclusions. However, as illustrated in Figure 1.3(d), for a wave propagating at higher frequency, there is no wave propagation, thus showing the band gap phenomenon.

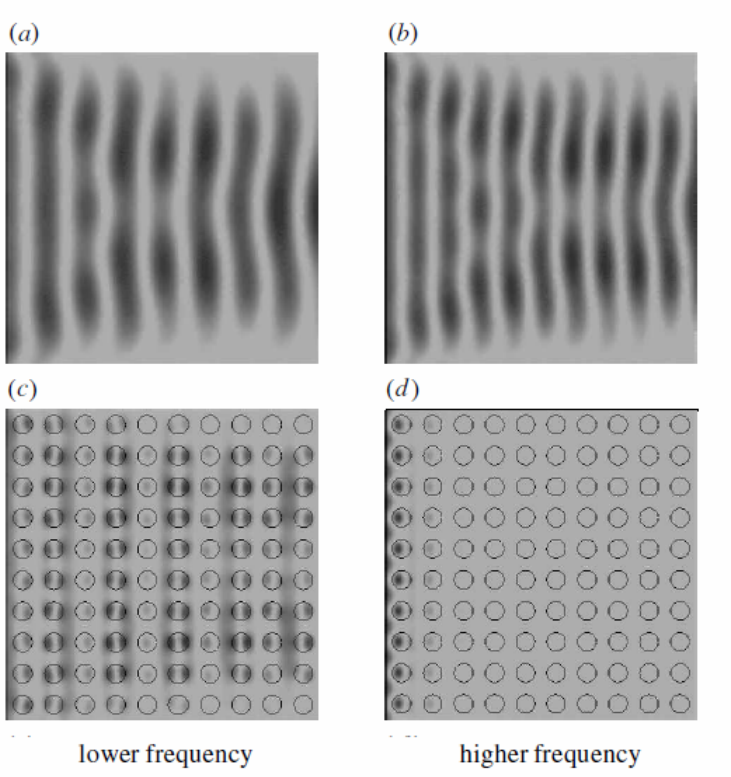

Figure 1.3: Illustration of wave propagation at different frequencies through 2D square domains, adopted from O. Sigmund and J. S. Jensen [26].

Wave propagation behaviour was further studied by A. Phani et al. [23] using various geometries of lattice structures. In their research, not only did they change the shape of the unit cell of the lattice structures, but they also changed the slenderness ratio of each strut constructing the unit cells of the lattice structures, with an aim to show the impact of each change on the wave propagation behaviour and its resulting dispersion curve.

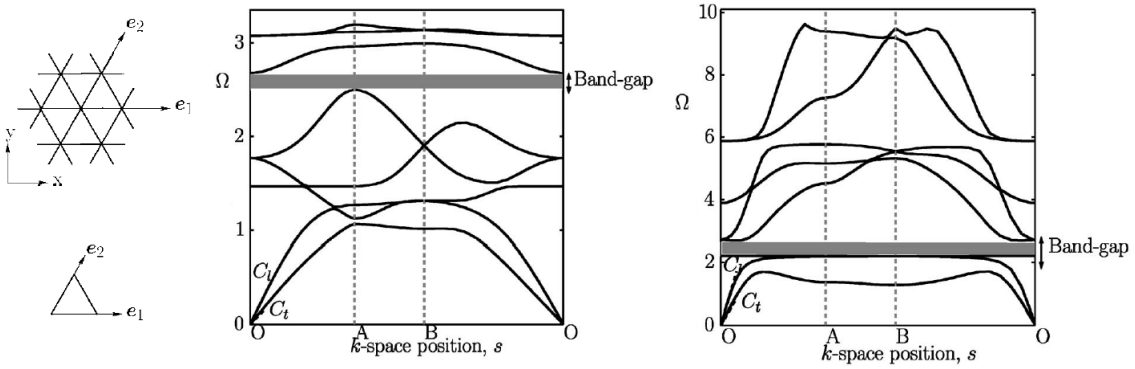

Figure 1.4: Illustration of wave propagation in a 2D triangular honeycomb lattice, from A. Phani et al. [23].

In Figure 1.4, the left figure illustrates a triangular honeycomb lattice structure and its unit cell, while the middle figure illustrates the dispersion curve obtained when the radius to length ratio is 0.1, and the right figure illustrates the dispersion curve obtained when the radius to length ratio is 0.02. As can be easily noted, the overall dispersion curve as well as band gap location is changed as the radius to length ratio of the strut is changed from 0.1 to 0.02.

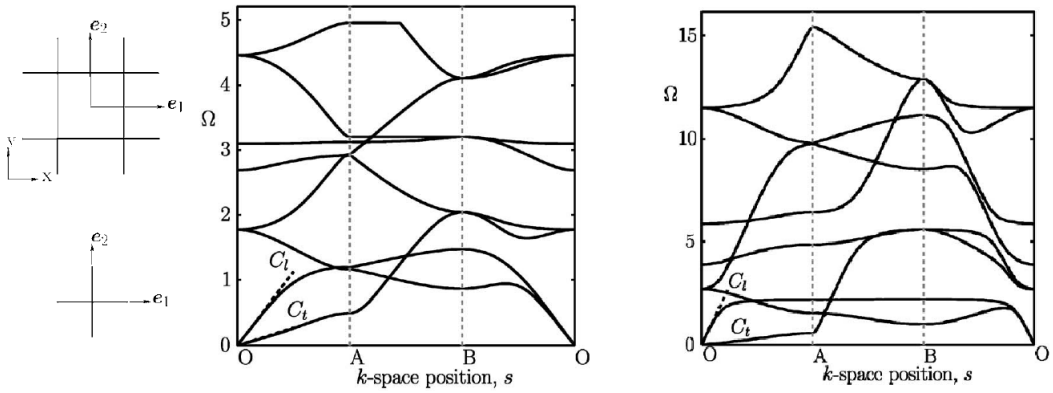

Figure 1.5: Illustration of wave propagation in a 2D square honeycomb lattice, from A. Phani et al. [23].

In Figure 1.5, the left figure illustrates a square honeycomb lattice structure and its unit cell, while the middle figure depicts the dispersion curve obtained when the radius to length ratio is 0.1 and the right figure shows the dispersion curve obtained when the radius to length ratio is 0.02. Compared to the two dispersion curves obtained from triangular honeycomb lattices, the dispersion curves obtained from square honeycomb lattices show entirely different dispersion curves, with no sign of a band gap for both radius to length ratios.

1.4 Project Scope

There already exist a numerical model of wave propagation behaviour in 3D lattice structures developed by Arya and Steeves [1]. This previous model is, therefore, used as a reference for this Master's thesis. The present thesis deeper analyzes the relationships between the shape, design variables, and the materials of the lattice structures and how these affect the resulting dispersion curves. Also, this thesis provides a comparison of symmetric and non-symmetric lattice structures. A symmetric lattice is a lattice structure where all the comprising struts share the same design variables and geometries; whereas a non-symmetric lattice comprises one or more struts that have different design variables to the other remaining struts. This study aimed to discover whether having non-symmetric lattices, achieved herein by introducing one or more modifications to the design variables, would allow a wider selection of options when tailoring the lattice structures for the maximum band gap at a desired frequency range.

1.5 Outline of the Thesis Structure

This thesis is be divided into five chapters as follows. In Chapter 2, a detailed review and analysis of lattice structures is covered. Also, this chapter will explain how tetrahedral and pyramidal lattice structures, the two lattice structures chosen for analysis in this thesis, are constructed. In Chapter 3, a numerical model for wave propagation in the lattice structures will be reviewed. Also, based on the numerical model, the results will be verified employing the finite element method and Floquet-Bloch analysis through comparison with the results from A. Phani et al. [23]. In Chapter 4, a detailed review and analysis of wave propagation in tetrahedral and pyramidal lattice structures will be performed, including what information can be obtained from the dispersion curves and how the wave propagation and dispersion curves change when the lattice structures are symmetric versus non-symmetric. In Chapter 5, the conclusions that can be gained from the research are present and future recommendations for further studies on 3D lattice structures are discussed.

Chapter 2

Periodic Lattice Structures

The main objective of this thesis is to construct 3D periodic lattice structures and then to analyze wave propagation behaviours in the corresponding periodic lattice structures. In this paper, the analysis of the wave propagations will be focused on tetrahedral and pyramidal 3D lattice structures. Also, a triangular 2D lattice structure is used to validate the numerical model for the analysis, through comparing the results with those from the past research performed by A. Phani et al. [23].

In this chapter, background on the lattice structures will be reviewed, such as generating the physical lattice structures and converting the physical lattices into the structure in wave-space, i.e. a reciprocal lattice structure. Afterwards, the special properties of the periodic lattice structures and the advantages of analyzing periodic lattice structures will be discussed.

2.1 Generating Physical Lattice Structures

In order to construct a periodic lattice structure, a primitive unit cell must be defined. The unit cell is constructed with multiple nodes and struts, arranged in specific angles to form a desired shape. The struts are originally in a local coordinate system, placed horizontally along the abscissa (the x-axis). Each of the struts in a local coordinate system are then transformed into a global coordinate system through Euler angle rotations, α, β, and γ, where α is the angle rotated about the y-axis, β is the angle rotated about the z-axis, and γ is the angle rotated about a struts central axis.

While the Euler angle rotations define the orientation of the struts of the lattice unit cell, nodes are required to be assigned at each end of the struts to define the nodal connectivity. For instance, one strut may have node A on the left end of the strut and node B on the right end, while another strut will have node C on its left end and node A on its right end. When connecting these two struts, the struts should be placed in such a way that the nodes of the same type, e.g. node A, from each strut should coincide. Following the above design mechanism, 2D triangular unit lattice cell, and 3D tetrahedral and pyramidal unit lattice cells can be generated.

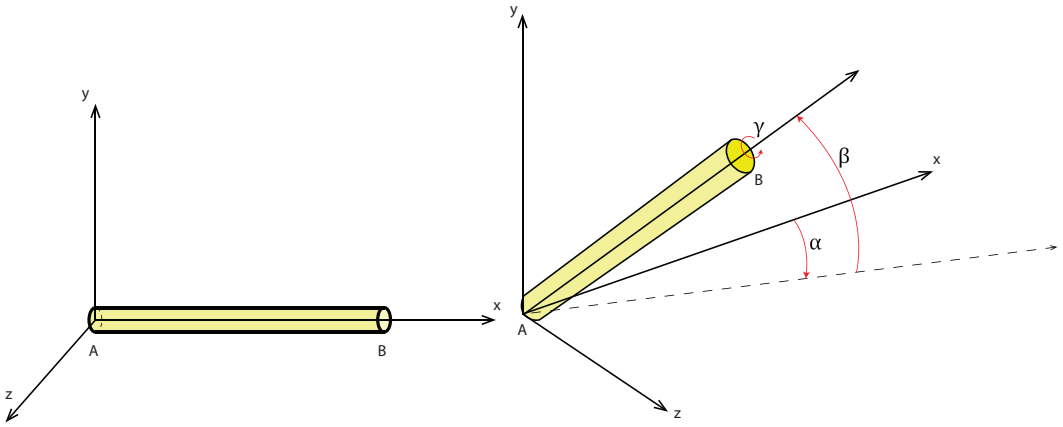

Figure 2.1: Illustration of a strut placed in a local coordinate system.

Tetrahedral Unit Cell	Global Coordinate		Euler Angle Rotation (radians)				Nodal Positions Cartesian Coord.		
Beams	Node A	Node B	α	β	γ	Nodes	x	y	z
Strut A	0	1	0	$\frac{\pi}{4}$	0	Basis	0	0	0
Strut B	0	2	$\frac{\pi}{2}$	$\frac{\pi}{4}$	0	Node 1	$\frac{L}{\sqrt{2}}$	$\frac{L}{\sqrt{2}}$	0
Strut C	3	0	$-\frac{3\pi}{4}$	0	0	Node 2	0	$\frac{L}{\sqrt{2}}$	$\frac{L}{\sqrt{2}}$
Strut D	1	2	$\frac{3\pi}{4}$	0	0	Node 3	$\frac{L}{\sqrt{2}}$	0	$\frac{L}{\sqrt{2}}$
Strut E	2	3	0	$-\frac{\pi}{4}$	0				
Strut F	1	3	$\frac{\pi}{2}$	$-\frac{\pi}{4}$	0				

Table 2.1: Table of the struts and nodes involved in the tetrahedral unit cell.

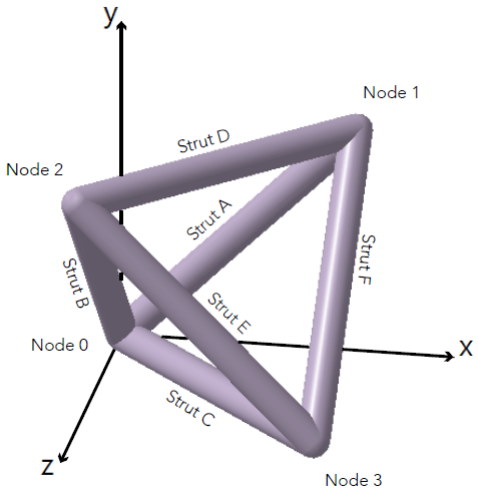

Figure 2.2: Illustration of the tetrahedral unit cell.

Pyramidal Unit Cell	Global Coordinate		Euler Angle Rotation (radians)			Nodal Positions Cartesian Coord.			
Beams	Node A	Node B	α	β	γ	Nodes	x	y	z
Strut A	0	1	$\frac{\pi}{2}$	0	0	Basis	0	0	0
Strut B	0	2	0	0	0	Node 1	0	0	L
Strut C	0	3	$\frac{\pi}{4}$	$\frac{\pi}{4}$	0	Node 2	L	0	0
Strut D	1	3	$-\frac{\pi}{4}$	$\frac{\pi}{4}$	0	Node 3	$\frac{L}{2}$	$\frac{L\sqrt{2}}{2}$	$\frac{L}{2}$
Strut E	4	3	$-\frac{3\pi}{4}$	$\frac{\pi}{4}$	0	Node 4	L	0	L
Strut F	2	3	$\frac{3\pi}{4}$	$\frac{\pi}{4}$	0				

Table 2.2: Table of the struts and nodes involved in the pyramidal unit cell.

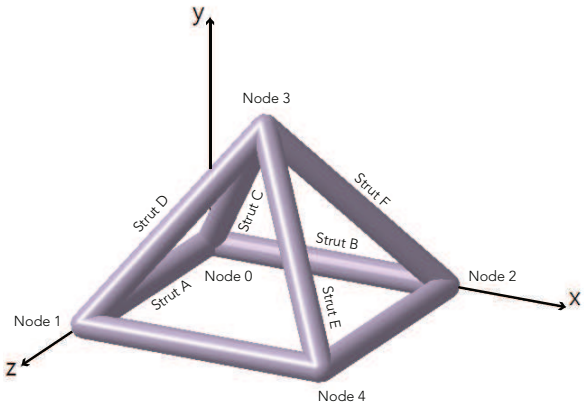

Figure 2.3: Illustration of the pyramidal unit cell.

The direct unit lattice contains n direct basis vectors, in which n is equal to the dimension of the lattice structure. The 2D triangular unit lattice, therefore, has two basis vectors, and the 3D tetrahedral and pyramidal unit lattice contains three basis vectors each. The direct basis vectors are defined such that the entire lattice structure can be formed by tessellating the direct lattice along the basis vectors e_i such as e_1, e_2, and e_3

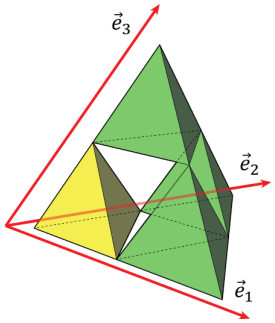

Figure 2.4: Illustration of the tetrahedral lattice structure with the basis vectors.

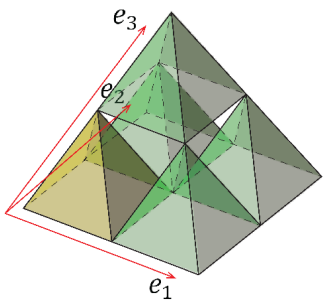

Figure 2.5: Illustration of the pyramidal lattice structure with the basis vectors.

2.2 Direct Lattice Structures in the Wave Space: Reciprocal Lattices

The reciprocal lattice is a non-physical lattice consisting of reciprocal basis vectors, which are derived from the direct lattice and its basis vectors. The reciprocal lattice is in k-space (momentum space), which is the set of all wave vectors k, while the wave vectors are a frequency analog of the position vector r. The reciprocal lattice is used through finite element analysis to obtain the wave propagation behaviour in the lattice structure. The set of reciprocal basis vectors, e_i^*, are defined by the following equations:
For three-dimensional lattice structure:

$$\begin{cases} e_1^* = 2\pi \frac{(e_2 \times e_3)}{e_1 \cdot (e_2 \times e_3)} \\ e_2^* = 2\pi \frac{(e_3 \times e_1)}{e_1 \cdot (e_2 \times e_3)} \\ e_3^* = 2\pi \frac{(e_1 \times e_2)}{e_1 \cdot (e_2 \times e_3)} \end{cases} \tag{2.1}$$

while e_i = direct lattice basis vectors
e_i^* = reciprocal lattice basis vectors

Following the governing relationship between direct basis vectors and reciprocal basis vectors, the reciprocal basis vectors for 3D tetrahedral and pyramidal lattice structures are obtained. Each of the tetrahedral and pyramidal lattice unit cells has three direct basis vectors and three reciprocal basis vectors. In Figure 2.6, the three diagrams depict how each reciprocal basis vector of the tetrahedral unit cell is defined based on the direct basis vectors of the unit cell. In the diagram, the red lines represent the direct basis vectors of the tetrahedral unit cell, namely e_1, e_2, and e_3, while the green lines represent the reciprocal basis vectors of the same unit cell, namely e_1^*, e_2^*, and e_3^*. The left diagram of Figure 2.6 illustrates how the reciprocal basis vector e_1^* is orthogonal to both the direct basis vectors e_2 and e_3, while the middle diagram shows that the reciprocal basis vector e_2^* is orthogonal to both the direct basis vectors e_1 and e_3, and the right diagram illustrates how the reciprocal basis vector e_3^* is orthogonal to both the direct basis vectors e_1 and e_2, with all of the reciprocal basis vectors having an absolute value of $\frac{2\pi}{unit\ cell\ length}$. The collection of the direct basis vectors of the tetrahedral unit cell is illustrated in the left diagram of Figure 2.7, while the collection of the reciprocal basis vectors of the tetrahedral unit cell is illustrated in the right diagram of Figure 2.7.

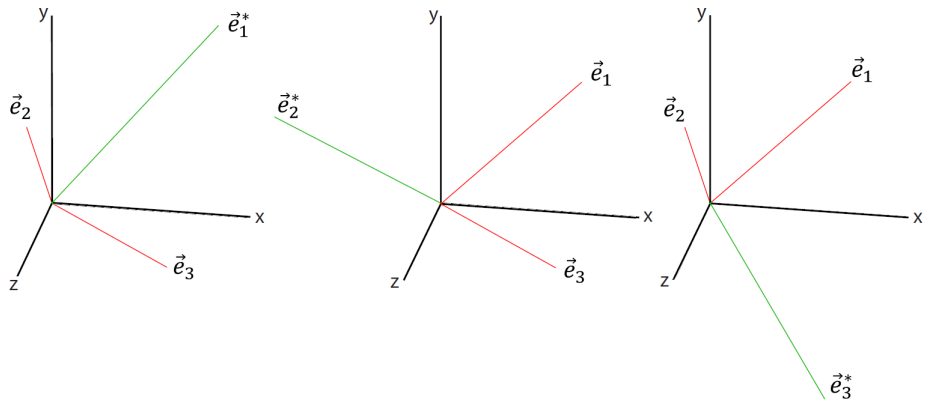

Figure 2.6: Illustration of the relationship between the direct basis vectors and the reciprocal basis vectors.

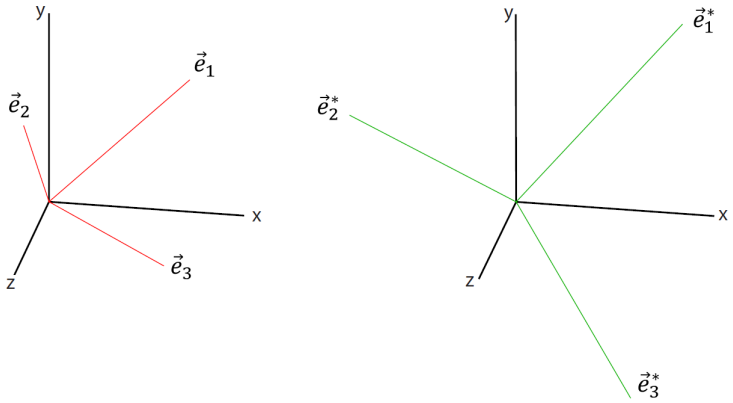

Figure 2.7: Illustration of the direct basis vectors and reciprocal basis vectors of the tetrahedral unit cell.

Similarly, the governing relationship described above is applied to construct direct and reciprocal basis vectors of the 3D pyramidal unit cell, which is illustrated in Figure 2.8. The left diagram of Figure 2.8 depicts the three direct basis vectors of the pyramidal unit cell, while the right diagram of Figure 2.8 depicts the three reciprocal basis vectors of the pyramidal unit cell.

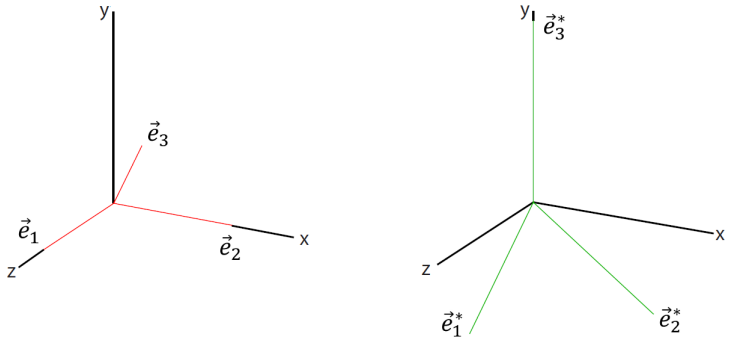

Figure 2.8: Illustration of the direct basis vectors and reciprocal basis vectors of the pyramidal unit cell.

2.3 Properties and Behaviour of Wave Propagation in an Infinite Lattice Structure

2.3.1 Brillouin Zone in a Reciprocal Lattice

The direct basis vectors define a direct lattice in physical space, while the reciprocal basis vectors define a reciprocal lattice in reciprocal space. The primitive unit cell of the direct lattice in the physical space is defined in such way that every lattice vector of the lattice is obtained as an integral linear combination of the direct basis vectors. On the other hand, the primitive unit cell of the reciprocal lattice in the reciprocal space is the Brillouin zone. The importance of constructing the first Brillouin zone comes from the information it holds. Arya and Steeves [1] state that, for any possible wave vector, a corresponding wave vector can be found in the first Brillouin zone with the same frequencies of propagation. This implies that the entire frequency response of the lattice is characterized by its frequency response to the wave vectors in the first Brillouin zone. Due to the periodicity of the frequency, any basic unit cell with the reciprocal basis vectors can be used to construct the first Brillouin zone. The simplest choice of the first Brillouin zone is a parallelepiped figure, whose sides are defined as reciprocal basis vectors.

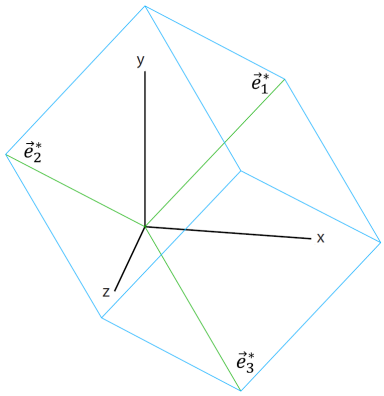

Figure 2.9: Illustration of the reciprocal basis vectors and the first Brillouin zone of a tetrahedral unit cell.

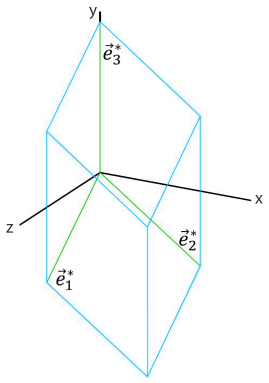

Figure 2.10: Illustration of the reciprocal basis vectors and the first Brillouin zone of a pyramidal unit cell.

2.3.2 Floquet and Bloch Theorem

Floquet's principal for one-dimensional (1D) lattice structures and Bloch's theorem in higher dimensional lattice structures are special cases of the wave equation in a periodic structure [23]. They are applied to impose periodic boundary conditions and to turn problems in infinite lattice structures into finite models, which enforce a plane wave solution in an infinite lattice. In 3D periodic structures with three basis vectors, according to Bloch's theorem, the classical equation to describe plane wave motion in the 3D periodic structure in terms of the relation between $\vec{r}_1$ (the position vector) and $\vec{r}_j$ (the j^{th} lattice point in the reference cell) is stated below.

$$q(\vec{r}) = q(\vec{r}_j)e^{n_1k_1+n_2k_2+n_3k_3} \tag{2.2}$$

while $\vec{r}_j$ = lattice points in reference cell
$\vec{r}$ = vector of lattice points in cell corresponding to
j^{th} point in reference cell
$q(\vec{r}_j)$ = displacement of a lattice point in reference cell
$k_i = \delta_i + i\epsilon_i$ = Wave vectors of plane wave
δ_i = Attenuation constants along basis vector e_i
ϵ_i = Phase constants
(n_1, n_2, n_3) = integer tuple that defines specific cell in the lattice,
which the cell is located at n_1 distance along e_1 direction,
n_2 distance along e_2 direction, and n_3 distance along e_3 direction
in relation to the reference cell

The wave vectors of a plane wave, k, are complex, containing a real part and an imaginary part, where the real part is the attenuation constant and the imaginary part is the phase constant [23]. Attenuation describes the gradual loss of intensity of a planar wave through a lattice structure. For waves propagating without attenuation in any lattice structure, the real part of the wave vector k is equal to zero, and the change in amplitude of the complex wave across the lattice structure does not depend on the location of the unit cell in the structure. Therefore, Bloch's theorem implies that one can study and understand wave propagation through the entire lattice structure by considering wave motion within a single unit cell, saving a large amount of time in the analysis of wave propagation in a lattice structure.

2.3.3 Coated Polymer Lattice Structure: An Ultralight Structure

At the beginning of the thesis, it was mentioned that periodic lattice structures can contribute to sustainable aviation as an application of ultralight materials. The following are two examples of periodic lattice structures with a radius to length ratio of 1 to 10, specifically with the radius being 1 mm and the length 10 mm. For the analysis of the wave propagation behaviour in 3D lattice structures throughout this thesis, the structures are considered to be coated with a nanometal. The radius and the length as well as the coating thickness of the struts are potential design variables, which can be modified to give different resulting dispersion curves and band gap phenomena in each lattice structure. For the coated prototype model shown below, the coating thickness for both samples was set at 25 microns. It should be noted that there is a thin layer of copper beneath the nickel layer, with the reason for this being so that there is a metal surface for the electrodeposition process of nickel. Otherwise, if the nickel layer

were put directly onto the polymer instead, it would become an electroless process, which would not produce as thick a coating as that from the electrodeposition process.

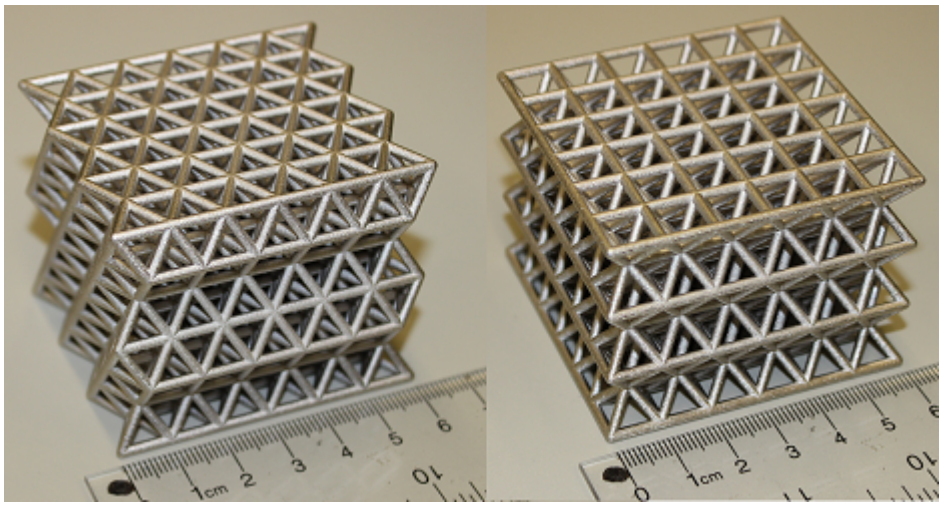

Figure 2.11: Illustration of the coated lattice structures.

The dimensions of the bounding box, the smallest rectangular prism box that envelops the lattice structure, for each lattice structure were measured. The volume of the bounding box represents the volume of the solid plate. Based on the volume of the bounding box and the volume of the lattice structure for each model, the relative density, which defines the volume fraction of the space filled with material as a percentage of the total volume of the lattice was measured. The tetrahedral lattice structure had 20.19% of material of relative density, while the pyramidal lattice structure had 20.62% of material of relative density.

$$\text{relative density} = \frac{\text{volume of the lattice structure}}{\text{volume of the solid plate (of the same bounding box dimensions)}} \tag{2.3}$$

	Lattice Geometry	
Properties	Tetrahedral Lattice	Pyramidal Lattice
Bounding Box	$6.2 \times 5.97 \times 5.098\ cm$	$6.2 \times 6.2 \times 4.44\ cm$
Volume of Bounding Box	$188.6974\ cm^3$	$170.6736\ cm^3$
Volume of Lattice Struc.	$38.098\ cm^3$	$35.1929\ cm^3$
Relative Density	20.19 %	20.62 %

Table 2.3: Table of the relative densities of tetrahedral and pyramidal lattice structures.

Chapter 3

Finite Element Analysis

In this chapter, finite element analysis on the wave propagation behaviour through a 3D lattice structure is discussed. The periodic lattice structures created from Chapter 2 will be used as the basic structure for the numerical analysis. This chapter will discuss various design variables of the coated lattice structures, and will then construct an eigenvalue problem through finite element analysis. By selecting the desired wave numbers, the eigenvalue problem will be solved to find eigenfrequencies and mode shapes of the wave propagating through the corresponding lattice structures.

3.1 Defining the Input Parameters

The coated lattice structure, constructed in the previous chapter, for the analysis of wave propagation contains five design variables: length of each strut of the lattice structure, radius of the polymer struts, thickness of each layer of coating, Young's modulus and the density of the polymer strut and of each layer of coating. As for the coating layers of the lattice structure, copper and nickel were used. First, based on the Young's modulus and the radius of the polymer substrate, as well as the Young's modulus and the thickness of the copper and nickel coating layers, the flexural rigidity of the overall coated structure was calculated.

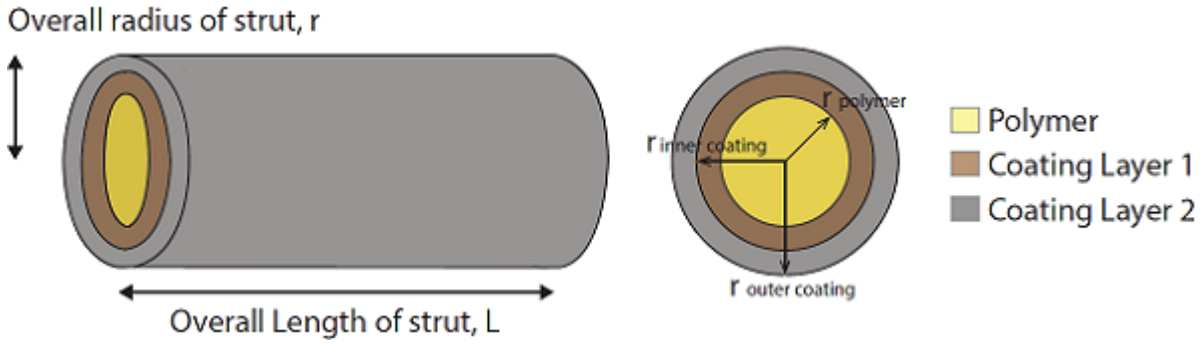

Figure 3.1: Illustration of a strut placed in a local coordinate system.

$$E_{overall}I_{overall} = E_{polymer}I_{polymer} + E_{copper}I_{copper} + E_{nickel}I_{nickel} \tag{3.1}$$

where E is the Young's modulus and I is the second moment of area of each section of the strut. The second moment of area for the solid polymer strut (cylindrical shape) and the second moment of area for the coating layers (hollowed cylindrical shape, annulus) are expressed as

$$I_{cylinder} = \frac{\pi r^4}{4} \tag{3.2}$$

$$I_{annulus} = \frac{\pi(r_{outer}^4 - r_{inner}^4)}{4} \tag{3.3}$$

For the prototype tetrahedral and pyramidal lattice structures, the input parameters were set as follows.

Design Variables	
$E_{polymer}$	2.115 Gpa
$\rho_{polymer}$	1170 $^{kg}/_{m^3}$
E_{copper}	58.6 Gpa
ρ_{copper}	8900 $^{kg}/_{m^3}$
E_{nickel}	157.6 Gpa
ρ_{nickel}	8900 $^{kg}/_{m^3}$
Radius of polymer strut	1 mm
Thickness of copper coating layer	0.0125 mm
Thickness of nickel coating layer	0.0125 mm
Length of each strut	10.25 mm

Table 3.1: Table of the design variables involved in the lattice structures.

Substituting the initial input values of the design variables into the equation above, the Young's modulus of the overall strut element was calculated to be 14.085 GPa. Also, the overall density could be calculated based on the volume and the density of the substrate and coating materials.

$$\rho_{overall}V_{overall} = \rho_{substrate}V_{substrate} + \rho_{coating}V_{coating} \tag{3.4}$$

where, the volume of the polymer strut is

$$V_{polymer} = \pi r_{polymer}^2 \times L_{polymer} \tag{3.5}$$

and the volume of the coating layers is

$$V_{Inner\ Coating} = (\pi(t_{Inner\ Coating} + r_{polymer})^2 \times L_{polymer}) - V_{polymer} \tag{3.6}$$

$$V_{Outer\ Coating} = (\pi(t_{Outer\ Coating}+t_{Inner\ Coating}+r_{polymer})^2 \times L_{polymer}) - V_{Inner\ Coating} - V_{polymer} \tag{3.7}$$

Substituting known values of the density and the volume, the density of the overall lattice structure was calculated to be 1542.5 $^{kg}/_{m^3}$.

3.2 Defining the Mesh Size and Meshed Elements

Once the strut's design variables are defined, and the struts of the lattice structure are rotated and coordinated as discussed in Chapter 2, the mesh size of the lattice structure is chosen. The mesh size defines the number of elements that each strut is divided into. The correct mesh size is critical as it impacts on the results of the analysis. Increasing the mesh size has positive impact on the computational result by increasing the accuracy and quality of the analysis, but, on the other hand, it also causes a negative impact by increasing the computational time. Therefore, an optimum mesh size that satisfies the requirements both for the accuracy of the result and a reasonable computational time must be applied. Selection of the optimum mesh size for the wave propagation analysis in this thesis is discussed in Chapter 4.

When a mesh size of n is applied to the lattice structure, every strut of the lattice is divided into n numbers of meshed elements and $n + 1$ number of nodes between each meshed elements. For convention, original struts prior to meshing are referred as the parent struts, while the meshed elements of the corresponding struts are referred to as child elements. As discussed in the previous chapter, parent struts contain Euler rotation angles, and a positive node and negative node at each end. Negative nodes refer to nodes at $x = 0$, while positive nodes refer to nodes at $x = L$, when the parent strut is placed in local coordinate system. When meshed elements are created, each child element inherits the same Euler rotation angle from its corresponding parent struts as well as the direction where the positive and negative nodes are located. The nodes at each end of the child elements are shared and bounded by the adjacent child elements.

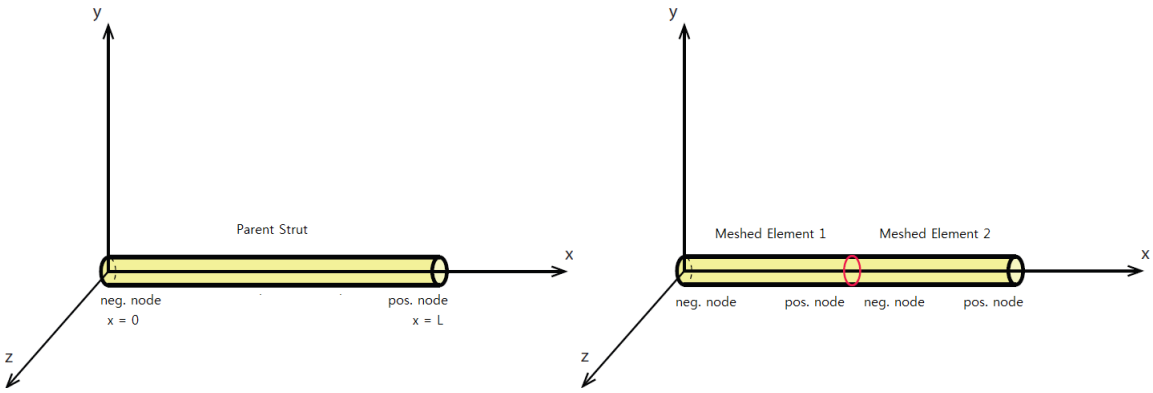

Figure 3.2: Illustration of the negative and positive nodes of the parent struts and meshed elements.

3.3 Defining the Nodes of the Structure

For an infinite lattice structure, Bloch's theorem relates the displacements at certain nodes in the unit cell to the displacements at the basis node[1]. Therefore, once the unit lattice structure is constructed, and the structure is meshed into the desired number of elements, the nodes must be defined into different categories: basis, internal, and boundary. Typically, a node located at the origin of the coordinate system is defined as the basis node, q_b, and is used as a base reference node to describe the boundary nodes. The

boundary nodes, q_{bnd}, are the nodes that can be reached by traversing the basis node along the direction of the direct basis vectors e_1, e_2, e_3. The boundary nodes are shared by other neighbouring unit cells in the lattice structures. Therefore, typically the nodes at the end of each parent strut in the direction of the direct basis vectors are defined as the boundary nodes. Lastly, nodes created between each of the meshed element are defined as internal nodes, q_i, which are not shared by the other neighbouring unit cells.

Tetrahedral	Negative Node	Positive Node
Strut A	Basis	Boundary e_1
Strut B	Basis	Boundary e_2
Strut C	Boundary e_3	Basis
Strut D	Boundary e_1	Boundary e_2
Strut E	Boundary e_2	Boundary e_3
Strut F	Boundary e_1	Boundary e_3

Table 3.2: Table of the internal, basis, and boundary nodes involved in the tetrahedral unit cell.

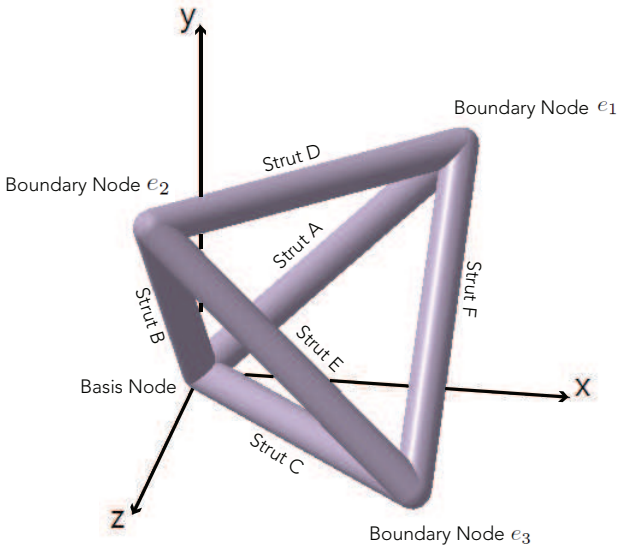

Figure 3.3: Illustration of the tetrahedral unit cell with the negative and the positive nodes of each strut defined in Table 3.2.

Pyramidal	Negative Node	Positive Node
Strut A	Basis	Boundary e_1
Strut B	Boundary e_2	Basis
Strut C	Basis	Boundary e_3
Strut D	Boundary e_1	Boundary e_3
Strut E	Boundary e_{12}	Boundary e_3
Strut F	Boundary e_2	Boundary e_3

Table 3.3: Table of the internal, basis, and boundary nodes involved in the pyramidal unit cell.

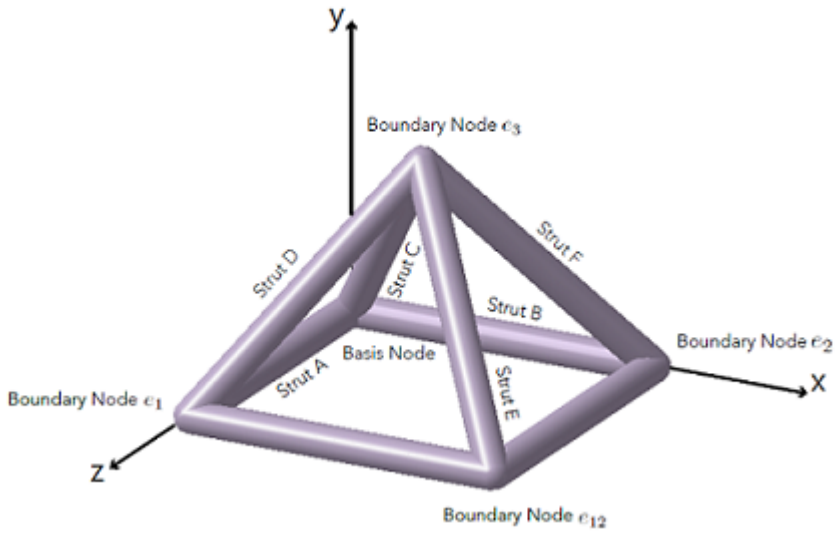

Figure 3.4: Illustration of the pyramidal unit cell with the negative and the positive nodes of each strut defined in Table 3.3.

3.4 Defining Direct Basis Vectors and Reciprocal Basis Vectors

After all the meshed elements and nodes are defined, three direct basis vectors, namely e_1, e_2, and e_3 are constructed, which are based on Cartesian coordinates as follows.

$$\begin{bmatrix} e_1 & e_2 & e_3 \end{bmatrix} = \begin{bmatrix} e_{1x} & e_{2x} & e_{3x} \\ e_{1y} & e_{2y} & e_{3y} \\ e_{1z} & e_{2z} & e_{3z} \end{bmatrix} \tag{3.8}$$

Based on the direct basis vectors, e_i, in the Cartesian form described above, the reciprocal basis vectors, $e^*{}_i$, can be obtained. While the geometrical relationship between the direct basis vectors and reciprocal basis vectors are defined in Chapter 2, the numerical relationship between the direct and the reciprocal basis vectors can be expressed as follows.

$$2\pi \begin{bmatrix} e_1 & e_2 & e_3 \end{bmatrix}^{-1} = \begin{bmatrix} e^*{}_1 & e^*{}_2 & e^*{}_3 \end{bmatrix}^T \tag{3.9}$$

Therefore, it can be seen that the reciprocal basis vectors are the inverse transpose of the direct basis vectors.

$$\left[2\pi \begin{bmatrix} e_1 & e_2 & e_3 \end{bmatrix}^{-1}\right]^T = \begin{bmatrix} e^*{}_1 & e^*{}_2 & e^*{}_3 \end{bmatrix} \tag{3.10}$$

3.5 Defining the Brillouin Zone

The Brillouin zone is defined by constructing a parallelepiped figure based on the reciprocal basis vectors. The Brillouin zone is turned into a 3D grid system (e^*_1, e^*_2, e^*_3), where each coordinate of the grid represents a wave vector, $k = (k_1, k_2, k_3)$. The grid size of the Brillouin zone affects the total number of wave vectors that can be obtained from the Brillouin zone. When the Brillouin zone is turned into an $n \times n \times n$ grid system, there are a total of $(n+3)^3$ numbers of wave vectors. The increase in the grid size gives a greater number of (finer) wave vectors to analyze, thus increasing the accuracy and quality of the results.

3.6 Defining Eigenvalue Problems

3.6.1 Timoshenko Beams and Nodal Displacements

The constructed lattice structures and meshed elements are considered as Timoshenko beams. Timoshenko beams are preferred and selected over Euler-Bernoulli beams, as the dispersion relation of the Euler-Bernoulli beam theory predicts that waves of short wavelength travel with unlimited speed, which is unrealistic. This unrealistic prediction arises due to two assumptions of the Euler-Bernoulli beam theory, namely that rotational effects are neglected and that the beam element remains rectangular during motion. However, in reality, waves of short wavelength will cause rotation and deformation of the beam element, hence leading to unrealistic predictions on the dispersion relation for short wavelengths. Contrary to Euler-Bernoulli beam theory, the Timoshenko beam theory takes account of the rotation and shear deformation of the beam element for waves of short wavelength, thus making it suitable for describing the dispersion relations of lattice structures.

Each 3D Timoshenko element has two nodes with six displacements for each node: υ, ν, ω, ϕ, ψ, θ. The υ, ν, and ω are the translational displacements along the x-axis, y-axis, and z-axis, in corresponding order, and the other three, ϕ, ψ, and θ, are rotational displacements about the x-axis, y-axis, and z-axis in corresponding order. Hence, the displacement of a single element q_{ele} with node A and node B can be described as

$$\begin{bmatrix} q_{ele} \end{bmatrix} = \begin{bmatrix} q_A & q_B \end{bmatrix}^T = \begin{bmatrix} \upsilon_A & \nu_A & \omega_A & \phi_A & \psi_A & \theta_A & \upsilon_B & \nu_B & \omega_B & \phi_B & \psi_B & \theta_B \end{bmatrix}^T \quad (3.11)$$

Therefore, displacements in a single strut q_{strut} meshed into three elements, with its containing nodes categorized into different types as discussed in the previous section, can be described as

$$\begin{bmatrix} q_{strut} \end{bmatrix} = \begin{bmatrix} q_{int1} & q_{int2} & q_{basis} & q_{boundary} \end{bmatrix}^T \quad (3.12)$$

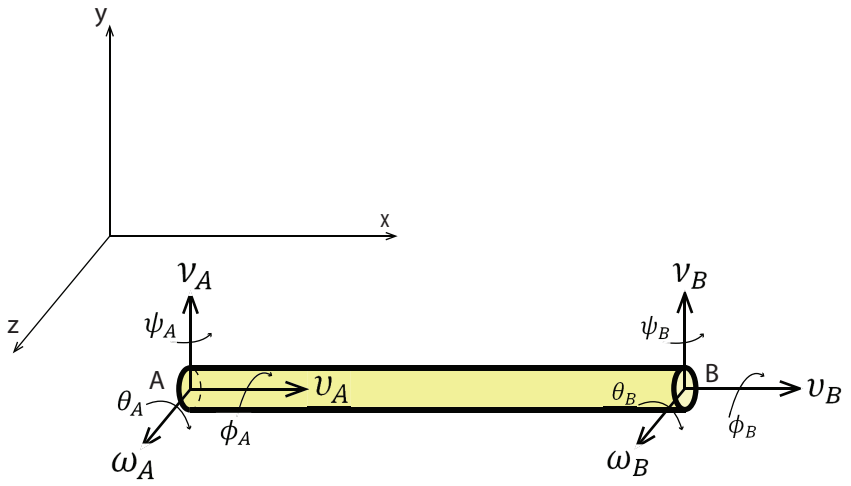

Figure 3.5: Illustration of the nodal displacements involved in each 3D strut.

3.7 Setting up the Shape Functions

According to the standard finite element procedure, the elastic deformation of an arbitrary point x of the 3D two-node meshed element, at time t can be expressed as[3]

$$\left[\ d\ \right] = \left[\ N\ \right] \cdot \left[\ q_{ele}\ \right] \tag{3.13}$$

where $[d]$ represents the elastic deformation vector of the meshed element, $[N]$ represents the matrix of shape functions, and q_{ele} represents the nodal displacement vector.

$$\upsilon(x,t) = a_i(x)q_{ele}(t) \tag{3.14a}$$
$$\nu(x,t) = b_i(x)q_{ele}(t) \tag{3.14b}$$
$$\omega(x,t) = c_i(x)q_{ele}(t) \tag{3.14c}$$
$$\phi(x,t) = d_i(x)q_{ele}(t) \tag{3.14d}$$
$$\psi(x,t) = e_i(x)q_{ele}(t) \tag{3.14e}$$
$$\theta(x,t) = f_i(x)q_{ele}(t) \tag{3.14f}$$

where,

$$\left[\ q_{ele}\ \right] = \left[\ \upsilon_A \quad \nu_A \quad \omega_A \quad \phi_A \quad \psi_A \quad \theta_A \quad \upsilon_B \quad \nu_B \quad \omega_B \quad \phi_B \quad \psi_B \quad \theta_B\ \right]^T \tag{3.15}$$

$$\begin{bmatrix} a_i \\ b_i \\ c_i \\ d_i \\ e_i \\ f_i \end{bmatrix}^T = \begin{bmatrix} a_1 & a_2 & a_3 & a_4 & a_5 & a_6 & a_7 & a_8 & a_9 & a_{10} & a_{11} & a_{12} \\ b_1 & b_2 & b_3 & b_4 & b_5 & b_6 & b_7 & b_8 & b_9 & b_{10} & b_{11} & b_{12} \\ c_1 & c_2 & c_3 & c_4 & c_5 & c_6 & c_7 & c_8 & c_9 & c_{10} & c_{11} & c_{12} \\ d_1 & d_2 & d_3 & d_4 & d_5 & d_6 & d_7 & d_8 & d_9 & d_{10} & d_{11} & d_{12} \\ e_1 & e_2 & e_3 & e_4 & e_5 & e_6 & e_7 & e_8 & e_9 & e_{10} & e_{11} & e_{12} \\ f_1 & f_2 & f_3 & f_4 & f_5 & f_6 & f_7 & f_8 & f_9 & f_{10} & f_{11} & f_{12} \end{bmatrix}^T \tag{3.16}$$

$$\begin{bmatrix} a_i \\ b_i \\ c_i \\ d_i \\ e_i \\ f_i \end{bmatrix}^T = \begin{bmatrix} a_1 & 0 & 0 & 0 & 0 & 0 & a_7 & 0 & 0 & 0 & 0 & 0 \\ 0 & b_2 & 0 & 0 & 0 & b_6 & 0 & b_8 & 0 & 0 & 0 & b_{12} \\ 0 & 0 & c_3 & 0 & c_5 & 0 & 0 & 0 & c_9 & 0 & c_{11} & 0 \\ 0 & 0 & 0 & d_4 & 0 & 0 & 0 & 0 & 0 & d_{10} & 0 & 0 \\ 0 & 0 & e_3 & 0 & e_5 & 0 & 0 & 0 & e_9 & 0 & e_{11} & 0 \\ 0 & f_2 & 0 & 0 & 0 & f_6 & 0 & f_8 & 0 & 0 & 0 & f_{12} \end{bmatrix}^T \tag{3.17}$$

The shape functions of a 3D Timoshenko beam element are defined as follows [1, 3]:

$$a_1 = 1 - \xi \tag{3.18a}$$
$$a_7 = \xi \tag{3.18b}$$

$$b_2 = \mu_z \left[1 - 3\xi^2 + 2\xi^3 + \eta_z(1 - \xi)\right] \tag{3.18c}$$
$$b_6 = L\mu_z \left[\xi - 2\xi^2 + \xi^3 + \frac{\eta_z}{2}(\xi - \xi^2)\right] \tag{3.18d}$$
$$b_8 = \mu_z \left[3\xi^2 - 2\xi^3 + \eta_z\xi\right] \tag{3.18e}$$
$$b_{12} = L\mu_z \left[-\xi^2 + \xi^3 + \frac{\eta_z}{2}(-\xi + \xi^2)\right] \tag{3.18f}$$

$$c_3 = \mu_y \left[1 - 3\xi^2 + 2\xi^3 + \eta_y(1 - \xi)\right] \tag{3.18g}$$
$$c_5 = -L\mu_y \left[\xi - 2\xi^2 + \xi^3 + \frac{\eta_y}{2}(\xi - \xi^2)\right] \tag{3.18h}$$
$$c_9 = \mu_y \left[3\xi^2 - 2\xi^3 + \eta_y\xi\right] \tag{3.18i}$$
$$c_{11} = -L\mu_y \left[-\xi^2 + \xi^3 + \frac{\eta_y}{2}(-\xi + \xi^2)\right] \tag{3.18j}$$

$$d_4 = 1 - \xi \tag{3.18k}$$
$$d_{10} = \xi \tag{3.18l}$$

$$e_3 = -\frac{6\mu_y}{L}\left[-\xi + \xi^2\right] \tag{3.18m}$$
$$e_5 = \mu_y \left[1 - 4\xi + 3\xi^2 + \eta_y(1 - \xi)\right] \tag{3.18n}$$
$$e_9 = -\frac{6\mu_y}{L}\left[\xi - \xi^2\right] \tag{3.18o}$$
$$e_{11} = \mu_z \left[-2\xi + 3\xi^2 + \eta_y\xi\right] \tag{3.18p}$$

$$f_2 = \frac{6\mu_z}{L}\left[-\xi + \xi^2\right] \tag{3.18q}$$
$$f_6 = \mu_z \left[1 - 4\xi + 3\xi^2 + \eta_z(1 - \xi)\right] \tag{3.18r}$$
$$f_8 = \frac{6\mu_z}{L}\left[\xi - \xi^2\right] \tag{3.18s}$$
$$f_{12} = \mu_z \left[-2\xi + 3\xi^2 + \eta_z\xi\right] \tag{3.18t}$$

$$\xi = \frac{x}{L} \tag{3.19a}$$

$$\eta_y = \frac{12EI_y}{\kappa GAL^2} \tag{3.19b}$$

$$\eta_z = \frac{12EI_z}{\kappa GAL^2} \tag{3.19c}$$

$$\mu_y = \frac{1}{1+\eta_y} \tag{3.19d}$$

$$\mu_z = \frac{1}{1+\eta_z} \tag{3.19e}$$

$$\kappa = \text{Shear correction factor} = \frac{6(1+\nu)}{7+6\nu} \tag{3.19f}$$

$$\nu = \text{Poisson's ratio} \tag{3.19g}$$

$$E = \text{Young's modulus} \tag{3.19h}$$

$$I_{y,z} = \text{Second moment of area} \tag{3.19i}$$

$$A = \text{Cross section of the strut element} \tag{3.19j}$$

$$L = \text{Length of the strut element} \tag{3.19k}$$

3.8 Kinetic Energy of a Timoshenko beam: Setting the Local Mass Matrix

First, the kinetic energy of a Timoshenko element is expressed in terms of the nodal displacements, while the kinetic energy of a particle i is described as

$$T_i = \frac{1}{2} m_i {v_i}^2 \tag{3.20}$$

and the total kinetic energy of the system becomes the sum of the kinetic energies of all particles in the system:

$$T_{sys} = \sum_{i=1}^{n} T_i = \sum_{i=1}^{n} \frac{1}{2} m_i {v_i}^2 \tag{3.21}$$

For a rigid body, such as a Timoshenko beam element, the equation becomes

$$T_{ele} = \int_m \frac{1}{2} |\vec{v}|^2 \, dm \tag{3.22}$$

To continue derivation of the kinetic energy equation of the Timoshenko element, the expression for the displacement field must be obtained. Figure 3.6 illustrates the motion of a particle p at an arbitrary location in 3D beam, and the location of the particle after displacement, p'.

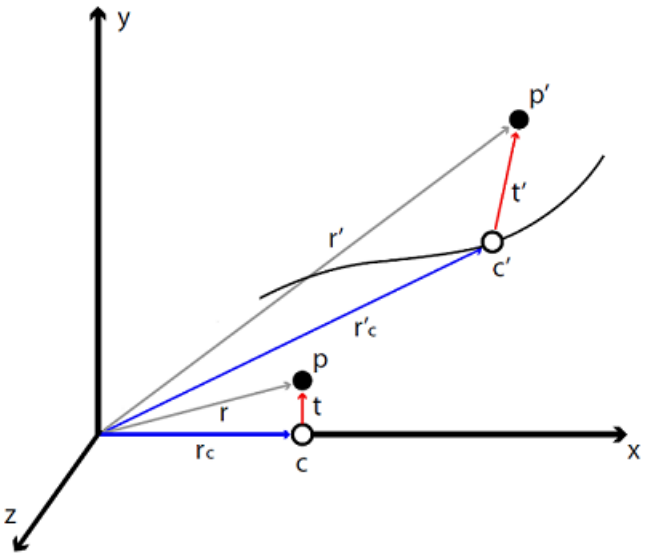

Figure 3.6: Illustration of the kinematics of a particle in a 3D strut [16].

Vector r, which describes the location of particle p, can be divided into two components: r_c and t, where r_c is the vector defining the location of the point c, which is point p projected onto the central axis (x-axis) and t is the vector from point c, directed to point p.

$$\begin{bmatrix} r \end{bmatrix} = \begin{bmatrix} x \\ y \\ z \end{bmatrix} \tag{3.23}$$

$$\begin{bmatrix} r_c \end{bmatrix} = \begin{bmatrix} x \\ 0 \\ 0 \end{bmatrix} \tag{3.24}$$

$$\begin{bmatrix} t \end{bmatrix} = \begin{bmatrix} 0 \\ y \\ z \end{bmatrix} \tag{3.25}$$

$$r = r_c + t \tag{3.26}$$

$$t = r - r_c \tag{3.27}$$

Likewise, the vector r' describing the location of the particle after the displacement, is expressed as

$$r' = r'_c + t' \tag{3.28}$$

Based on Euler-Chasles' theorem, the rotation of vector t can be described by the rotational matrix R [16]:

$$t' = Rt \tag{3.29}$$

where,

$$R = \begin{bmatrix} 1 & -\theta & \psi \\ \theta & 1 & -\phi \\ -\psi & \phi & 1 \end{bmatrix} \tag{3.30}$$

Therefore,

$$r' = r'_c + Rt \tag{3.31}$$

substituting $t = r - r_c$,

$$r' = r'_c + R(r - r_c) \tag{3.32}$$

Noting that point c' is the point c after displacement by $[\upsilon \quad \nu \quad \omega]^T$

$$r'_c = r_c + \begin{bmatrix} \upsilon \\ \nu \\ \omega \end{bmatrix} \tag{3.33}$$

the displacement field is expressed as follows

$$u = \begin{bmatrix} u_x \\ u_y \\ u_z \end{bmatrix} = r' - r \tag{3.34}$$

since

$$r' = r'_c + R(r - r_c) \tag{3.35}$$

$$u = r'_c + R(r - r_c) - r \tag{3.36}$$

substituting (3.33) into the equation gives,

$$u = r_c - r + \begin{bmatrix} \upsilon \\ \nu \\ \omega \end{bmatrix} + R(r - r_c) \tag{3.37}$$

$$u = \begin{bmatrix} x \\ 0 \\ 0 \end{bmatrix} - \begin{bmatrix} x \\ y \\ z \end{bmatrix} + \begin{bmatrix} \upsilon \\ \nu \\ \omega \end{bmatrix} + \begin{bmatrix} 1 & -\theta & \psi \\ \theta & 1 & -\phi \\ -\psi & \phi & 1 \end{bmatrix} \cdot \begin{bmatrix} 0 \\ y \\ z \end{bmatrix} \tag{3.38}$$

$$u = \begin{bmatrix} 0 \\ -y \\ -z \end{bmatrix} + \begin{bmatrix} \upsilon \\ \nu \\ \omega \end{bmatrix} + \begin{bmatrix} 0 & -y\theta & z\psi \\ 0 & y & -z\phi \\ 0 & y\phi & z \end{bmatrix} \tag{3.39}$$

The resulting displacement field $[u]$ is

$$u = \begin{bmatrix} u_x \\ u_y \\ u_z \end{bmatrix} = \begin{bmatrix} \upsilon & -y\theta & z\psi \\ \nu & 0 & -z\phi \\ \omega & y\phi & 0 \end{bmatrix} \tag{3.40}$$

Revisiting the kinetic energy equation for a Timoshenko element,

$$T_{ele} = \int_m \frac{1}{2}|\vec{v}|^2 \, dm = \int_m \frac{1}{2}(\dot{u_x}^2 + \dot{u_y}^2 + \dot{u_z}^2) \, dm \tag{3.41}$$

where

$$|\vec{v}|^2 = \dot{u}^2 = \dot{u_x}^2 + \dot{u_y}^2 + \dot{u_z}^2 \tag{3.42a}$$

$$\dot{u} = \begin{bmatrix} \dot{u}_x \\ \dot{u}_y \\ \dot{u}_z \end{bmatrix} = \begin{bmatrix} \dot{\upsilon} & -y\dot{\theta} & z\dot{\psi} \\ \dot{\nu} & 0 & -z\dot{\phi} \\ \dot{\omega} & y\dot{\phi} & 0 \end{bmatrix} \tag{3.42b}$$

$$dm = \rho d\upsilon = \rho dx dA \tag{3.42c}$$

$$\int_m dm = \int_0^L \int_A \rho dA dx \tag{3.42d}$$

The equation then becomes

$$T_{ele} = \frac{1}{2}\int_0^L \int_A \rho(\dot{u_x}^2 + \dot{u_y}^2 + \dot{u_z}^2) \, dA dx \tag{3.43}$$

Substituting the above equations into the kinetic energy equation, the following expression can be derived

$$T_{ele} = \frac{1}{2}\int_0^L \int_A [(\dot{u} - y\dot{\theta} + z\dot{\psi})^2 + (\dot{\upsilon} - z\dot{\phi})^2 + (\dot{\omega} - y\dot{\phi})^2] \, \rho dx dA \tag{3.44}$$

Further expansion of the above equation gives

$$T_{ele} = \frac{1}{2}\int_0^L \int_A [\dot{u}^2 + y^2\dot{\theta}^2 + z^2\dot{\psi}^2 + 2y\dot{\theta}\dot{u} + 2z\dot{u}\dot{\psi} - 2yz\dot{\theta}\dot{\psi} + \dot{\upsilon}^2 + z^2\dot{\phi}^2 - 2z\dot{\upsilon}\dot{\phi} + \dot{\omega}^2 + y^2\dot{\phi}^2 + 2y\dot{\omega}\dot{\phi}] \, \rho dx dA \tag{3.45}$$

Afterwards, the equation is further re-ordered and expanded by multiplying $\int_A \rho dA$ to each term.

$$\begin{aligned} T_{ele} = \frac{1}{2}\int_0^L [&\dot{u}^2\rho\int_A dA + \dot{\theta}^2\rho\int_A y^2 dA + \dot{\psi}^2\rho\int_A z^2 dA + 2\dot{\theta}\dot{u}\rho\int_A y dA + 2\dot{u}\dot{\psi}\rho\int_A z dA - 2\dot{\theta}\dot{\psi}\rho\int_A yz dA \\ &+ \dot{\upsilon}^2\rho\int_A dA + \dot{\phi}^2\rho\int_A z^2 dA - 2\dot{\upsilon}\dot{\phi}\rho\int_A z dA + \dot{\omega}^2\rho\int_A dA + \dot{\phi}^2\rho\int_A y^2 dA + 2\dot{\omega}\dot{\phi}\rho\int_A y dA] dx \end{aligned} \tag{3.46}$$

From the equation above, the following expressions give the beam cross-sectional parameters. When the cross section of the beam is symmetric, three of the parameters, namely A_y, A_z, and J, are zero.

$$\int_A dA = A \tag{3.47a}$$

$$\int_A ydA = A_y = 0 \tag{3.47b}$$

$$\int_A zdA = A_z = 0 \tag{3.47c}$$

$$\int_A z^2 dA = I_y \tag{3.47d}$$

$$\int_A y^2 dA = I_z \tag{3.47e}$$

$$\int_A yzdA = J = 0 \tag{3.47f}$$

After substituting the cross-sectional parameters, the equation becomes

$$T_{ele} = \frac{1}{2}\int_0^L \left[A\rho(\dot{u}^2 + \dot{v}^2 + \dot{\omega}^2) + I_y\rho\dot{\psi}^2 + I_z\rho\dot{\theta}^2 + (I_y + I_z)\rho\dot{\phi}^2\right] dx \tag{3.48}$$

By applying shape function relations into the above equation, the final form of the equation can be derived:

$$\begin{aligned} T_{ele} &= \sum_{ij} \frac{1}{2}\dot{q}_i\dot{q}_j \int_0^L \left[A\rho(a_i a_j + b_i b_j + c_i c_j) + I_y\rho e_i e_j + I_z\rho f_i f_j + (I_y + I_z)\rho d_i d_j\right] dx \\ &= \frac{1}{2}\dot{q}_i\dot{q}_j m_{ij} \end{aligned} \tag{3.49}$$

where m_{ij} is the mass matrix of the element.

$$m_{ij} = \int_0^L \left[A\rho(a_i a_j + b_i b_j + c_i c_j) + I_y\rho e_i e_j + I_z\rho f_i f_j + (I_y + I_z)\rho d_i d_j\right] dx \tag{3.50}$$

The equation for the kinetic energy of a Timoshenko element in a local coordinate system is simplified to

$$T_{ele} = \frac{1}{2}\dot{q_{ele}}_i \dot{q_{ele}}_j m_{ele\,ij} = \frac{1}{2}\dot{q_{ele}}^T m_{ele}\dot{q_{ele}} \tag{3.51}$$

3.9 Setting the Local Stiffness Matrix

After the kinetic energy relation and the mass matrix of the Timoshenko element are found, the strain potential energy of the Timoshenko element is calculated.

$$U_{ele} = \int_V \hat{U}\, dV \tag{3.52}$$

where $\hat{U}$ is the expression for the strain energy density:

$$\hat{U} = \int_0^{\epsilon_{ij}} \sigma_{ij} d\epsilon_{ij} \tag{3.53}$$

For the strain energy density of isotropic materials, Hooke's Law states that

$$\sigma_{ij} = C_{ijkl}\epsilon_{kl} = \lambda\epsilon_{kk}\delta_{ij} + 2G\epsilon_{ij} \tag{3.54}$$

where λ is Lamé's first parameter and G is Lamé's second parameter. The strain energy density equation then becomes

$$\hat{U} = \int_0^{\epsilon_{ij}} C_{ijkl}\epsilon_{kl} d\epsilon_{ij} = \frac{1}{2} C_{ijkl}\epsilon_{kl}\epsilon_{ij} \tag{3.55}$$

Substituting the strain energy density equation and Hooke's law for an isotropic material, the strain potential energy equation for a Timoshenko element can be expressed as

$$U_{ele} = \int_V \frac{1}{2} C_{ijkl}\epsilon_{kl}\epsilon_{ij} dV = \frac{1}{2}\int_V (\lambda\epsilon_{kk}\delta_{ij} + 2G\epsilon_{ij})\epsilon_{ij}\, dV \tag{3.56}$$

Expanding and re-ordering,

$$U_{ele} = \frac{1}{2}\int_V (\lambda\epsilon_{ij}\epsilon_{kk}\delta_{ij} + 2G\epsilon_{ij}\epsilon_{ij})\, dV \tag{3.57}$$

where,

$$\epsilon_{ij}\epsilon_{kk}\delta_{ij} = \left[\sum_{k=1}^{3} \epsilon_{kk}\right]^2 \tag{3.58}$$

and

$$\epsilon_{ij}\epsilon_{ij} = \sum_{i=1}^{3}\sum_{j=1}^{3}(\epsilon_{ij}^2) \tag{3.59}$$

$$[\epsilon] = \begin{bmatrix} \epsilon_{11} & \epsilon_{12} & \epsilon_{13} \\ \epsilon_{21} & \epsilon_{22} & \epsilon_{23} \\ \epsilon_{31} & \epsilon_{32} & \epsilon_{33} \end{bmatrix} \tag{3.60}$$

Revisiting the displacement field obtained above, the 3D stress-strain relations components can be expressed as follows, where u_x, u_y, u_z are the components of the displacement field.

$$\epsilon_{11} = \frac{\partial u_x}{\partial x} = u' - y\theta' + z\psi' \tag{3.61a}$$

$$\epsilon_{22} = \frac{\partial u_y}{\partial y} = 0 \tag{3.61b}$$

$$\epsilon_{33} = \frac{\partial u_z}{\partial z} = 0 \tag{3.61c}$$

$$\epsilon_{12} = \epsilon_{21} = \frac{1}{2}\left(\frac{\partial u_x}{\partial y} + \frac{\partial u_y}{\partial x}\right) = \frac{1}{2}\left(\upsilon' - z\phi' - \theta\right) \tag{3.61d}$$

$$\epsilon_{13} = \epsilon_{31} = \frac{1}{2}\left(\frac{\partial u_x}{\partial z} + \frac{\partial u_z}{\partial x}\right) = \frac{1}{2}\left(\omega' + y\phi' + \psi\right) \tag{3.61e}$$

$$\epsilon_{23} = \epsilon_{32} = \frac{1}{2}\left(\frac{\partial u_y}{\partial z} + \frac{\partial u_z}{\partial y}\right) = 0 \tag{3.61f}$$

Therefore, the strain potential energy equation becomes,

$$\begin{aligned} U_{ele} &= \frac{1}{2}\int_V \left[\lambda(\epsilon_{11})^2 + 2G(\epsilon_{11}^2 + 2\epsilon_{12}^2 + 2\epsilon_{13}^2)\right] dV \\ &= \frac{1}{2}\int_V \left[\lambda(\epsilon_{11}^2) + 2G(\epsilon_{11}^2) + 4G(\epsilon_{12}^2) + 4G(\epsilon_{13}^2)\right] dV \\ &= \frac{1}{2}\int_V \left[(\lambda + 2G)(\epsilon_{11}^2) + 4G(\epsilon_{12}^2) + 4G(\epsilon_{13}^2)\right] dV \end{aligned} \tag{3.62}$$

Substituting the strain expressions above,

$$\begin{aligned} U_{ele} &= \frac{1}{2}\int_V \left[(\lambda + 2G)[(u' - y\theta' + z\psi')^2] + 4G[(\frac{1}{2}\left(\upsilon' - z\phi' - \theta\right))^2] + 4G[(\frac{1}{2}\left(\omega' + y\phi' + \psi\right))^2]\right] dV \\ &= \frac{1}{2}\int_V \left[(\lambda + 2G)[(u' - y\theta' + z\psi')^2] + G\left(\upsilon' - z\phi' - \theta\right)^2 + G\left(\omega' + y\phi' + \psi\right)^2\right] dV \end{aligned} \tag{3.63}$$

Replacing,

$$\int_V dV = \int_0^L \int_A dA dx \tag{3.64}$$

the equation becomes

$$U_{ele} = \frac{1}{2}\int_0^L \int_A \left[(\lambda + 2G)[(u' - y\theta' + z\psi')^2] + G\left(\upsilon' - z\phi' - \theta\right)^2 + G\left(\omega' + y\phi' + \psi\right)^2\right] dA dx \tag{3.65}$$

Expanding,

$$U_{ele} = \frac{1}{2}\int_0^L \int_A [(\lambda + 2G)(u'^2 - 2yu'\theta' + 2zu'\psi' - 2yz\theta'\psi' + y^2\theta'^2 + z^2\psi'^2) + G(\upsilon'^2 - 2z\upsilon'\phi' - 2\upsilon'\theta + 2z\phi'\theta + z^2\phi'^2 + \theta^2) + G(\omega'^2 + 2y\omega'\phi' + 2\omega'\psi + 2y\phi'\psi + y^2\phi'^2 + \psi^2)]dAdx \quad (3.66)$$

Afterwards, the equation can be further re-ordered and expanded by multiplying $\int_A dA$ to each term

$$U_{ele} = \frac{1}{2}\int_0^L [(\lambda+2G)(u'^2\int_A dA - 2u'\theta'\int_A ydA + 2u'\psi'\int_A zdA - 2\theta'\psi'\int_A yzdA + \theta'^2\int_A y^2dA + \psi'^2\int_A z^2dA) + G(\upsilon'^2\int_A dA - 2\upsilon'\phi'\int_A zdA - 2\upsilon'\theta\int_A dA + 2\phi'\theta\int_A zdA + \phi'^2\int_A z^2dA + \theta^2\int_A dA) + G(\omega'^2\int_A dA + 2\omega'\phi'\int_A ydA + 2\omega'\psi\int_A dA + 2\phi'\psi\int_A ydA + \phi'^2\int_A y^2dA + \psi^2\int_A dA)]dx \quad (3.67)$$

Afterwards, the expressions for the symmetric beam cross-sectional parameters are substituted into the equation above to simplify the expression.

$$\int_A dA = A \quad (3.68a)$$

$$\int_A ydA = A_y = 0 \quad (3.68b)$$

$$\int_A zdA = A_z = 0 \quad (3.68c)$$

$$\int_A z^2dA = I_y \quad (3.68d)$$

$$\int_A y^2dA = I_z \quad (3.68e)$$

$$\int_A yzdA = J = 0 \quad (3.68f)$$

A reduced form of the equation can be found:

$$U_{ele} = \frac{1}{2}\int_0^L [\lambda(Au'^2 + I_y\psi'^2 + I_z\theta'^2) + 2G(Au'^2 + I_y\psi'^2 + I_z\theta'^2) + G(A\upsilon'^2 - 2A\upsilon'\theta + A\theta^2 + I_y\phi'^2) + G(A\omega'^2 + 2A\omega'\psi + I_z\phi'^2 + A\psi^2)]dx \quad (3.69)$$

Expanding the above equation and re-ordering,

$$U_{ele} = \frac{1}{2}\int_0^L [\lambda(Au'^2 + I_y\psi'^2 + I_z\theta'^2) + 2G(Au'^2 + I_y\psi'^2 + I_z\theta'^2) + GA(\upsilon'^2 - 2\upsilon'\theta + \theta^2) + GA(\omega'^2 + 2\omega'\psi + \psi^2) + G(I_y\phi'^2 + I_z\phi'^2)]dx$$
$$= \frac{1}{2}\int_0^L [\lambda(Au'^2+I_y\psi'^2+I_z\theta'^2)+2G(Au'^2+I_y\psi'^2+I_z\theta'^2)+GA((\upsilon'-\theta)^2+(\omega'+\psi)^2)+G(I_y+I_z)\phi'^2)]dx \tag{3.70}$$

By substituting the expressions for the shape functions into the above derivative terms, and incorporating the shear correction factor κ, the following form is derived.

$$U_{ele} = \frac{1}{2}\int_0^L [\lambda(A(q_i a_i')^2 + I_y(q_i e_i')^2 + I_z(q_i f_i')^2) + 2\kappa G(A(q_i a_i')^2 + I_y(q_i e_i')^2 + I_z(q_i f_i')^2) + \kappa GA((q_i b_i' - q_i f_i)^2 + (q_i c_i' + q_i e_i)^2) + \kappa G(I_y + I_z)(q_i d_i')]dx \tag{3.71}$$

$$U_{ele} = \sum_{ij}\frac{1}{2}q_i q_j \int_0^L [\lambda(Aa_i'a_j' + I_y e_i'e_j' + I_z f_i'f_j') + 2\kappa G(Aa_i'a_j' + I_y e_i'e_j' + I_z f_i'f_j') + \kappa GA((b_i' - f_i)(b_j' - f_j) + (c_i' + e_i)(c_j' + e_j)) + \kappa G(I_z + I_y)(d_i'd_j')]dx = \frac{1}{2}q_i q_j k_{ij}$$
$$\text{where } k_{ij} = \int_0^L [\lambda(Aa_i'a_j' + I_y e_i'e_j' + I_z f_i'f_j') + 2\kappa G(Aa_i'a_j' + I_y e_i'e_j' + I_z f_i'f_j') + \kappa GA((b_i' - f_i)(b_j' - f_j) + (c_i' + e_i)(c_j' + e_j)) + \kappa G(I_z + I_y)(d_i'd_j')]dx \tag{3.72}$$

where, k_{ij} is the mass matrix of the element.

$$k_{ij} = \int_0^L [\lambda(Aa_i'a_j' + I_y e_i'e_j' + I_z f_i'f_j') + 2\kappa G(Aa_i'a_j' + I_y e_i'e_j' + I_z f_i'f_j') + \kappa GA((b_i' - f_i)(b_j' - f_j) + (c_i' + e_i)(c_j' + e_j)) + \kappa G(I_z + I_y)(d_i'd_j')]dx \tag{3.73}$$

The equation for the strain potential energy of a Timoshenko element in a local coordinate system can be simplified to

$$U_{ele} = \frac{1}{2}q_{ele\ i}q_{ele\ j}k_{ele\ ij} = \frac{1}{2}q_{ele}^T k_{ele} q_{ele} \tag{3.74}$$

where λ and G are the first and the second Lamé's parameters of the coated struts of the lattice structures. First, Lamé's second parameter, G(shear modulus), is evaluated by the following, knowing that the shear modulus, G, can be related with shear stress and shear strain:

$$G = \frac{\text{Shear Stress}}{\text{Shear Strain}} = \frac{\tau_{xy}}{\gamma_{xy}} = \frac{F/A}{\triangle x/l} = \frac{Fl}{A\triangle x} \tag{3.75}$$

where,

F = Shear force
A = Area of cross section
l = Length of the strut element
$\triangle x$ = Transverse displacement

re-ordering the equation, and equating to Shear Force,

$$F = \frac{GA\triangle x}{l} \tag{3.77}$$

$$\frac{GA\triangle x}{l}_{overall} = \frac{GA\triangle x}{l}_{polymer} + \frac{GA\triangle x}{l}_{copper} + \frac{GA\triangle x}{l}_{nickel} \tag{3.78}$$

Knowing that all the components of the coated strut have the same strut length and transverse displacement, $\triangle x$ and l can be eliminated from all the terms, resulting in the following equation

$$GA_{overall} = GA_{polymer} + GA_{copper} + GA_{nickel} \tag{3.79}$$

Once $G_{overall}$ is calculated, Lamé's first parameter can be found by using the following equation.

$$\lambda = \frac{G(E - 2G)}{3G - E} \tag{3.80}$$

where E is the Young's modulus of the overall coated strut found at the beginning of this chapter.

3.10 Evaluating the Shape Functions Involved in the Mass and Stiffness Matrices

In the previous section, expressions for the local element mass and stiffness matrices, m_{ij} and k_{ij}, were found based on the kinetic and strain potential energy equations.

$$m_{ij} = \int_0^L [A\rho(a_i a_j + b_i b_j + c_i c_j) + I_y \rho e_i e_j + I_z \rho f_i f_j + (I_y + I_z)\rho d_i d_j]\, dx \tag{3.81}$$

$$k_{ij} = \int_0^L [\lambda(Aa'_i a'_j + I_y e'_i e'_j + I_z f'_i f'_j) + 2\kappa G(Aa'_i a'_j + I_y e'_i e'_j + I_z f'_i f'_j) + \kappa GA((b'_i - f_i)(b'_j - f_j) + (c'_i + e_i)(c'_j + e_j)) + \kappa G(I_z + I_y)(d'_i d'_j)]dx \tag{3.82}$$

The alphabetical terms, a_i, a_j, ... f_i, f_j are the basic shape functions that were described in the previous section, while a'_i, a'_j, ... f'_i, f'_j are the derivatives of the corresponding shape functions. Both the element mass and stiffness matrices in a local coordinate system involve multiplication of the shape functions and its derivatives, such as $a_i a_j$, which must be evaluated with the Gauss quadrature method.

Consider a term involving multiplication of two shape functions a_1 and a_2:

$$I = \int_{a=0}^{b=L} a_1 a_2 dx \tag{3.83}$$

Both shape functions a_1 and a_2 require five inputs to be computed: ξ, η_y, η_z, μ_y, and μ_z. The $\eta_{y,z}$ and $\mu_{y,z}$ are easily calculated with the information of E, $I_{y,z}$, κ, G, A, L, and ν, which were obtained in the previous steps of the finite element analysis. However, ξ requires the Gauss quadrature method to be evaluated.

$$\xi_i = \frac{1}{2}(0 + L) + \frac{1}{2}(P_i)(L - 0) \tag{3.84}$$

where, P is the position of the Gauss points and L is the length of the element. Noting that ξ is expressed in terms of P_i, which has four different values and its own corresponding weights, W_i, the multiplication of the two shape functions must be evaluated with all four different Gauss points and weights.

i	Gauss points, P_i	Weights, W_i
1	-0.8611363116	0.3478548451
2	-0.3399810436	0.6521451549
3	+0.3399810436	0.6521451549
4	+0.8611363116	0.3478548451

Table 3.4: Table of the Gauss quadrature points and corresponding weights.

$$\sum_{i=1}^{4} \left[\frac{L}{2} W_i \Big(a_1(\xi_i, \eta_y, \eta_z, \mu_y, \mu_z) \quad a_2(\xi_i, \eta_y, \eta_z, \mu_y, \mu_z) \Big) \right] \tag{3.85}$$

3.11 Construction of the Local and Global Mass and Stiffness Matrices

The mass and stiffness matrices of the Timoshenko elements obtained above, m_{ij} and k_{ij}, are in a local coordinate system. The two local element mass and stiffness matrices must then represented in the matrices in a global coordinate system by applying a rotational matrix R.

$$R_{ele} = \begin{bmatrix} \begin{bmatrix} \\ r_y r_z r_x \\ \\ \end{bmatrix} & \mathbf{0} & \mathbf{0} & \mathbf{0} \\ \mathbf{0} & \begin{bmatrix} 1 & 0 & 0 \\ 0 & 1 & 0 \\ 0 & 0 & 1 \end{bmatrix} & \mathbf{0} & \mathbf{0} \\ \mathbf{0} & \mathbf{0} & \begin{bmatrix} \\ r_y r_z r_x \\ \\ \end{bmatrix} & \mathbf{0} \\ \mathbf{0} & \mathbf{0} & \mathbf{0} & \begin{bmatrix} 1 & 0 & 0 \\ 0 & 1 & 0 \\ 0 & 0 & 1 \end{bmatrix} \end{bmatrix}$$

$$r_y = \begin{bmatrix} \cos\alpha & 0 & -\sin\alpha \\ 0 & 1 & 0 \\ \sin\alpha & 0 & \cos\alpha \end{bmatrix} \quad r_z = \begin{bmatrix} \cos\beta & -\sin\beta & 0 \\ \sin\beta & \cos\beta & 0 \\ 0 & 0 & 1 \end{bmatrix} \quad r_x = \begin{bmatrix} 1 & 0 & 0 \\ 0 & \cos\gamma & \sin\gamma \\ 0 & -\sin\gamma & \cos\gamma \end{bmatrix} \tag{3.86}$$

By applying the following relations, the global mass matrix $M_{element}$ and stiffness matrix $K_{element}$ can be found.

$$K_{ele} = R_{ele} k_{ele} R_{ele}^T \tag{3.87}$$

$$M_{ele} = R_{ele} m_{ele} R_{ele}^T \tag{3.88}$$

Once all the mass and stiffness matrices for all the elements are converted from a local to a global coordinate system, all the elements' mass matrices are collected into one global mass matrix M_{ij} of the lattice structure based on the nodal connectivities of each of the elements. Similarly, all the elements' stiffness matrices are collected into one global stiffness matrix K_{ij} of the lattice structure based on the nodal connectivities of each of the elements. For example, consider a structure involving two elements ($E1$, $E2$) at the element level, each element holds a negative node A and a positive node B. However, when the elements are connected together, the structure holds three nodes (n1, n2, n3). At the structure level, the first element $E1$ has a negative node of n1 and a positive node of n2, and the second element $E2$ has a negative node of n2 and a positive node of n3, where the two elements are connected by node n2.

	Nodes in local		Nodes in Global	
Elements	-ve node	+ve node	-ve node	+ve node
E1	A	B	n1	n2
E2	A	B	n2	n3

Table 3.5: Table of nodal connectivities in local and global coordinate systems.

The global mass matrix can be divided into four quadrants, where each quadrant relates to the specific nodes of the element:

$$\left[\ M_{E1}\ \right] = \begin{bmatrix} +ve\ node\ +ve\ node & +ve\ node\ -ve\ node \\ -ve\ node\ +ve\ node & -ve\ node\ -ve\ node \end{bmatrix} = \begin{bmatrix} AA & AB \\ BA & BB \end{bmatrix} \tag{3.89}$$

The global matrix of the first element, E1, can be expressed as

$$\left[\ M_{E1}\ \right] = \begin{bmatrix} A_{E1}A_{E1} & A_{E1}B_{E1} \\ B_{E1}A_{E1} & B_{E1}B_{E1} \end{bmatrix}_{in\ element\ level} \tag{3.90}$$

and the global mass matrix of the second element, E2, can be expressed as

$$\left[\ M_{E2}\ \right] = \begin{bmatrix} A_{E2}A_{E2} & A_{E2}B_{E2} \\ B_{E2}A_{E2} & B_{E2}B_{E2} \end{bmatrix}_{in\ element\ level} \tag{3.91}$$

The two element mass matrices are then collected into a single matrix, representing the mass matrix of

the overall lattice structure:

$$\left[\ M_{structure}\ \right] = \begin{bmatrix} n1,n1 & n1,n2 & n1,n3 \\ n2,n1 & n2,n2 & n2,n3 \\ n3,n1 & n3,n2 & n3,n3 \end{bmatrix} \tag{3.92}$$

The location, where each quadrant of the element matrices fits into the collected structure matrix, is defined by how the negative and positive nodes of each element (nodes A and B) are represented as nodes in the structure level (nodes n1, n2, and n3). For the first element, E1, the location of each quadrant of the element matrix is defined as

$$\left[\ M_{E1}\ \right]_{collected} = \begin{bmatrix} n1,n1 & n1,n2 \\ n2,n1 & n2,n2 \end{bmatrix}_{location\ in\ structure\ matrix} = \begin{bmatrix} A_{E1}A_{E1} & A_{E1}B_{E1} & 0 \\ B_{E1}A_{E1} & B_{E1}B_{E1} & 0 \\ 0 & 0 & 0 \end{bmatrix} \tag{3.93}$$

and the location of each quadrant of the second element matrix, E2, is defined as

$$\left[\ M_{E2}\ \right]_{collected} = \begin{bmatrix} n2,n2 & n2,n3 \\ n3,n2 & n3,n3 \end{bmatrix}_{location\ in\ structure\ matrix} = \begin{bmatrix} 0 & 0 & 0 \\ 0 & A_{E2}A_{E2} & A_{E2}B_{E2} \\ 0 & B_{E2}A_{E2} & B_{E2}B_{E2} \end{bmatrix} \tag{3.94}$$

Finally, by taking the sum of $[M_{E1}]_{collected}$ and $[M_{E2}]_{collected}$, the collected mass matrix of the structure in the global coordinate system is expressed as

$$\left[\ M_{structure}\ \right] = \begin{bmatrix} A_{E1}A_{E1} & A_{E1}B_{E1} & 0 \\ B_{E1}A_{E1} & B_{E1}B_{E1} + A_{E2}A_{E2} & A_{E2}B_{E2} \\ 0 & B_{E2}A_{E2} & B_{E2}B_{E2} \end{bmatrix} \tag{3.95}$$

Similarly, the stiffness matrix, K, of the structure in a global coordinate system can be obtained as well. The equation for kinetic energy and strain potential energy of the lattice structure in a global coordinate system is simplified to

$$T_{structure} = \frac{1}{2}\dot{q}_i\dot{q}_j M_{ij} = \frac{1}{2}\dot{q}^T M\dot{q} \tag{3.96}$$

$$U_{structure} = \frac{1}{2}q_i q_j K_{ij} = \frac{1}{2}q^T Kq \tag{3.97}$$

3.12 Obtaining the Equation of Motion

The equation of motion can be obtained by using Lagrange's equation:

$$\frac{\partial}{\partial t}\frac{\partial L}{\partial \dot{q}_i} - \frac{\partial L}{\partial q_i} = f \tag{3.98}$$

where, $T = \frac{1}{2}\dot{q}_i\dot{q}_j M_{ij} = \frac{1}{2}\dot{q}^T M\dot{q}$
$U = \frac{1}{2}q_i q_j K_{ij} = \frac{1}{2}q^T Kq$
L = Lagrangian = Kinetic energy - potential energy = $T - U$
f = force

Lagrange's equation can be simplified to

$$M\ddot{q} + Kq = f \tag{3.99}$$

where q is the collection of all nodal displacements of all nodes in the lattice unit cell, M is the collected mass matrix of the lattice unit cell in the global coordinate system, and K is the collected stiffness matrix of the lattice unit cell in the global coordinate system.

Revisiting Bloch's theorem and the related equation described in the previous chapter,

$$q_{bnd} = q_b e^{n_1 k_1 + n_2 k_2 + n_3 k_3} \tag{3.100}$$

Bloch's theorem expresses that the displacement at the boundary nodes can be defined by the displacement at the corresponding basis node. Hence, in the previous section, all the collection of nodes in the entire lattice unit cell are categorized into three different types: internal, (q_i), basis, (q_b), and boundary, ($q_{bnd} = q_{1,2,3}$). In order to describe the boundary node in reference to the basis node, the transformation matrix, $[T]$, is required:

$$\left[\ q_{bnd}\ \right] = \left[\ T\ \right] \cdot \left[\ q_b\ \right] \tag{3.101}$$

For example, the boundary node q_1 is the nodal displacement that can be explained by the displacement at the basis node q_b tessellated in the e_1 direction, while q_{12} is the nodal displacement that can be expressed by the displacement at the basis node tessellated in the e_1 and e_2 directions. While all the boundary nodes are defined by the basis node, each internal node can only be defined by itself.

$$\left[\ q\ \right] = \left[\ T\ \right] \cdot \left[\ \tilde{q}\ \right] = \begin{bmatrix} q_i \\ q_b \\ q_1 \\ q_2 \\ q_3 \\ q_{12} \\ q_{13} \\ q_{23} \\ q_{123} \end{bmatrix} = \begin{bmatrix} I & 0 \\ 0 & I \\ 0 & T_1 \\ 0 & T_2 \\ 0 & T_3 \\ 0 & T_{12} \\ 0 & T_{13} \\ 0 & T_{23} \\ 0 & T_{123} \end{bmatrix} \cdot \begin{bmatrix} q_i \\ q_b \end{bmatrix} \tag{3.102}$$

For example, the relationship between q_{12}, T_{12}, and q_b can be expressed as follows:

$$\left[\ q_{12}\ \right] = \left[\ T_{12}\ \right] \cdot \left[\ q_b\ \right] = \begin{bmatrix} u_{12} \\ v_{12} \\ w_{12} \\ \phi_{12} \\ \psi_{12} \\ \theta_{12} \end{bmatrix} = \begin{bmatrix} e^{k_1+k_2} & 0 & 0 & 0 & 0 & 0 \\ 0 & e^{k_1+k_2} & 0 & 0 & 0 & 0 \\ 0 & 0 & e^{k_1+k_2} & 0 & 0 & 0 \\ 0 & 0 & 0 & e^{k_1+k_2} & 0 & 0 \\ 0 & 0 & 0 & 0 & e^{k_1+k_2} & 0 \\ 0 & 0 & 0 & 0 & 0 & e^{k_1+k_2} \end{bmatrix} \cdot \begin{bmatrix} u_b \\ v_b \\ w_b \\ \phi_b \\ \psi_b \\ \theta_b \end{bmatrix} \tag{3.103}$$

k_1, k_2, and k_3 are the wave numbers in the directions of e_1, e_2, and e_3 basis vectors, in the corresponding order:

$$\vec{k} = n_1\vec{k}\vec{e_1} + n_2\vec{k}\vec{e_2} + n_3\vec{k}\vec{e_3} = n_1k_1 + n_2k_2 + n_3k_3 \tag{3.104}$$

where $\vec{k}$ is the wave vector, and n_i defines any other neighbouring unit lattice cell obtained by n_i translation along the e_i direction. The overall transformation matrix looks as follows:

$$\begin{bmatrix} q_i \\ q_b \\ q_1 \end{bmatrix} = \begin{bmatrix} I & 0 \\ 0 & I \\ 0 & T_1 \end{bmatrix} . \begin{bmatrix} q_i \\ q_b \end{bmatrix} \tag{3.105}$$

$$\begin{bmatrix} u_i \\ v_i \\ w_i \\ \phi_i \\ \psi_i \\ \theta_i \\ u_b \\ v_b \\ w_b \\ \phi_b \\ \psi_b \\ \theta_b \\ u_1 \\ v_1 \\ w_1 \\ \phi_1 \\ \psi_1 \\ \theta_1 \end{bmatrix} = \begin{bmatrix} 1 & 0 & 0 & 0 & 0 & 0 & 0 & 0 & 0 & 0 & 0 & 0 \\ 0 & 1 & 0 & 0 & 0 & 0 & 0 & 0 & 0 & 0 & 0 & 0 \\ 0 & 0 & 1 & 0 & 0 & 0 & 0 & 0 & 0 & 0 & 0 & 0 \\ 0 & 0 & 0 & 1 & 0 & 0 & 0 & 0 & 0 & 0 & 0 & 0 \\ 0 & 0 & 0 & 0 & 1 & 0 & 0 & 0 & 0 & 0 & 0 & 0 \\ 0 & 0 & 0 & 0 & 0 & 1 & 0 & 0 & 0 & 0 & 0 & 0 \\ 0 & 0 & 0 & 0 & 0 & 0 & 1 & 0 & 0 & 0 & 0 & 0 \\ 0 & 0 & 0 & 0 & 0 & 0 & 0 & 1 & 0 & 0 & 0 & 0 \\ 0 & 0 & 0 & 0 & 0 & 0 & 0 & 0 & 1 & 0 & 0 & 0 \\ 0 & 0 & 0 & 0 & 0 & 0 & 0 & 0 & 0 & 1 & 0 & 0 \\ 0 & 0 & 0 & 0 & 0 & 0 & 0 & 0 & 0 & 0 & 1 & 0 \\ 0 & 0 & 0 & 0 & 0 & 0 & 0 & 0 & 0 & 0 & 0 & 1 \\ 0 & 0 & 0 & 0 & 0 & 0 & e^{k_1} & 0 & 0 & 0 & 0 & 0 \\ 0 & 0 & 0 & 0 & 0 & 0 & 0 & e^{k_1} & 0 & 0 & 0 & 0 \\ 0 & 0 & 0 & 0 & 0 & 0 & 0 & 0 & e^{k_1} & 0 & 0 & 0 \\ 0 & 0 & 0 & 0 & 0 & 0 & 0 & 0 & 0 & e^{k_1} & 0 & 0 \\ 0 & 0 & 0 & 0 & 0 & 0 & 0 & 0 & 0 & 0 & e^{k_1} & 0 \\ 0 & 0 & 0 & 0 & 0 & 0 & 0 & 0 & 0 & 0 & 0 & e^{k_1} \end{bmatrix} . \begin{bmatrix} u_i \\ v_i \\ w_i \\ \phi_i \\ \psi_i \\ \theta_i \\ u_b \\ v_b \\ w_b \\ \phi_b \\ \psi_b \\ \theta_b \end{bmatrix} \tag{3.106}$$

Substituting the above expressions into the collected equations of motion will give the following equation

$$MT\ddot{\tilde{q}} + KT\tilde{q} = f \tag{3.107}$$

$$T^HMT\ddot{\tilde{q}} + T^HKT\tilde{q} = T^Hf \tag{3.108}$$

where T^H is a conjugate transpose of the transformation matrix, and $\tilde{M} = T^H$ M and $\tilde{K} = T^H$ K. Noting that

$$T^HMT = \tilde{M} \tag{3.109}$$

$$T^HKT = \tilde{K} \tag{3.110}$$

The equation is further simplified to

$$\tilde{M}\ddot{\tilde{q}} + \tilde{K}\tilde{q} = T^Hf \tag{3.111}$$

Bloch's theorem can be extended onto the expression for force. While the expression

$$f_{bnd} = \left[\ T\ \right] .\ f_b \tag{3.112}$$

defines the force applied at the boundary node with respect to the force applied at the corresponding basis node, the expression

$$f_b = \left[\ T^H\ \right] .\ f_{bnd} \tag{3.113}$$

represents the force applied at the basis node, with respect to the force applied at the corresponding boundary node. Therefore, for the tetrahedral and pyramidal unit cell that undergoes a boundary condition of zero external forces, the right-hand side of the reduced equation of motion, $T^H f$, is expressed as

$$T^H f = \begin{bmatrix} I & 0 & 0 & 0 & 0 \\ 0 & I & T_1^H & T_2^H & T_3^H \end{bmatrix} \begin{bmatrix} F_{q_i} \\ F_{q_b} \\ F_{q_1} \\ F_{q_2} \\ F_{q_3} \end{bmatrix} = \begin{bmatrix} F_{q_i} & 0 & 0 & 0 & 0 \\ 0 & F_{q_b} & T_1^H F_{q_1} & T_2^H F_{q_2} & T_3^H F_{q_3} \end{bmatrix} \tag{3.114}$$

Since there are no external forces applied, there are no forces applied to the internal nodes.

$$F_{q_i} = 0 \tag{3.115}$$

As F_{q_b} defines the force applied to the basis node by all neighbouring boundary nodes,

$$F_{q_b} = T^H F_{q_{bnd}} = -\left(T_1^H F_{q_1} + T_2^H F_{q_2} + T_3^H F_{q_3}\right) \tag{3.116}$$

Therefore,

$$T^H f = \begin{bmatrix} F_{q_i} & 0 & 0 & 0 & 0 \\ 0 & F_{q_b} & T_1^H F_{q_1} & T_2^H F_{q_2} & T_3^H F_{q_3} \end{bmatrix} = \begin{bmatrix} 0 \\ 0 \end{bmatrix} \tag{3.117}$$

Substituting the force term obtained through the application of Bloch's theorem, the reduced equation of motion can be simplified as follows:

$$\tilde{M}\ddot{\tilde{q}} + \tilde{K}\tilde{q} = 0 \tag{3.118}$$

where $\tilde{M}$ = Hermitian Mass Matrix
$\tilde{K}$ = Hermitian Stiffness Matrix
$\tilde{q}$ = nodal displacement
$\ddot{\tilde{q}}$ = nodal acceleration

The reduced equation of motion is converted into an eigenvalue problem by substituting $\tilde{q}$, which is the classical equation describing plane wave motion through a lattice with a wave vector k, radial frequency ω and amplitude A at a point r and at time t:

$$\tilde{q} = Ae^{i(\vec{k}\cdot\vec{r}-\omega t)} \tag{3.119}$$

$$\tilde{q} = A[cos(\vec{k}\cdot\vec{r}-\omega t) + isin(\vec{k}\cdot\vec{r}-\omega t)] \tag{3.120}$$

where $\vec{k}$ = Wave vector of plane wave
$\vec{r}$ = vector of lattice points in cell corresponding to
jth point in reference cell
ω = radial frequency
t = time

Then, $\ddot{\tilde{q}}$ is found by taking the second derivative of the real part of $\tilde{q}$:

$$\tilde{q} = Acos(\vec{k} \cdot \vec{r} - \omega t) \tag{3.121}$$

$$\ddot{\tilde{q}} = -\omega^2 Acos(\vec{k} \cdot \vec{r} - \omega t) \tag{3.122}$$

Substituting the expressions for $\tilde{q}$ and $\ddot{\tilde{q}}$ into the reduced equation of motion, the eigenvalue problem describing free wave motion in the frequency domain is obtained:

$$\tilde{K}\phi = \omega^2 \tilde{M}\phi \tag{3.123}$$

where ϕ = eigenvector
$\omega^2 = \lambda$ = eigenvalues

There are two solutions for the eigenvalue problem: eigenvectors and eigenvalues. While the eigenvalues obtained from the eigenvalue problem can be used to create a dispersion surface, in which the number of resulting dispersion surfaces is equal to the number of eigenvalues in the problem, the eigenvectors are used to analyze the mode shapes of the lattice structure undergoing wave propagation.

Chapter 4

Wave propagation analysis

4.1 Plotting Dispersion Curves

Dispersion curves of waves propagating in lattice structures are plotted by taking the eigenfrequencies and plotting them against the wave numbers, which are the inputs and the solutions of the eigenvalue problem derived through the finite element analysis. A 2D lattice structure has two reciprocal basis vectors, e_1^* and e_2^*. Therefore, to plot a dispersion curve for the 2D lattice structure, a 3D plot is required, in which the x-axis and y-axis of the graph plot the wave numbers k_1 and k_2, while the z-axis of the graph plots the eigenfrequencies. Likewise, a 3D lattice structure has three reciprocal basis vectors: e_1^*, e_2^*, and e_3^*. Therefore, to plot a dispersion curve for the 3D lattice structure, a four dimensional (4D) plot is required, where three dimensions are required for the wave numbers along the directions of the three different reciprocal basis vectors and one dimension is required for the frequencies of the wave propagation. A generic dispersion curve can be generated by computing the eigenvalue problem and finding eigenfrequencies solutions for all the wave vectors in the first Brillouin zone, and then plotting them against each corresponding wave vector. This thesis focuses on the analysis and comparison of symmetric and non-symmetric lattice structures with an aim to find an improved way to tailor and locate the band gap at a desired frequency range in the dispersion curve, which is performed by comparing the dispersion relations of waves propagating along different directions. Hence, this thesis focuses on the analysis of the wave vectors propagating along the reciprocal basis vectors, e_1^* and e_2^*. Therefore, the dispersion curves of the 3D lattice structures presented in this thesis are in 2D plot of frequency (the ordinate) against the wave vector (the abscissa).

Prior to moving on to the following section of the thesis, it is important to make clear the understanding between symmetric/non-symmetric lattice structures, and symmetric/asymmetric dispersion relations. The symmetric lattice structure refers to a structure in which all the struts have equal design variables, while the non-symmetric lattice structure refers to a structure in which one or more but not all the struts are modified to have different design variables. On the other hand, the dispersion relation is symmetric when the resulting dispersion curves of a wave propagating in one direction is symmetric to the dispersion curves of a wave propagating in a different direction; whereas the dispersion relation is considered asymmetric, when the resulting dispersion curves of a wave propagating in one direction is different from the dispersion curves of a wave propagating in a different direction.

4.2 Modifying the Design Variables to Tailor the Dispersion Curve

As described in Chapter 3, the constructed lattice structure contains multiple design variables, which can be modified to tailor the lattice structure as well as the band gap of the dispersion curve.

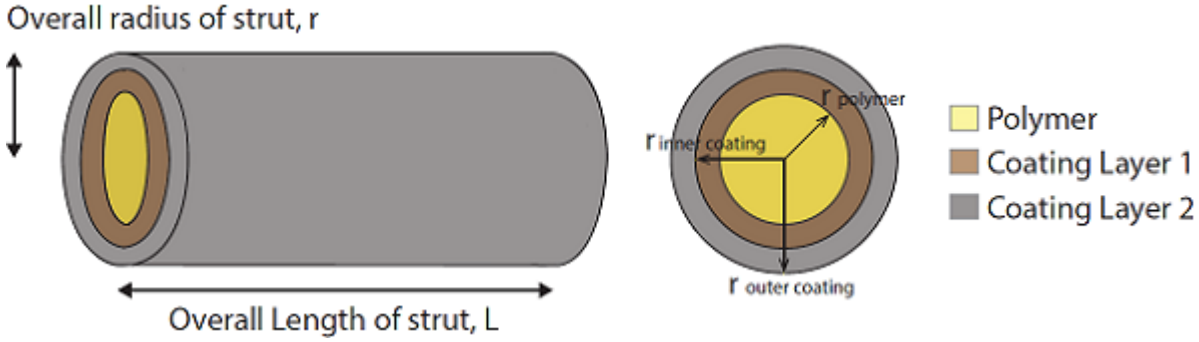

Figure 4.1: Illustration of a structural configuration of the struts of a lattice structure.

The design variables and components of the lattice struts that can be modified to tailor the lattice structure are listed in Table 4.1

Design Variables	Components of lattice structure
Young's modulus, E	Polymer substrate, Coating layers
Density, ρ	Polymer substrate, Coating layers
radius, r	Polymer substrate
Thickness, t	Coating layers
Length, L	Lattice strut

Table 4.1: Table of the design variables involved in different sections of the lattice struts.

One or more design variables in Table 4.1 can be increased or decreased to tailor the lattice structure, which would affect the dispersion curve and band gap phenomenon. For application of the lattice structure in aerospace industries, structures with a high stiffness (Young's modulus) and low density are preferred. Therefore, for the analysis of the current thesis, the design variables are modified to provide an increase or decrease in the Young's modulus and density.

Table 4.2 lists the material combinations and corresponding design variables set for the structural configuration illustrated in Figure 4.1. Based on the material combinations and the values of each of the design variables in Table 4.2, the Young's modulus and the density of the overall lattice structure can be modified in various ways through modifying the radius of the substrate and the thickness of each coating layer of the lattice struts. For instance, compared to the design variables listed in Table 4.2, increasing the radius of the polymer substrate, while maintaining the overall strut radius, causes the thickness of the coating layers to be slimmer than before, and thereby decreases both the Young's modulus and the

density of the overall lattice strut. On the other hand, decreasing the radius of the polymer substrate, while maintaining the overall strut radius, increases both the Young's modulus and the density of the overall lattice strut. When the radius of the polymer substrate is kept the same but the thicknesses of both coating layers are decreased, both the Young's modulus and the density of the overall lattice strut decreases. However, if both thickness of the two coating layers are increased, both the Young's modulus and the density of the overall lattice strut increases. As such, various combinations of modification on the radius of the polymer substrate and the thickness of the coating layers will cause a change in the Young's modulus and in the density of the lattice structure.

The importance of the material combinations listed in Table 4.2 is based on the flexibility of how the Young's modulus and the density of the lattice structure can be modified. In Table 4.2, it can be also seen that copper and nickel are used as the coating materials, and that both materials have the same value of density, but differ in their values of the Young's modulus. For this reason, referring to Figure 4.1, when the radius of the polymer substrate and the radius of the outer coating remain constant, and only the radius of the inner coating is modified, the Young's modulus of the overall lattice strut can be modified independently without changing the density of the lattice strut. With the material combination and design variables defined in Table 4.2, the Young's modulus of overall strut is calculated as 14.085 Gpa, and the density of the overall strut is calculated as 1542.5 $^{kg}/_{m^3}$. For example, with the design variables defined in Table 4.2, while maintaining the radius of the polymer substrate at 1 mm, but reducing the thickness of the copper coating layer by 0.01 mm and increasing the thickness of the nickel coating layer by 0.01 mm, the Young's modulus of the overall strut is changed to 17.754 Gpa, while the density of the overall strut remains constant. This change occurs as the amount of nickel, which has the highest Young's modulus, is increased significantly, while the amount of copper, which has a lower Young's modulus, is decreased by the same volume. Using such a method, the Young's modulus and the density of the overall lattice strut can be modified independently for analysis of the dispersion curves of various lattice configurations.

Alternatively, the Young's modulus and the density of the lattice strut can be modified by changing the material combinations, such as using different coating materials for the lattice structure. To change the density of the lattice strut, metals of different types with differing densities can be mixed through an alloying process. For example, nickel with the density of 8900 $^{kg}/_{m^3}$ can be alloyed with another metal that has a higher or lower density, and the modified density of the strut can be obtained based on a rule of mixtures approach, which the material is the electrodeposited alloy. Again, the Young's modulus of the lattice strut can be modified if a stiffer material is added through an alloying process, which the material is electrodeposited alloy as well.

The material combinations and the design variables are described in Table 4.2 and were used for the default lattice configuration for the tetrahedral and the pyramidal lattice structures. The dispersion curves of this default lattice configuration are analyzed and then used throughout the analysis section of the thesis, and will also be compared with dispersion curves of various configurations of the lattice structures.

Design Variables	
$E_{polymer}$	2.115 Gpa
$\rho_{polymer}$	1170 $^{kg}/_{m^3}$
E_{copper}	58.6 Gpa
ρ_{copper}	8900 $^{kg}/_{m^3}$
E_{nickel}	157.6 Gpa
ρ_{nickel}	8900 $^{kg}/_{m^3}$
Radius of polymer strut	1 mm
Thickness of copper coating layer	0.0125 mm
Thickness of nickel coating layer	0.0125 mm
Length of each strut	10.25 mm

Table 4.2: Table of the design variables involved in the lattice structures.

4.3 Properties of Dispersion Curves

4.3.1 Velocity of Wave Propagation

Dispersion curves tell us how waves are propagating at different velocities at different frequencies. In the dispersion curves, two types of velocities can be found: phase velocity (ν_p) and group velocity(ν_g). The secant slope, the slope of the straight line connecting the origin to the point of interest, represents the phase velocity, while the tangent slope, the slope of the tangent line at the point of the dispersion curve, represents the group velocity [23]. The dispersion curves plot the frequencies against the corresponding wave numbers. The frequencies, are in units of radians per second (rad/s), while the wave numbers are in units of radians per unit distance. Since the frequencies are plotted on the y-axis and the wave numbers are plotted on the x-axis, the slopes of the dispersion curves are measured as follows

$$\text{Slope of the curve} = \frac{\text{frequencies}}{\text{wave numbers}} = \frac{\frac{\text{radians}}{\text{second}}}{\frac{\text{radians}}{\text{meter}}} = \frac{\text{meter}}{\text{second}} = \text{Velocity} \tag{4.1}$$

4.3.2 Dispersion Branches, Veering Effect and Natural Frequencies

First, the dispersion curves for a tetrahedral 3D lattice structure were plotted as shown in Figure 4.2, with the design variables described in Table 4.2. The dispersion curves for waves propagating along e_1^* are plotted with blue solid lines, with wave numbers of varying k_1 component, but zero k_2 and k_3 components. When the eigenvalue problems are solved for each input wave number, multiple eigenfrequencies are obtained as solutions for each wave number. The lowest eigenfrequency solutions of each wave number are then connected into a line, forming the first dispersion branch of the dispersion curve, while the second lowest eigenfrequency solutions of each wave number are connected into another line, forming the second dispersion branch. Through repeating this procedure, dispersion curves were plotted for the first 14 dispersion branches. The number of dispersion branches appearing in the plot was manually selected to display the band gap phenomena in the resulting dispersion curves of the lattice structure.

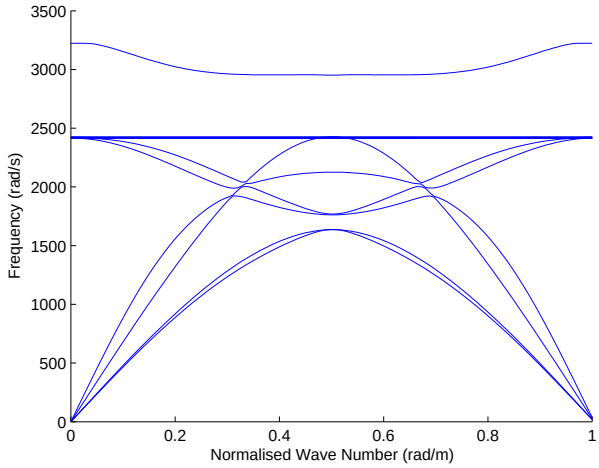

Figure 4.2: Illustration of the dispersion curves of the tetrahedral lattice with the design variables in Table 4.2.

Often, when the dispersion curves are plotted based on frequency (ordinate) against the wave vector (abscissa), the observed dispersion branches look as if they are crossing each other. However, the dispersion branches that seem to be crossing each other are in fact just coming close to each other, then they make a steep change in direction at some point. In reality, the dispersion branches never cross each other in the dispersion curve. This phenomenon is called veering [22].

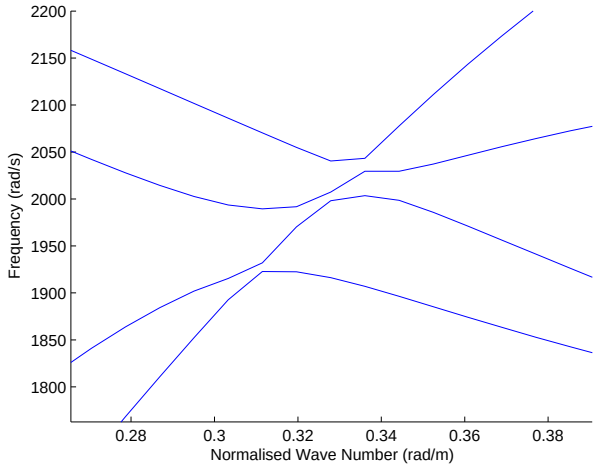

Figure 4.3: Illustration of the four dispersion branches experiencing the veering effect.

Paying attention to 3^{rd}, 4^{th}, 5^{th}, and 6^{th} dispersion branches of the dispersion curves, the four dispersion branches seem as if they are crossing each other. However, as illustrated in Figure 4.3, when the plot is magnified to display the four dispersion branches between the normalised wave numbers of 0.28 and 0.38, and the frequency range of 1800 and 2200 rad/s, it can be observed that these are in fact, four separate dispersion branches that do not cross each other.

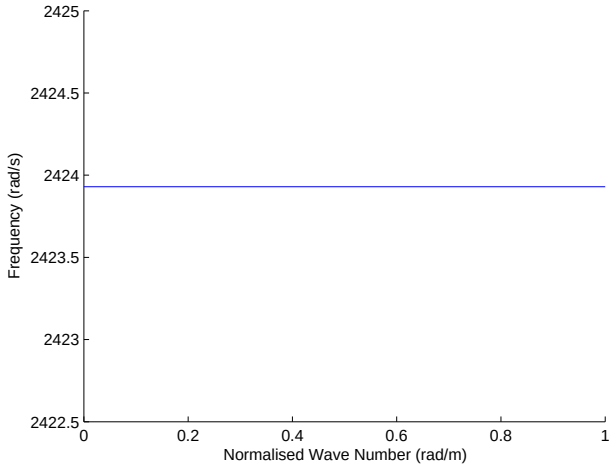

Figure 4.4: Illustration of the dispersion branch representing the natural frequency of the lattice structure.

Other information that can be obtained from the dispersion curves is the natural frequency of the lattice structure. The flat dispersion branch in the middle Figure 4.2 represents natural frequency, the frequency at which the lattice structure tends to vibrate. As illustrated in Figure 4.4, when no other dispersion branches are present except for the natural frequency, the natural frequency occurs at a frequency of 2424 rad/s, representing 11^{th} dispersion branch.

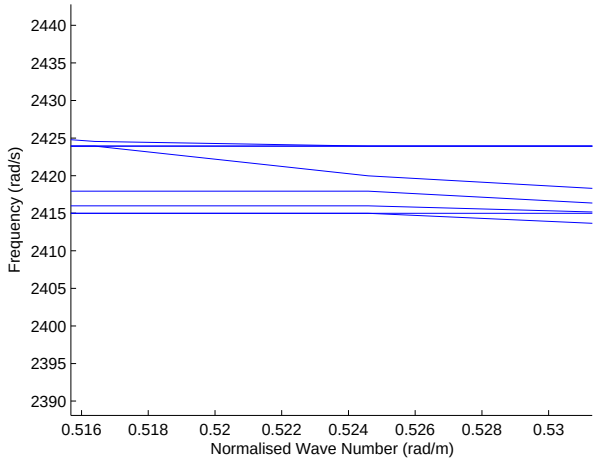

Figure 4.5: Illustration of multiple dispersion branches located close to each other.

While it was aforementioned that the dispersion curves illustrated in Figure 4.2 are plotted for 14 dispersion branches, the dispersion curves appear to only contain eight dispersion branches. The reason for this is that there are multiple dispersion branches that are tightly close to each other near the dispersion branch representing the natural frequency. Figure 4.5 provides magnified representation of the multiple dispersion branches that are located close to each other. These dispersion branches never

cross each other, and among the dispersion branches depicted in Figure 4.5, only one dispersion branch is flat, with a uniform eigenfrequency, representing the natural frequency.

4.3.3 Band Gap Phenomenon

In the dispersion curve, if there is a gap between the dispersion branches, the gap is referred as a band gap in solid-state physics, where no wave propagation occurs within the band gap region. In other words, phononic waves, which are of primary interest in this thesis, will not propagate in any direction at frequencies associated with band gaps. Figure 4.6 illustrates the band gap phenomenon and its location in dispersion curves. A band gap appears between the 13^{th} and 14^{th} dispersion branches at the frequency range of 2424-2957 rad/s, in which there are no waves propagating within this frequency range.

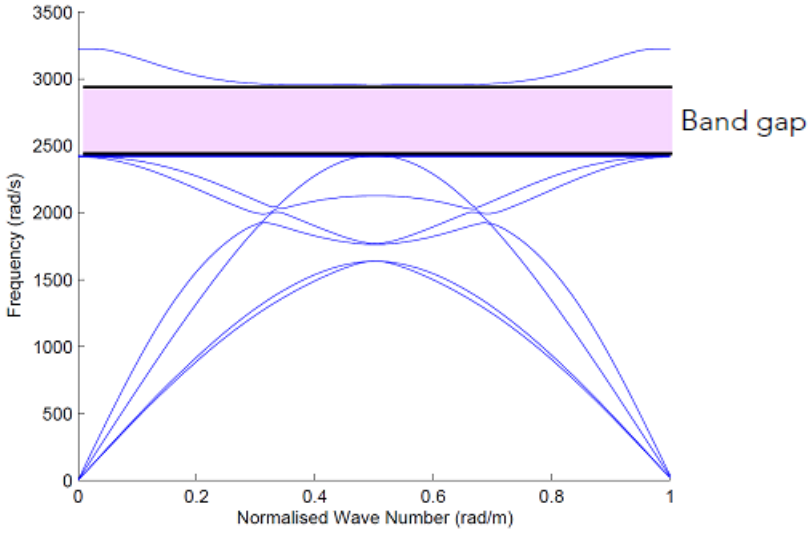

Figure 4.6: Illustration of the band gap in the dispersion curves of the tetrahedral lattice structure with the design variables in Table 4.2.

4.4 Validation Through Two-dimensional Triangular Lattices

The numerical model was verified through comparing the dispersion curves generated from the numerical model with the dispersion curves calculated by A. Phani et al. [23]. In their research, wave propagation through a 2D triangular lattice structure with a radius to length ratio of 0.1 was performed. As their report did not define specific values of the Young's modulus and the density of the struts, the numerical model in this thesis used arbitrary values of other design variables, but with matching the radius to length ratio. First, a triangular lattice structure with a radius to length ratio of 0.1 was compared, as shown in Figure 4.7.

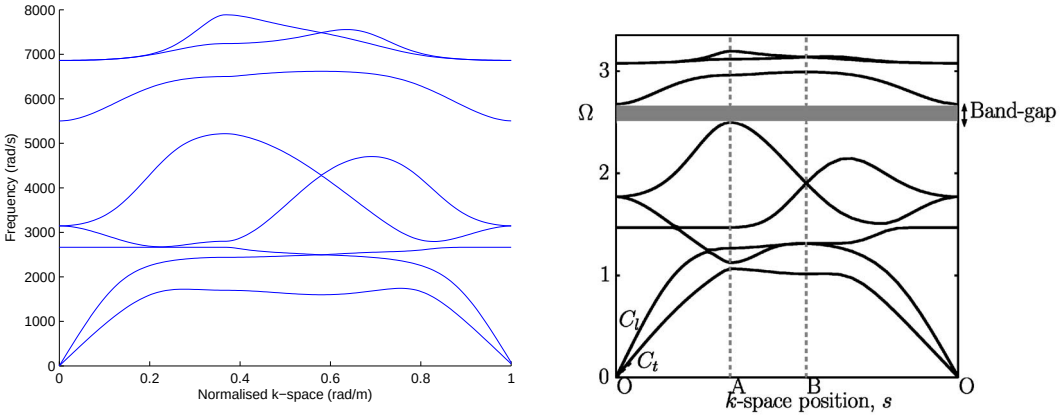

Figure 4.7: Comparison of the dispersion curves of a 2D triangular lattice with a radius to length ratio of 0.1 through finite element analysis (left) and the dispersion curves adopted from A. Phani et al. [23] (right).

The two dispersion curves show close resemblance of their band structures, with a band gap located in the high frequency range. The first band gap of the dispersion curves occurs between the 5^{th} and 6^{th} dispersion branches, while the second band gap of the dispersion curves occurs between the 6^{th} and 7^{th} dispersion branches for both plots.

Next, a triangular lattice structure with a radius to length ratio of 0.02 was then compared, as illustrated in Figure 4.8. The two plots show close resemblance of dispersion surfaces, with a band gap located in the low frequency range between the 3^{rd} and 4^{th} dispersion surfaces from the bottom.

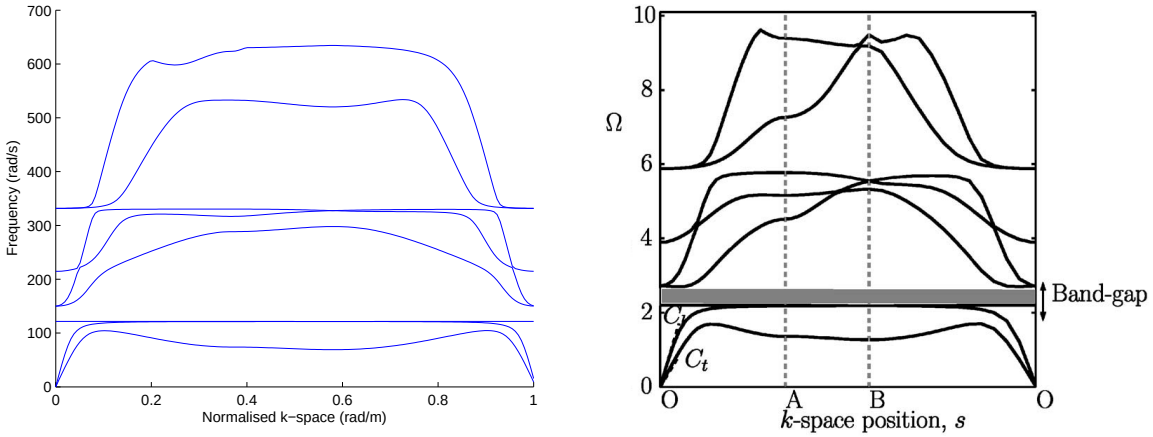

Figure 4.8: Comparison of the dispersion curves of a 2D triangular lattice with a radius to length ratio of 0.02 through finite element analysis (left) and the dispersion curves adopted from A. Phani et al. [23] (right).

4.5 Gaining a Physical Understanding of the Lattice Structure

It is of interest to understand what happens in the physical space in a physical lattice structure when a wave propagates along a strut of the lattice structure. For this purpose, wave vectors propagating along the direction of the direct basis vector e_1 of each tetrahedral and pyramidal lattice structure were used as inputs for the eigenvalue problem to solve it for the eigenvectors ϕ.

$$\tilde{K}\phi = \omega^2 \tilde{M}\phi \tag{4.2}$$

The eigenvector solution of the eigenvalue problem is in the form of a matrix, with the rows of the matrix representing nodal displacement of all the nodes existing in the lattice structure, and the columns of the matrix representing the nodal displacements of different mode shapes. The nodal displacements of the first mode are incorporated with the original location of the nodes of the lattice structures to demonstrate the first mode of the deformation of the tetrahedral and pyramidal lattice structures. The struts in light blue colour represent undeformed struts of the tetrahedral or pyramidal lattice structure, while the struts in orange colour represent the deformed struts of the lattice structures. While the deformation is demonstrated for the first mode, some struts have frequency of one, while some struts exhibit a frequency of two. This can be explained by intuitively performing nodal rotations for each node of the struts in each lattice structure. For this, first, pick a node at the end of one strut of an undeformed structure. By performing nodal rotation on the selected node, the struts sharing this node are expected to deform in one mode as the nodes at the other end of the strut are considered fixed. Afterwards, move on to the remaining nodes of the lattice structure and perform nodal rotation while trying to maintain the deformation of each strut having one mode only. By repeating this procedure, it is impossible to keep all the struts having only a single mode. Therefore, it is inevitable that there will be at least one strut with two modes.

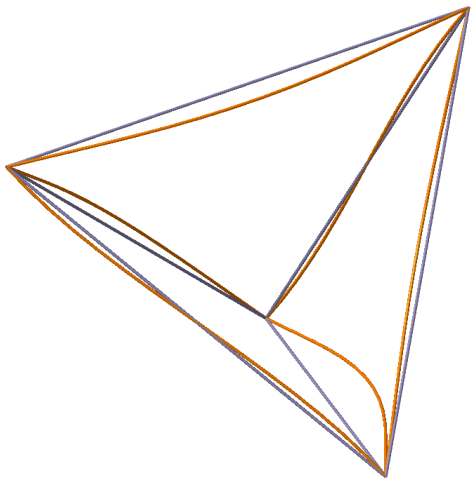

Figure 4.9: Illustration of the first mode deformation of a tetrahedral lattice structure for waves propagating along strut A (along the direct basis vector e_1).

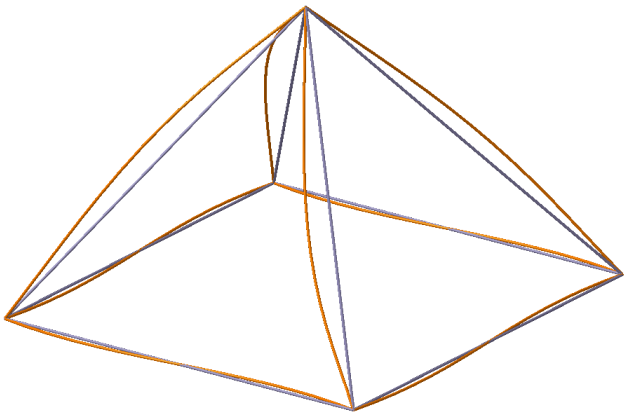

Figure 4.10: Illustration of the first mode deformation of a pyramidal lattice structure for waves propagating along strut A (along the direct basis vector e_1).

4.6 Wave Propagation Through a Tetrahedral Lattice Structure with a Radius to Length Ratio of 0.1

In this section, the wave propagation behaviour of a 3D tetrahedral lattice structure with a radius to length ratio of 0.1 is analyzed. First, the wave propagation behaviour through the symmetric lattice structure was examined, in which all the struts of the structure have equal design variables, such as radius and length of the lattice struts, thickness of the coating layers, and materials used for the struts and coating layers. Afterwards, wave propagation behaviour through the non-symmetric lattice structure was analyzed, in which one or more struts of the structure had modified design variables. The dispersion curves were plotted for the frequencies of wave propagation for the corresponding wave vectors propagating in the direction of the reciprocal basis vector e_1^* (wave vector with a varying k_1 component, while the k_2 and k_3 components are zero), and another dispersion curves were plotted for the waves propagating in the direction of the reciprocal basis vector e_2^* (wave vector with a varying k_2 component, while the k_1 and k_3 components are zero). Analysis of the non-symmetric lattice was performed to measure the symmetric and asymmetric dispersion relation behaviours in the non-symmetric lattice structures. Also, analysis of the different combinations of modified struts were performed to measure the changes in the resulting dispersion curves. Moreover, analysis of the non-symmetric lattice was performed whereby the total number of modified struts of the lattice structure were increased gradually, in order to identify the impact of such changes on the band structures of the dispersion curves. The frequencies of the resulting dispersion curves were normalized, to make the location and the changes in the band gaps easier to comprehend.

4.6.1 Initial Symmetric Lattice Structure

Dispersion curves of the initial symmetric tetrahedral lattice structure with a radius to length ratio of 0.1 are illustrated in Figure 4.11. All the struts of the unit cell share the same design variables defined previously in Table 4.2. Dispersion curves are plotted for waves propagating in two different directions. The dispersion curves for waves propagating along e_1^* are plotted with blue dotted lines, while the dispersion curves for waves propagating along e_2^* are plotted with red solid lines. The dispersion curves

are plotted for first 14 dispersion branches, in which the number of the displayed dispersion branches are predefined to present the band gap phenomena in the resulting dispersion curves.

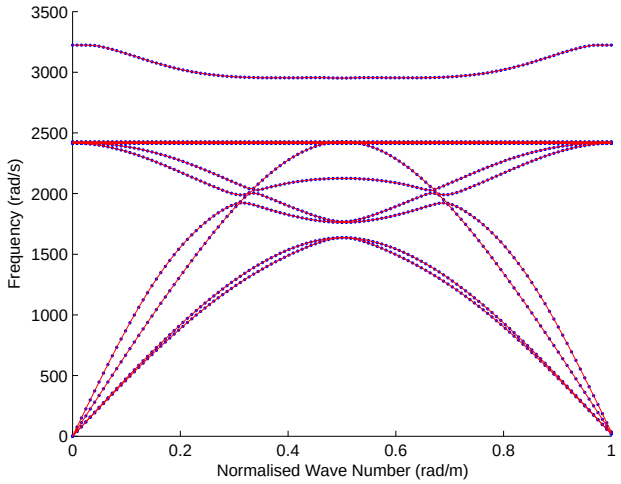

Figure 4.11: Dispersion curve of a symmetric tetrahedral lattice with a r:l ratio of 0.1 for waves propagating along e_1^* (blue dotted lines) and for waves propagating along e_2^* (red solid lines).

First, as the definition of the dispersion curves illustrates, the plot provides information on how waves propagate at different frequencies in different phase velocities and group velocities. The phase velocity of a point can be obtained by connecting a straight line between the origin and the point of interest, then find the slope of the straight line. On the other hand, the group velocity of the point can be obtained by forming a line tangent to the point on the curve, and then taking the slope of the tangent line. For example, for the first dispersion branch, phase velocities and group velocities of each waves were measured and are plotted below to demonstrate how waves propagate at different speeds as the wave numbers of wave vectors are gradually increased (or as the wave length of the wave vectors are gradually reduced).

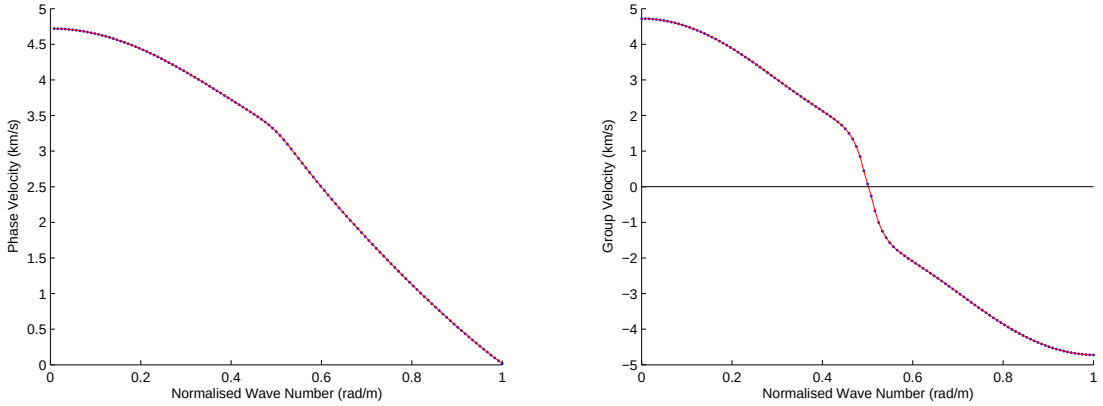

Figure 4.12: Phase velocity (left) and group velocity (right) of the first dispersion branch for waves propagating along e_1^* (blue dotted lines) and for waves propagating along e_2^* (red solid lines).

As the plots illustrate, with the increasing wave number of the wave vectors (i.e. decreasing wave length), the phase velocity of the corresponding wave numbers are gradually decreased from 4.721 km/s to 0.0184 km/s. On the other hand, the group velocity of the first dispersion branch gradually decreases from a positive 4.721 km/s, reaching zero velocity at a normalised wave number of 0.5. However, beyond this point, the group velocity goes into the negative region, while the magnitude of the velocity begins to increase. This change from a positive to a negative region implies a change in the direction of the group velocity relative to the phase velocity. When the group velocity is in a positive region, the group velocity is moving in the same direction as the phase velocity. However, when the group velocity is in a negative region, the group velocity is moving in the opposite direction to the phase velocity.

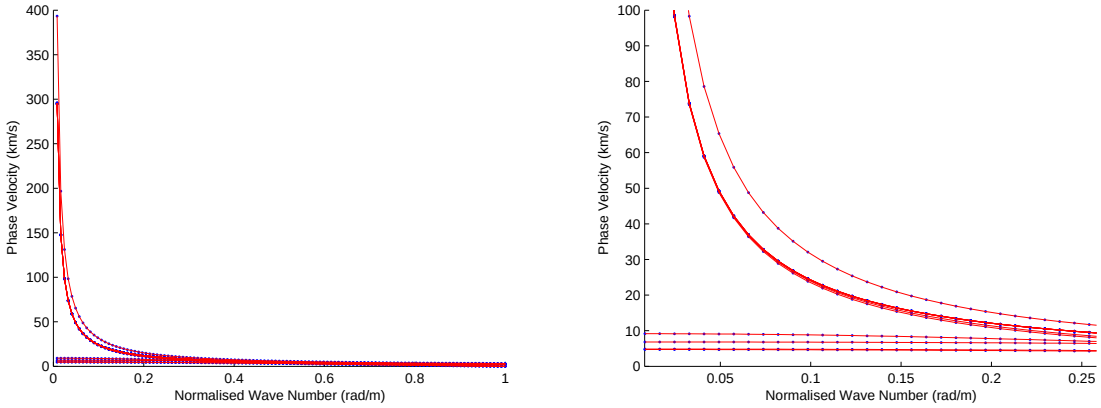

Figure 4.13: Phase velocity plot of the first 14 dispersion branches (left), and a close look of the plot at small wave numbers (right).

The phase velocities for all 14 dispersion branches are plotted in Figure 4.13. The left plot shows the change in phase velocity over all the ranges of wave numbers, while the right plot shows the change in phase velocity over the ranges of the normalised wave numbers from 0 to 0.25. Compared to the first four dispersion branches, in which the waves with small wave numbers propagate in the low frequency range, the remaining dispersion branches propagate at much higher frequencies for the same corresponding wave numbers. Therefore, the 5^{th} and higher dispersion branches show the phase velocities decaying exponentially as the wave numbers increase.

The second significant information that the dispersion curves provide is information on the band gap phenomenon and its location. A band gap appears between the 13^{th} and 14^{th} dispersion branches at the frequency range of 2424-2957 rad/s, in which contains no waves propagating within this frequency range. For the initial symmetric tetrahedral lattice structure, the dispersion relations of the waves propagating in the direction of the reciprocal basis vector e_1^* are equal to the dispersion relations of the waves propagating in the direction of the reciprocal basis vector e_2^*, thus demonstrating symmetric behaviours. Hence, the dispersion curves and the band gaps overlap with each other.

4.6.2 Impact of Changing the Design Variables E and ρ for All the Struts of the Lattice Structure

As was well described in Section 4.2, the lattice structure can have a different Young's modulus or density when the lattice structure is made of different materials or if the radius of the polymer substrate or the thickness of the coating layers are changed. In this section, analysis was performed in order to understand the impact on the resulting dispersion curves when the Young's modulus or the density is changed for all the struts of the lattice structure. The dispersion curves of the modified symmetric tetrahedral lattice structure with the Young's modulus multiplied by 10 for all the struts are illustrated in Figure 4.14, using the method described in section 4.2. The dispersion curves for waves propagating along e_1^* were plotted with blue dotted lines, while the dispersion curves for waves propagating along e_2^* were plotted with red solid lines. The dispersion curves were plotted for the first 14 dispersion branches.

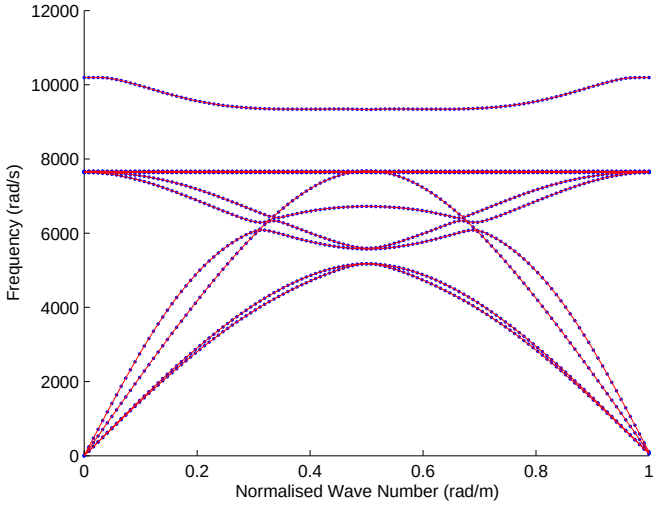

Figure 4.14: Dispersion curve of a symmetric tetrahedral lattice with a r:l ratio of 0.1 for waves propagating along e_1^* (blue dotted lines) and for waves propagating along e_2^* (red solid lines), which all the struts are modified to have their Young's modulus multiplied by 10.

As the figure illustrates, the dispersion relations of the waves propagating in the direction of the reciprocal basis vector e_1^* is equal to the dispersion relations of the waves propagating in the direction of the reciprocal basis vector e_2^*, thus demonstrating symmetric behaviours. Compared to the dispersion curves of the initial symmetric tetrahedral lattice structure illustrated in Figure 4.11, the dispersion curves of the modified symmetric lattice structure in Figure 4.14 show an exactly equal band structure, but the waves propagate at much higher frequency ranges. For example, just as the band gap is located in the initial symmetric lattice structure, the band gap for the modified symmetric lattice structure appears between the 13^{th} and 14^{th} dispersion branches, but at the frequency range between 7665 and 9350 rad/s, whereby the frequency range is much higher compared to the location of the band gap of the initial symmetric lattice structure between 2424 and 2957 rad/s. This can be explained by revisiting the

expression for the mass matrix and stiffness matrix derived in the previous chapter.

$$m_{ij} = \int_0^L [A\rho(a_i a_j + b_i b_j + c_i c_j) + I_y \rho e_i e_j + I_z \rho f_i f_j + (I_y + I_z)\rho d_i d_j]\, dx \tag{4.3}$$

$$\begin{aligned} k_{ij} = \int_0^L [&\lambda(A a_i' a_j' + I_y e_i' e_j' + I_z f_i' f_j') + 2G(A a_i' a_j' + I_y e_i' e_j' + I_z f_i' f_j') \\ &+ \kappa G A((b_i' - f_i)(b_j' - f_j) + (c_i' + e_i)(c_j' + e_j)) + \kappa G(I_z + I_y)(d_i' d_j')]dx \end{aligned} \tag{4.4}$$

where m_{ij} is the mass matrix of an individual strut in a global coordinate system and k_{ij} is the stiffness matrix of an individual strut in a global coordinate system. If the radius and length of the struts remain constant, the density ρ becomes the only variable in the equation of the mass matrix. Therefore, when the radius and length of the strut are fixed, the mass matrix of a strut can be re-expressed as

$$m_{ij} = \rho \int_0^L [A(a_i a_j + b_i b_j + c_i c_j) + I_y e_i e_j + I_z f_i f_j + (I_y + I_z) d_i d_j]\, dx = \rho m_{ij}' \tag{4.5}$$

where

$$m_{ij}' = \int_0^L [A(a_i a_j + b_i b_j + c_i c_j) + I_y e_i e_j + I_z f_i f_j + (I_y + I_z) d_i d_j]\, dx \tag{4.6}$$

In the stiffness matrix equation, the design variables λ, G, and E are involved. However, as the shear modulus and Young's modulus are related,

$$G = \frac{E}{2(1+\nu)} \tag{4.7}$$

and since Lamé's first parameter is related with the shear modulus and Young's modulus:

$$\lambda = \frac{G(E - 2G)}{3G - E)} \tag{4.8}$$

where λ and G can be expressed in terms of E, and the stiffness matrix equation can be re-expressed as follows:

$$\begin{aligned} k_{ij} = E \int_0^L [&(A a_i' a_j' + I_y e_i' e_j' + I_z f_i' f_j') + (A a_i' a_j' + I_y e_i' e_j' + I_z f_i' f_j') \\ &+ ((b_i' - f_i)(b_j' - f_j) + (c_i' + e_i)(c_j' + e_j)) + (I_z + I_y)(d_i' d_j')]dx \\ &= E k_{ij}' \end{aligned} \tag{4.9}$$

The collection of mass and stiffness matrices of the individual struts (A, B, C, D, E, F) to form the mass and stiffness matrices of the entire structure in the global coordinate system (M_{struc}, K_{struc}) can be

expressed as

$$M_{struc} = (m_A + m_B + m_C + m_D + m_E + m_F) = \rho m'_A + \rho m'_B + \rho m'_C + \rho m'_D + \rho m'_E + \rho m'_F \quad (4.10)$$

$$K_{struc} = (k_A + k_B + k_C + k_D + k_E + k_F) = Ek'_A + Ek'_B + Ek'_C + Ek'_D + Ek'_E + Ek'_F \quad (4.11)$$

For a symmetric lattice structure, an equal value of the Young's modulus or the density is applied for each individual strut. Since the remaining terms of the mass matrix and stiffness matrix equations remain constant for all the struts, and are independent from the change in ρ and E, the global mass and stiffness matrices of the entire structure can be expressed as

$$M_{struc} = \rho M'_{struc} \quad (4.12)$$

where,

$$M'_{struc} = m'_A + m'_B + m'_C + m'_D + m'_E + m'_F \quad (4.13)$$

and

$$K_{struc} = EK'_{struc} \quad (4.14)$$

where,

$$K'_{struc} = k'_A + k'_B + k'_C + k'_D + k'_E + k'_F \quad (4.15)$$

This relationship can be extended to the reduced global mass and stiffness matrices.

$$\tilde{M}_{struc} = \rho \tilde{M'}_{struc} \quad (4.16)$$

$$\tilde{K}_{struc} = E\tilde{K'}_{struc} \quad (4.17)$$

Applying the above relations, the eigenvalue problem for the initial symmetric lattice structure can be expressed as

$$E_1 \tilde{K'}_1 \phi = \omega_1^2 \rho_1 \tilde{M'}_1 \phi \quad (4.18)$$

while, the eigenvalue problem for the modified symmetric lattice structure can be expressed as

$$E_2 \tilde{K'}_2 \phi = \omega_2^2 \rho_2 \tilde{M'}_2 \phi \quad (4.19)$$

Knowing that the mass and stiffness matrices, $\tilde{K'}$ and $\tilde{M'}$, for both the initial symmetric lattice structure and the modified symmetric lattice structure are equal only when the Young's modulus or the density is changed for all the struts,

$$\tilde{K'}_1 = \tilde{K'}_2 = \tilde{K'} \quad (4.20)$$

$$\tilde{M'}_1 = \tilde{M'}_2 = \tilde{M'} \quad (4.21)$$

then, the relationship between the two eigenvalue problems can be equated as follows:

$$E_1 \tilde{K'} \phi = \omega_1^2 \rho_1 \tilde{M'} \phi \quad (4.22)$$

$$E_2 \tilde{K'} \phi = \omega_2^2 \rho_2 \tilde{M'} \phi \quad (4.23)$$

Hence, the relationship between the initial and the modified symmetric lattice structures, when the Young's modulus and/or the density of all the struts are modified, can be expressed by a scalar factor of the ratio between the Young's modulus and the density.

$$\sqrt{\frac{E}{\rho}} \tag{4.24}$$

This relationship can be verified through comparison of the locations of the band gaps between the initial and modified symmetric lattice structures in the above example, in which the Young's modulus of the modified symmetric lattice structure is multiplied by a factor of 10 while the density is unchanged.

$$\rho_2 = \rho_1 \tag{4.25}$$

$$E_2 = 10E_1 \tag{4.26}$$

It is expected that the dispersion curve of the modified symmetric lattice structure will be scaled by a factor of $\sqrt{10}$, at which eigenfrequencies of all wave numbers of the dispersion curves are multiplied by the same factor of $\sqrt{10}$, compared to the dispersion curve of the initial symmetric lattice structure. When the initial lattice structure has a band gap in the frequency range of 2424-2957 rad/s, the frequency range at which the band gap of the modified symmetric lattice will appear can be calculated by multiplying by this factor at each the lower bound and upper bound of the frequency range at which the band gap appeared in the initial lattice structure.

$$\begin{aligned} \text{Lower bound in second dispersion curve} &= 2424 \times \sqrt{\frac{10}{1}} = 7665 \\ \text{Upper bound in second dispersion curve} &= 2957 \times \sqrt{\frac{10}{1}} = 9350 \end{aligned} \tag{4.27}$$

Through the above relation, the frequency range at which the band gap will appear for the modified symmetric lattice structure is expected to be at 7665-9350 rad/s, which matches with the result from the finite element analysis. Therefore, in symmetric lattice structures, changing the value of the Young's modulus and/or the density simply scales the dispersion curve by factor of $\sqrt{\frac{E}{\rho}}$, This relation can be applied to any 2D lattice structure as well as to any 3D lattice structure with any design variables as long as the lattice structures are symmetric and only the Young's modulus and the density are changed.

The above relation plays an important role when tailoring the band gap location of the dispersion curves. Based on the expression, increasing the Young's modulus or reducing the density using the method described in Section 4.2 provides dispersion curves with the same band structure, but with waves propagating at a higher frequency range, which the frequency ranges and the band gap location is multiplied by a factor of $\sqrt{\frac{E}{\rho}}$. On the other hand, reducing Young's modulus or increasing the density provides dispersion curves with the same band structure, but with waves propagating at reduced frequency ranges. Therefore, when a band gap is present in the dispersion curves of the lattice structure, but is desired to be placed at a different frequency range, Young's modulus can be changed by maintaining the radius of the polymer substrate and the overall strut radius, while only modifying the ratio of the thickness of the two coating layers to achieve such a requirement. However, while this relation may seem strong and an easy method to tailor the band gap location, it holds one factor that may be

considered a weakness. As this relation simply scales the entire dispersion curve by the factor derived above, it also scales the frequency range at which the band gap occurs. Therefore, not only does this relation shift the location of the band gap, but it also increases or decreases the size of the band gap, which may be an unintentional consequence.

4.6.3 Impact of Changing the Design Variables E and ρ for a Non-Symmetric Lattice Structure

Strut A Modified

Next, the wave propagation behaviour in non-symmetric lattice structures was studied to analyze the differences in dispersion relations compared to in the symmetric lattice structures. The non-symmetric lattice structures were created by modifying the design variables of one or more, but not all the struts of the unit lattice cell. First, strut A, which was oriented along the direct basis vector e_1, was modified to have its Young's modulus multiplied by 10, while the other five struts remained unchanged. As Figure 4.15 illustrates, the dispersion curves of the wave propagating along e_1^* (blue dotted lines in the left plot) and the dispersion curves of the wave propagating along e_2^* (red dotted lines in the right plot) were plotted and compared with the dispersion curves of the initial symmetric lattice structure (black solid lines in both plots).

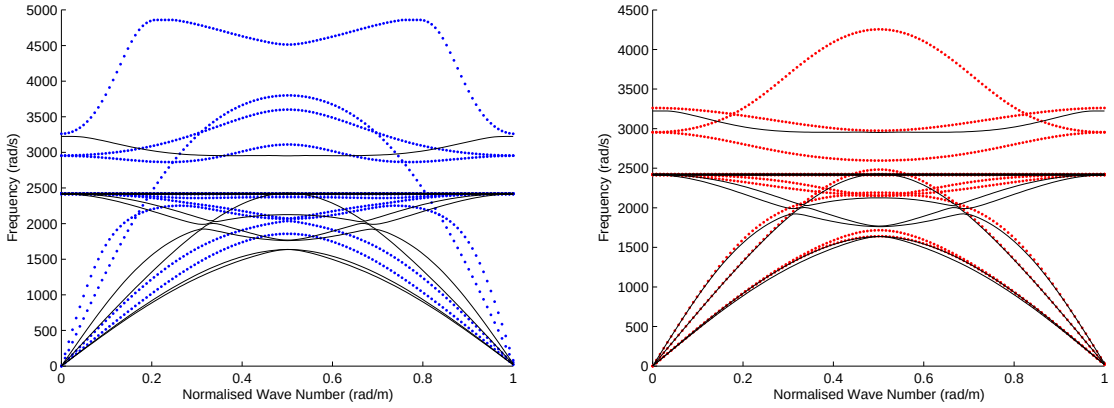

Figure 4.15: Dispersion curves of the non-symmetric tetrahedral lattice structure for waves propagating along e_1^* (blue dotted lines in the left plot) and for waves propagating along e_2^* (red dotted lines in the right plot), with strut A modified to have increased Young's modulus by 10 times, compared with the dispersion curves of the initial symmetric lattice structure shown in Figure 4.11 (black solid lines in both plots)

The dispersion curves for waves propagating along e_1^* were plotted with blue dotted lines, and the dispersion curves for waves propagating along e_2^* were plotted in red dotted lines, while the dispersion curves of the initial symmetric lattice analyzed in Figure 4.11 were plotted with black solid lines. The dispersion curves are plotted for the first 14 dispersion branches. Starting with the dispersion curves of the waves propagating along e_1^*, it can be seen that as one of the struts was modified to have a higher stiffness, the waves propagate at much higher frequency ranges. In the initial symmetric lattice structure, the first 14 dispersion branches show waves propagating within the frequency ranges of 39.74-3224 rad/s. How-

ever, for the non-symmetric lattice structure, the first 14 dispersion branches show waves propagating up to the frequency range of 4858 rad/s. Also, waves of each individual dispersion branch of the non-symmetric lattice structure propagate at a higher frequency range compared to the corresponding waves of each of the dispersion branches of the initial symmetric lattice structure, implying the waves of the non-symmetric lattice structures propagate at a higher phase velocity than the waves of the initial symmetric lattice structures. The dispersion curves of the waves propagating along e_2^* of the non-symmetric lattice show a similar phenomenon. As the first 14 dispersion branches show waves propagating up to the frequency range of 4255 rad/s, the waves propagate at much higher frequency than the waves propagating through the initial symmetric lattice structure. Also, for each dispersion branch, waves in non-symmetric lattice structure propagate at a higher frequency than the waves in the corresponding dispersion branches in symmetric lattice structure, showing that the waves in the non-symmetric lattice structure propagate with a higher phase velocity than the waves in the symmetric lattice structure. In terms of the band gap phenomenon, there is no complete band gap for waves propagating along e_1^*, but there exists one band gap for waves propagating along e_2^* in the frequency range of 2483-2597 rad/s.

The first significant difference between the dispersion relations of the waves propagating in the above non-symmetric lattice structure and the initial symmetric lattice structure comes from the difference in the band structure. In the previous section, when the initial symmetric lattice structure was modified so that all the struts of the lattice structures would have an increased Young's modulus, it was observed that the band structures remained the same and the dispersion curves were simply scaled by a certain factor. However, when only one strut was modified to have an increased Young's modulus, the scalar relation did not apply, thereby leading to different band structures in the dispersion curves. This can be explained by re-visiting the energy equations involving the mass and stiffness matrices. While a symmetric lattice structure defines that the change in design variables are applied to all the struts in the lattice structure, a non-symmetric lattice structure implies that only one or a few struts (but not all) of the lattice structure have their design variables changed. Thus at first, when Young's modulus or the density is changed in a symmetric lattice structure, a change in the design variable is also applied to every strut of the lattice structure.

$$M_1 = (m_{1A} + m_{1B} + m_{1C} + m_{1D} + m_{1E} + m_{1F}) = \rho m'_{1A} + \rho m'_{1B} + \rho m'_{1C} + \rho m'_{1D} + \rho m'_{1E} + \rho m'_{1F} \quad (4.28)$$

$$K_1 = (k_{1A} + k_{1B} + k_{1C} + k_{1D} + k_{1E} + k_{1F}) = Ek'_{1A} + Ek'_{1B} + Ek'_{1C} + Ek'_{1D} + Ek'_{1E} + Ek'_{1F} \quad (4.29)$$

As the terms involving the shape functions, m' and k', remain constant for all the struts, and as the terms are independent from the change in ρ, the global mass matrix of the symmetric structure can be expressed as

$$M_1 = \rho M'_1 \quad (4.30)$$

$$K_1 = EK'_1 \quad (4.31)$$

where,

$$M'_1 = m'_{1A} + m'_{1B} + m'_{1C} + m'_{1D} + m'_{1E} + m'_{1F} \quad (4.32)$$

$$K'_1 = k'_{1A} + k'_{1B} + k'_{1C} + k'_{1D} + k'_{1E} + k'_{1F} \quad (4.33)$$

However, when a change in the Young's modulus or the density is only applied to a single strut, strut A, this turns the lattice into a non-symmetric lattice structure,

$$M_2 = (m_{2A}+m_{2B}+m_{2C}+m_{2D}+m_{2E}+m_{2F}) = 10\rho m'_{2A}+\rho m'_{2B}+\rho m'_{2C}+\rho m'_{2D}+\rho m'_{2E}+\rho m'_{2F} \quad (4.34)$$

$$K_2 = (k_{2A}+k_{2B}+k_{2C}+k_{2D}+k_{2E}+k_{2F}) = 10Ek'_{2A}+Ek'_{2B}+Ek'_{2C}+Ek'_{2D}+Ek'_{2E}+Ek'_{2F} \quad (4.35)$$

reducing the equation, it becomes

$$M_2 = \rho M'_2 = \rho(10m'_{2A}+m'_{2B}+m'_{2C}+m'_{2D}+m'_{2E}+m'_{2F}) \quad (4.36)$$

$$K_2 = EK'_2 = E(10k'_{2A}+k'_{2B}+k'_{2C}+k'_{2D}+k'_{2E}+k'_{2F}) \quad (4.37)$$

where,

$$M'_2 = (10m'_{2A}+m'_{2B}+m'_{2C}+m'_{2D}+m'_{2E}+m'_{2F}) \quad (4.38)$$

$$K'_2 = (10k'_{2A}+k'_{2B}+k'_{2C}+k'_{2D}+k'_{2E}+k'_{2F}) \quad (4.39)$$

Hence, M'_1 and K'_1 are not equal to M'_2 and K'_2, and these mass and stiffness matrices of the two different lattice structures cannot be expressed by a scalar (multiplicative by the factor of ratio of $\sqrt{\frac{E}{\rho}}$) relationship anymore. Therefore, when applying different values of design variables, such as Young's modulus or density on the non-symmetric lattice structure, a different band structure is expected in the resulting dispersion curves compared to the band structure of the symmetric lattice structure.

The second significant observation is the difference in the dispersion relations between waves propagating in different directions. As Figure 4.16 illustrates, the dispersion curves of waves propagating along e_1^* and the dispersion curves of waves propagating along e_2^* are different, and show asymmetric dispersion relations. The dispersion curves for waves propagating along e_1^* were plotted with blue dotted lines, and the dispersion curves for waves propagating along e_2^* were plotted with red solid lines.

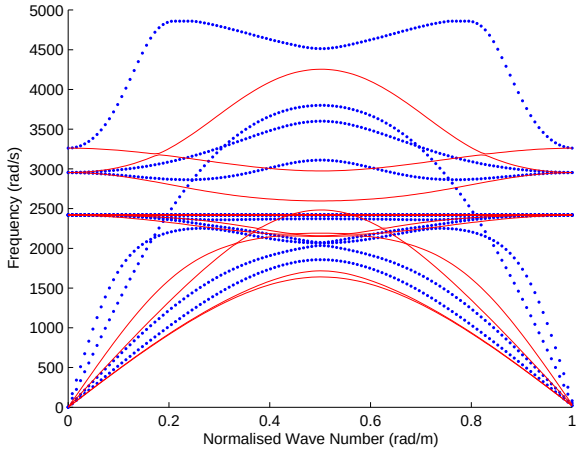

Figure 4.16: Collapsed dispersion curves of a non-symmetric tetrahedral lattice structure for waves propagating along e_1^* (blue dotted lines) and for waves propagating along e_2^* (red solid lines), with strut A modified to have increased Young's modulus by 10 times.

As described in the previous chapter, Bloch theorem can be applied to describe displacements of all the nodes of the unit lattice cell, to be expressed by the displacements of the internal and the basis nodes. To achieve this, a transformation matrix was created. The transformation matrix is in the form of

$$T = \begin{bmatrix} I \\ \tau \end{bmatrix} \tag{4.40}$$

The top part of the transformation matrix is related to the internal and the basis nodes, and is simply an n×n identity matrix, where n is the total number of internal and basis nodes. On the other hand, the bottom part of the transformation matrix (τ) is related to the boundary nodes, which is in the following form:

$$\tau = \begin{bmatrix}
0 & 0 & 0 & \cdots & 0 & 0 & 0 & e^{k_1} & 0 & 0 & 0 & 0 & 0 \\
0 & 0 & 0 & \cdots & 0 & 0 & 0 & 0 & e^{k_1} & 0 & 0 & 0 & 0 \\
0 & 0 & 0 & \cdots & 0 & 0 & 0 & 0 & 0 & e^{k_1} & 0 & 0 & 0 \\
0 & 0 & 0 & \cdots & 0 & 0 & 0 & 0 & 0 & 0 & e^{k_1} & 0 & 0 \\
0 & 0 & 0 & \cdots & 0 & 0 & 0 & 0 & 0 & 0 & 0 & e^{k_1} & 0 \\
0 & 0 & 0 & \cdots & 0 & 0 & 0 & 0 & 0 & 0 & 0 & 0 & e^{k_1} \\
0 & 0 & 0 & \cdots & 0 & 0 & 0 & e^{k_2} & 0 & 0 & 0 & 0 & 0 \\
0 & 0 & 0 & \cdots & 0 & 0 & 0 & 0 & e^{k_2} & 0 & 0 & 0 & 0 \\
0 & 0 & 0 & \cdots & 0 & 0 & 0 & 0 & 0 & e^{k_2} & 0 & 0 & 0 \\
0 & 0 & 0 & \cdots & 0 & 0 & 0 & 0 & 0 & 0 & e^{k_2} & 0 & 0 \\
0 & 0 & 0 & \cdots & 0 & 0 & 0 & 0 & 0 & 0 & 0 & e^{k_2} & 0 \\
0 & 0 & 0 & \cdots & 0 & 0 & 0 & 0 & 0 & 0 & 0 & 0 & e^{k_2} \\
0 & 0 & 0 & \cdots & 0 & 0 & 0 & e^{k_3} & 0 & 0 & 0 & 0 & 0 \\
0 & 0 & 0 & \cdots & 0 & 0 & 0 & 0 & e^{k_3} & 0 & 0 & 0 & 0 \\
0 & 0 & 0 & \cdots & 0 & 0 & 0 & 0 & 0 & e^{k_3} & 0 & 0 & 0 \\
0 & 0 & 0 & \cdots & 0 & 0 & 0 & 0 & 0 & 0 & e^{k_3} & 0 & 0 \\
0 & 0 & 0 & \cdots & 0 & 0 & 0 & 0 & 0 & 0 & 0 & e^{k_3} & 0 \\
0 & 0 & 0 & \cdots & 0 & 0 & 0 & 0 & 0 & 0 & 0 & 0 & e^{k_3}
\end{bmatrix} \tag{4.41}$$

From the above matrix, k_1, k_2, and k_3 are three components (wave numbers) of a wave vector. For waves propagating along e_1^*, k_1 varies, while k_2 and k_3 are fixed as zero; whereas, for waves propagating along e_2^*, k_2 varies, while k_1 and k_3 are fixed as zero. Therefore, the transformation matrix for waves propagating in the e_1^* direction and e_2^* direction are different. Then the transformation matrices are multiplied to the global mass and stiffness matrices to create reduced global mass and stiffness matrices, where T^H is the conjugate transpose of the transformation matrix,

$$T^H M T = \tilde{M} \tag{4.42}$$

$$T^H K T = \tilde{K} \tag{4.43}$$

since the transformation matrices for waves propagating along e_1^* are different to those from e_2^*, there exists two different sets of reduced mass and stiffness matrices. However, as illustrated in Figures 4.11 and 4.14, when the eigenvalue problems are solved for the symmetric lattice structures with the different sets of reduced mass and stiffness matrices, symmetric eigen solutions can be obtained for waves propagating in the e_1^* and e_2^* directions. On the other hand, as illustrated in Figure 4.16, when the eigenvalue

problems are solved for a non-symmetric lattice structure with strut A modified to have higher stiffness, asymmetric solutions are obtained for waves propagating in the e_1^* and e_2^* directions. This difference in symmetric/asymmetric dispersion curves is related to the geometrical symmetry of the lattice structure and how the modification of the design variables impacts on the symmetry with respect to each direction of wave propagation. First, recall the orientation of the tetrahedral unit lattice cell in Cartesian coordinates illustrated in Figure 4.17 (left); with a certain rotation of the unit cell, as illustrated in Figure 4.17 (right), the tetrahedral unit cell can be viewed as symmetric with respect to the plane created by the y-axis and direct basis vector e_3 (the red line in Figure 4.15 b), in which the right region involving e_1^* is symmetric to the left region involving e_2^*.

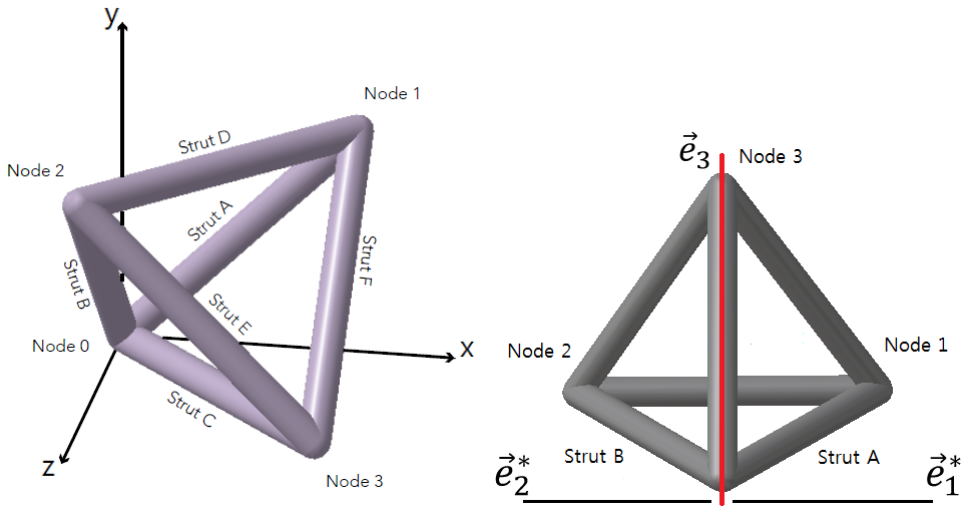

Figure 4.17: Illustration of the symmetric view on a tetrahedral unit cell with respect to e_1^* and e_2^*.

Next, consider two waves, with one wave propagating along e_1^*, and another wave propagating along e_2^*. For symmetric lattice structures, in which all the struts of the lattice structure are modified equally and are geometrically symmetric, the dispersion relation of the wave propagating along e_1^* is symmetric to the dispersion relation of the wave propagating along e_2^*. On the other hand, for a non-symmetric lattice structure, in which only strut A is modified, due to the modification on one strut, the lattice unit cell is no longer geometrically symmetric with respect to each direction of wave propagation. Therefore, the dispersion relation of the wave propagating along e_1^* is asymmetric to the dispersion relation of the wave propagating along e_2^*, also with different dispersion curves and band structures. As emphasized at the beginning of this chapter, it is important to make clear understanding of the differences between symmetric/non-symmetric lattice structures and symmetric/asymmetric dispersion relations. A symmetric lattice structure refers to a structure, in which all the struts have equal design variables, while a non-symmetric lattice structure refers to a structure, in which one or more but not all of struts are modified to have different design variables. On the other hand, the dispersion relation is symmetric when the resulting dispersion curves of the wave propagating in one direction are identical to the dispersion curves of a wave propagating in a different direction, and the dispersion relation is asymmetric when the resulting dispersion curves of a wave propagating in one direction is different from the dispersion curves of a wave propagating in a different direction. To carry out deeper analysis and better characterization of the asymmetric dispersion relations of non-symmetric lattice structures, three cases are considered

here: a) a non-symmetric lattice structure, where modifications applied with respect to the e_1^* direction, are applied on the struts located geometrically symmetric with respect to the e_2^* direction instead; b) a non-symmetric lattice structure where modifications to the lattice structure are applied on struts located geometrically symmetric with respect to both directions of the wave propagation; c) a non-symmetric lattice structure where modifications of the design variables are concentrated on one side of the lattice structure, and the location of the modifications applied are geometrically non-symmetric with respect to each direction of the wave propagation.

Non-Symmetric Lattice Structure, Where the Modifications Applied with respect to the e_1^* Direction, is Applied Equally with respect to the e_2^* Direction Instead

The first case involved observation of the impact of modifying different struts, where the previous modification was applied with respect to the e_1^* direction of the wave propagation, but is now applied at the strut placed at the geometrically symmetric location with respect to the e_2^* direction of the wave propagation. In other words, in the previous case, strut A was modified and the waves were propagating along e_1^* and e_2^*. In the current section, the focus was made to analyze and compare the dispersion curve when strut B was modified instead, and to measure the dispersion relations of the waves propagating along e_1^* and e_2^* directions, as illustrated in Figure 4.18.

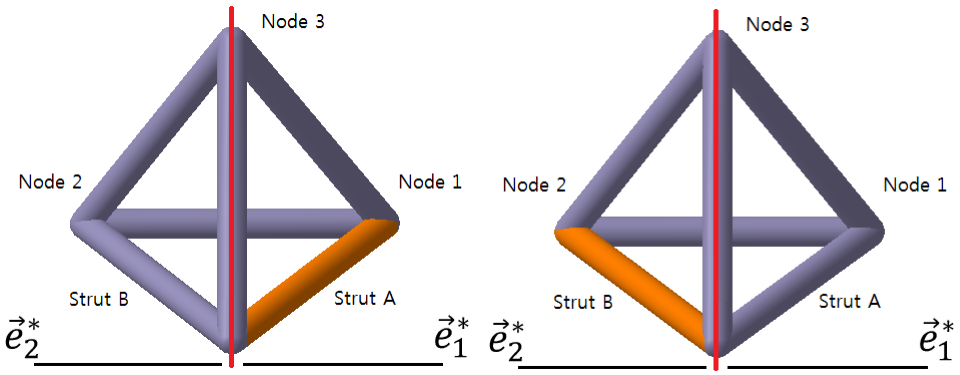

Figure 4.18: Illustration of strut A of tetrahedral unit cell modified (left) and strut B of tetrahedral unit cell modified (right). The modified strut is in orange colour.

The dispersion curves of the non-symmetric lattice structure, in which strut B was modified are plotted in Figure 4.19 below. As discussed in the previous section, since the modification applied to the lattice structure is geometrically non-symmetric with respect to each direction of the wave propagation, the dispersion relations between the waves propagating along e_1^* and e_2^* are asymmetric. The dispersion curves for waves propagating along e_1^* was plotted with blue dotted lines, while the dispersion curves for waves propagating along e_2^* was plotted with red solid lines.

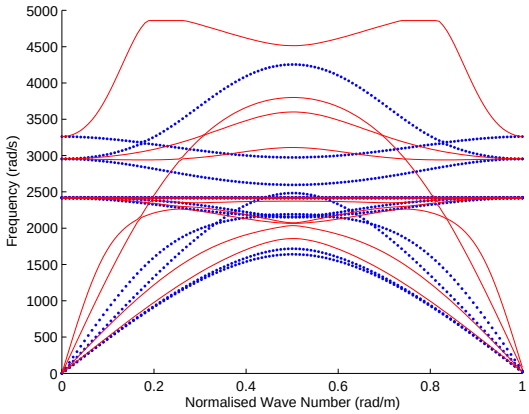

Figure 4.19: Collapsed dispersion curves of a non-symmetric tetrahedral lattice structure for waves propagating along e_1^* (blue dotted lines) and for waves propagating along e_2^* (red solid lines), with strut A modified to have increased Young's modulus by 10 times.

When the above dispersion curves are compared with the dispersion curves of waves propagating through the non-symmetric lattice structure when strut A is modified, as illustrated in Figure 4.16, it can be seen that the band structures of the dispersion curves are identical. However, as Figure 4.20 illustrates, the dispersion curves of waves propagating along e_2^* of the non-symmetric lattice structure with strut B modified, are symmetric with the dispersion curves of the waves propagating along e_1^* of the non-symmetric lattice structure with strut A modified. Likewise, the dispersion curves of waves propagating along e_1^* of the non-symmetric lattice structure with strut B modified, are symmetric with the dispersion curves of the waves propagating along e_2^* of the non-symmetric lattice structure with strut A modified. The dispersion curves from Figure 4.16 are plotted with blue dotted lines, and the current dispersion curves are plotted with red solid lines.

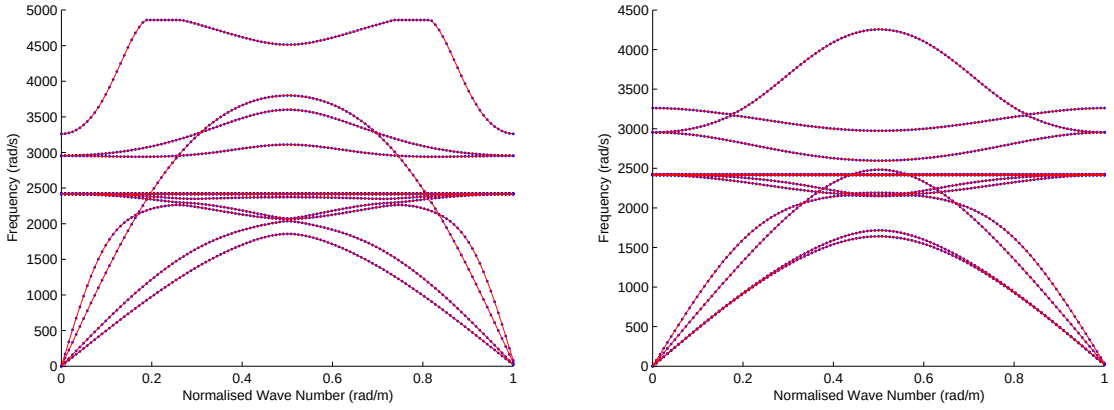

Figure 4.20: Comparisons of the dispersion curves for waves propagating along e_1^* when strut A is modified (blue dotted lines on the left) and for waves propagating along e_2^* when strut B is modified (red solid lines on the left) and the dispersion curves for waves propagating along e_2^* when strut A is modified (blue dotted lines on the right) and for waves propagating along e_1^* when strut B is modified (red solid lines on the right).

Therefore, when a new modification is applied at the geometrically symmetrical location compared to the location of the previous modification with respect to each direction of wave propagation, the previous dispersion curves for waves propagating along e_1^* are symmetric to the new dispersion curves for waves propagating along e_2^*. Similarly, the previous dispersion curves for waves propagating along e_2^* are symmetric to the new dispersion curves for waves propagating along e_1^*. This relation is applied to a non-symmetric lattice structure when different modifications are applied. For instance, dispersion curves of waves propagating along e_1^* of the lattice structure with strut F modified are equivalent to dispersion curves of the waves propagating along e_2^* of the lattice structure with strut E modified. Hence, this relation allows swapping of the dispersion curves between waves propagating in different directions.

Non-Symmetric Lattice Structure, where Modifications on the Lattice Structure are Geometrically Symmetric with respect to Both Directions of Wave Propagation

The second case involved analyzing the impact of applying modifications on struts in which the changes were geometrically symmetric with respect to both waves propagating along the e_1^* and e_2^* directions equally at the same time. Hence, this section focuses on the analysis and comparisons of the dispersion curve when both strut A and strut B are modified to have an increased value of Young's modulus, as illustrated in Figure 4.21.

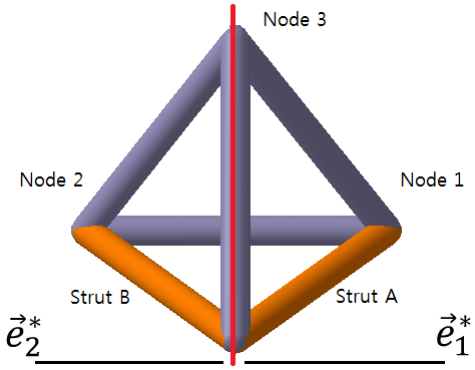

Figure 4.21: Illustration of strut A and strut B of tetrahedral unit cell modified. Modified struts are in orange color.

The dispersion curves of the non-symmetric lattice structure in which struts A and B are both modified, are plotted in Figure 4.22 below. The dispersion curves for waves propagating along e_1^* were plotted with blue dotted lines, while the dispersion curves for waves propagating along e_2^* were plotted with red solid lines. The dispersion curves are plotted for the first 14 dispersion branches.

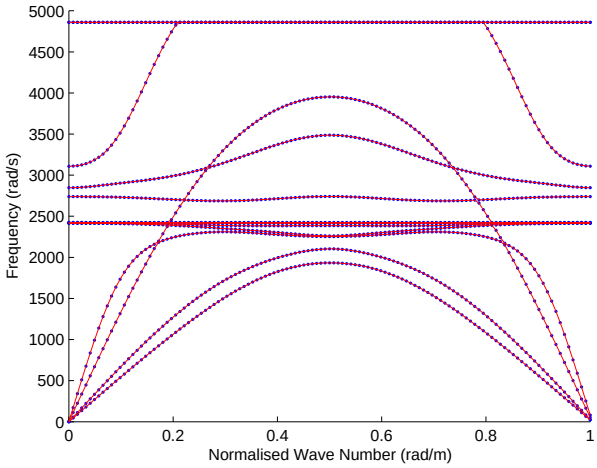

Figure 4.22: Collapsed dispersion curves of a non-symmetric tetrahedral lattice structure for waves propagating along e_1^* (blue dotted lines) and for waves propagating along e_2^* (red solid lines), with struts A and B modified to have increased Young's modulus by 10 times.

One distinct change compared to the previous experiment is the symmetric dispersion relations between waves propagating in the e_1^* and e_2^* directions. In the previous experiment case, in which only either strut A or strut B was modified, the dispersion curves of the waves propagating in two different directions were asymmetric. The asymmetric solutions were a result of the modifications made on the lattice structure not being geometrically symmetric with respect to each direction of wave propagation. However, when both strut A and B were modified, the modification applied on the lattice structure was symmetric with respect to both directions of wave propagation, resulting in the symmetric dispersion relations between waves propagating along e_1^* and e_2^*. This relationship could be extended to other non-symmetric lattice structures with different modifications, in which the modifications applied are geometrically symmetric with respect to waves propagating in different directions. For instance, modifying struts A, B, and C all together would result in symmetric dispersion relations as the modifications applied are geometrically symmetric with respect to both directions of the wave propagation. It is important to note that when struts are modified, the same changes in the design variables are applied for the modified struts.

4.6.4 Impact of Modifying Different Combinations of Struts of the Lattice Structure

In the previous experiments on non-symmetric lattice structures, the relationship between the location of the modifications and the symmetric/asymmetric dispersion relations were discussed. In this section, in order to explore how various different asymmetric relations can be obtained, and to further analyze the significance of having asymmetric dispersion relations for waves propagating in different directions, the thesis focuses on modifications skewed to one location, in which case the modifications applied on the struts would impact one side of the unit lattice structure, while affecting the other side of the unit lattice structure as little as possible. In this section and onward, the modifications are applied to impact node 1, the boundary node located at the end of strut A, (along the direct basis vector e_1) as much as possible, while affecting node 2, the boundary node located at the end of strut B, (along the direct basis

vector e_2) as little as possible. This skewed modification was applied to ensure that the dispersion relations for waves propagating along the e_1^* and e_2^* directions are asymmetric. In this section, the impact of applying a modification on different combinations of struts are tested, and the resultant changes in the dispersion curves are analyzed. First, two struts, strut A and strut D, of the tetrahedral unit cell were modified to have Young's modulus increased by 10 times. Two dispersion curves for waves propagating along e_1^* and e_2^*, are illustrated in Figure 4.23.

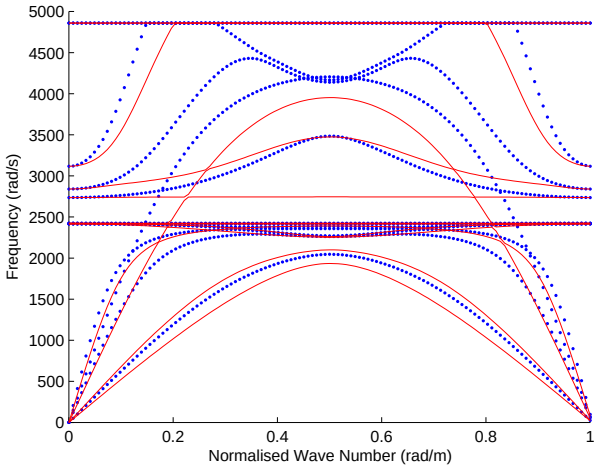

Figure 4.23: Collapsed dispersion curves of the non-symmetric tetrahedral lattice structure for waves propagating along e_1^* (blue dotted lines) and for waves propagating along e_2^* (red solid lines), with the struts A and D modified to have increased Young's modulus by 10 times.

The dispersion curves for waves propagating along e_1^* were plotted with blue dotted lines, while the dispersion curves for waves propagating along e_2^* were plotted with red solid lines. The dispersion curves were plotted for the first 14 dispersion branches. As discussed in previous sections, as the modifications applied on the struts are not geometrically symmetric with respect to each direction of wave propagation, the resulting dispersion relations for each directions are asymmetric. Also, compared to the dispersion curves of the initial symmetric lattice structure in Figure 4.11, the waves of the first 14 dispersion branches propagate at a higher frequency ranges. When the dispersion curves of waves propagating along e_1^* and e_2^* are compared, it can be seen that the dispersion branches of waves propagating along e_1^* are propagating at a higher frequency range than the corresponding dispersion branches of waves propagating along e_2^*. This implies that waves along e_1^* are propagating with higher phase velocity, when comparing each dispersion branches. Figure 4.24 illustrates the change in phase velocity of each dispersion branch, as the wave number is increased. The plot focuses on the region of small wave numbers for easier comprehension of the differences in phase velocity between each of the dispersion curves. The phase velocity of the dispersion branches of the waves propagating along e_1^* was plotted with blue dotted lines, while the phase velocity of dispersion branches of the waves propagating along e_2^* was plotted with red solid lines. As illustrated in Figure 4.23, it can be observed that the significant differences in the frequency ranges in which the waves propagate occur at the dispersion branches of 1 to 4 and 11 to 13, and for those dispersion branches, Figure 4.24 illustrates that the phase velocity of the waves propagating along e_1^* are higher than the phase velocity of the waves propagating along e_2^*.

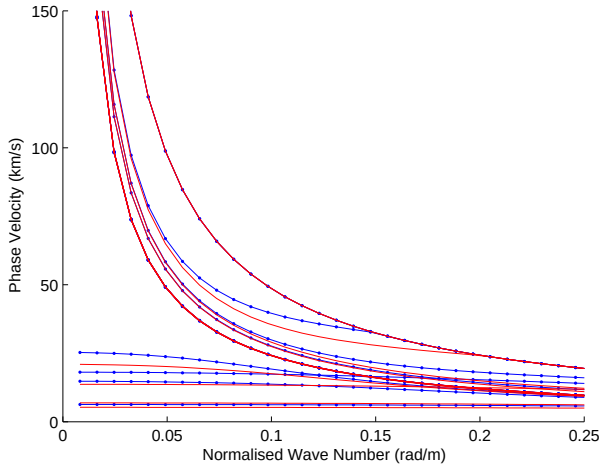

Figure 4.24: Phase velocity plot of the first 14 dispersion branches, focused on the small wave numbers.

Next, the dispersion curves were analyzed for different combinations of modified struts, while maintaining the total number of modified struts to be unchanged. Here, two struts, strut A and strut F, of the tetrahedral unit cell were modified to have Young's modulus increased by 10 times. As the purpose of the current section of the thesis is to observe the changes in dispersion curves when different combinations of struts are modified, the dispersion curves for waves propagating along e_1^* of the current non-symmetric lattice structure, in which strut A and F are modified, were compared with the dispersion curves for waves propagating along e_1^* of the previous non-symmetric lattice structure, in which strut A and D were modified (Figure 4.25). The dispersion curves of the current lattice structure were plotted with blue dotted lines, while the dispersion curves of the previous lattice structure were plotted with red solid lines.

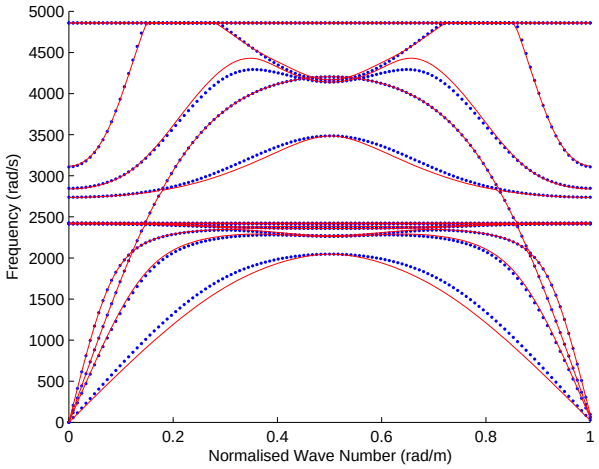

Figure 4.25: Comparisons of the dispersion curves for waves propagating along e_1^* when the struts A and D were modified (blue dotted lines) and for waves propagating along e_1^* when the struts A and F were modified (red solid lines).

Similarly, the dispersion curves for waves propagating along e_2^* of the current non-symmetric lattice structure, in which struts A and F were modified, was compared with the dispersion curves for waves propagating along e_2^* of the previous non-symmetric lattice structure, in which struts A and D were modified (Figure 4.26). The dispersion curves of the current lattice structure were plotted with blue dotted lines, while the dispersion curves of the previous lattice structure were plotted with red solid lines.

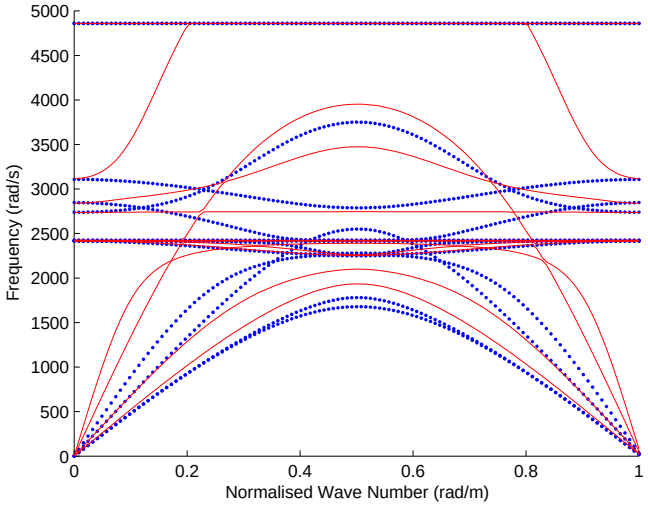

Figure 4.26: Comparisons of the dispersion curves for waves propagating along e_2^* when the struts A and D were modified (blue dotted lines) and for waves propagating along e_2^* when the struts A and F were modified (red solid lines).

When comparing Figures 4.25 and 4.26, it can be seen that the frequency range, at which the waves propagate, are unaffected, as for both cases waves propagate between 39.81 and 4859 rad/s. From Figure 4.23, it can be seen that the dispersion curves of waves propagating along e_1^* of the current lattice structure have different band structure than the dispersion curves of waves propagating along e_1^* of the previous lattice structure, but they show close resemblance to each other. There are, however, minor-but-noticeable differences occurring at the dispersion branches of 1, 10, and 12, in which waves propagate at different frequency ranges. Also, there exists no complete band gap for waves propagating along e_1^* for both combinations of strut modifications. From Figure 4.24, the dispersion curves of waves propagating along e_2^* of the current lattice structure have different band structure than the dispersion curves of waves propagating along e_2^* of the previous lattice structure, but they show much significant differences in their band structure. Due to the significant changes in the dispersion curves, when modifications are applied on the different strut combinations, a complete band gap appears at the frequency range between 3751 and 4859 rad/s. The difference in magnitude of the change in band structure is related to the number of nodes affected by the strut modifications that are connected to each boundary node of the lattice structure, and how the changes in the nodes affect the global and reduced mass and stiffness matrices.

When the direction of the wave propagation is considered and the dispersion curves are plotted for waves propagating along e_1^*, the part of the global mass and stiffness matrices corresponding to the

internal nodes connected to the boundary node e_1 (node 1 of the tetrahedral lattice structure, which is located at the end of strut A along the direction of the direct basis vector e_1) and the boundary node e_1 itself are multiplied by a factor of e^{k_1}, while the part of the matrices corresponding to the internal nodes connected to the other boundary nodes and the other boundary nodes themselves are multiplied by a factor of 1, since k_2 and k_3 are fixed at zero. As the wave number k_1 increases, the values at the part of the reduced mass and stiffness matrices corresponding to the internal nodes connected to boundary node e_1 and the boundary node e_1 itself, would be changed as well, while the values at the parts corresponding to the other internal nodes connected to other boundary nodes remain constant as they are multiplied by 1. Therefore, for wave vectors propagating along the e_1^* direction, changes in the values at the part of the global mass and stiffness matrices corresponding to the internal nodes that are connected to the boundary node e_1 would cause significant differences on the resulting eigen solution for the same corresponding wave vectors. Knowing that the total number of internal nodes connected to each boundary node are fixed for the same geometry of unit cell, the only factor that would cause changes to the values at the parts of the global mass and stiffness matrices corresponding to the internal nodes connected to the boundary node e_1 is the changes in the design variables due to the modifications. Therefore, when different combinations of modifications are considered for waves propagating along e_1^*, if the total number of internal nodes affected by the modifications, which are connected to the boundary node e_1, changes, then the differences in the dispersion curves and the band structures are likely to be significant as there will be significant differences in the reduced mass and stiffness matrices. On the other hand, considering that there are no changes in the number of internal nodes affected by modifications and which are connected to the boundary node e_1, the changes in the values at the parts of the global mass and stiffness matrices corresponding to other internal nodes that are connected to the other boundary nodes (the boundary nodes e_2 and e_3) would cause minor differences in the resulting eigen solution for the same corresponding wave vectors, in which the minor differences occur from the differences in the global mass and stiffness matrices.

Similarly, when the direction of the wave propagation is considered and the dispersion curves are measured for waves propagating along e_2^*, the parts in the global mass and stiffness matrices corresponding to the internal nodes connected to the boundary node e_2 (node 2 of the tetrahedral lattice structure, which is located at the end of strut B along the direction of direct basis vector e_2) and the boundary node e_2 itself are multiplied by the factor of e^{k_2}, while the parts of the matrices corresponding to the internal nodes connected to the other boundary nodes and the other boundary nodes themselves are multiplied by a factor of 1 (since k_1 and k_3 are fixed at zero). As the wave number k_2 increases, the values at the parts of the reduced mass and stiffness matrices corresponding to the internal nodes connected to the boundary node e_2 and the boundary node e_2 itself would be changed as well, while the values at the parts of the matrices corresponding to the other internal nodes connected to the other boundary nodes remain constant as they are multiplied by 1. Therefore, for the wave vectors propagating along the e_2^* direction, changes in the values at the parts of global mass and stiffness matrices corresponding to the internal nodes that are connected to the boundary node e_2 would cause significant differences in the resulting eigen solution for the same corresponding wave vectors. Knowing that the total number of internal nodes connected to each boundary node are fixed for the same geometry of unit cell, the only factor that could cause changes in the values at the parts of the global mass and stiffness matrices corresponding to the internal nodes connected to the boundary node e_2, is the changes in the design

variables due to the modification. Therefore, when different combinations of strut modifications are considered for waves propagating along e_2^*, if the total number of modified internal nodes connected to the boundary node e_2 changes, the differences in the dispersion curves and the band structures are significant as there are significant differences in the reduced mass and stiffness matrices. On the other hand, considering that there are no changes in the number of modified internal nodes connected to the boundary node e_2, changes in the values at the parts of the global mass and stiffness matrices corresponding to the other internal nodes that are connected to the other boundary nodes (boundary nodes e_1 and e_3) would cause minor differences on the resulting eigen solution for the same corresponding wave vectors, in which the minor differences occur from the differences in the global mass and stiffness matrices.

In the above, when the modified struts were changed from struts A and D to struts A and F, the total number of modified internal nodes connected to the boundary node e_1 remained the same, while the total number of modified internal nodes connected to the boundary node e_2 changed. When the dispersion curves of the waves propagating along e_1^* for each combination were compared, minor differences could be seen in the band structure, although the band structures showed a close resemblance to each other. On the other hand, when the dispersion curves of waves propagating along e_2^* for each combination were compared, there were significant differences in the resulting band structures. The above relation can be applied to other combinations of modifications, providing the same number of struts are modified. Also, for different combinations of modifications, when the same number of struts are modified, the frequency ranges at which the waves propagate in the dispersion curves do not change. For all the different combinations of modifications, as long as only two struts are modified, the maximum frequency range at which the waves propagate, at least for the first 14 dispersion branches, occurs at 4859 rad/s.

4.6.5 Impact of Increasing the Number of Struts Being Modified

In this section, the impact of increasing the number of struts being modified is analyzed. The modifications were applied to impact node 1, the boundary node located at the end of strut A, (along the direct basis vector e_1) as much as possible, while affecting node 2, the boundary node located at the end of strut B, (along the direct basis vector e_2) as little as possible. This skewed modification was applied to ensure that the dispersion relations for the waves propagating along e_1^* and e_2^* were asymmetric. First, three struts, namely strut A, C, and F, of the tetrahedral unit cell were modified to have Young's modulus increased by 10 times. As the purpose of the current section of the thesis is to observe the changes in the dispersion curves when the number of modified struts are increased, the dispersion curves for the waves propagating along the e_1^* directions of the current (three struts, A, C, and F, modified) non-symmetric lattice structure are compared with the dispersion curves for the waves propagating along the e_1^* directions of the previous (two struts, A and F, modified) non-symmetric lattice structure. The dispersion curves of the current lattice structure were plotted with blue dotted lines, while the dispersion curves of the previous lattice structure (red solid line from Figure 4.25) were plotted with red solid lines.

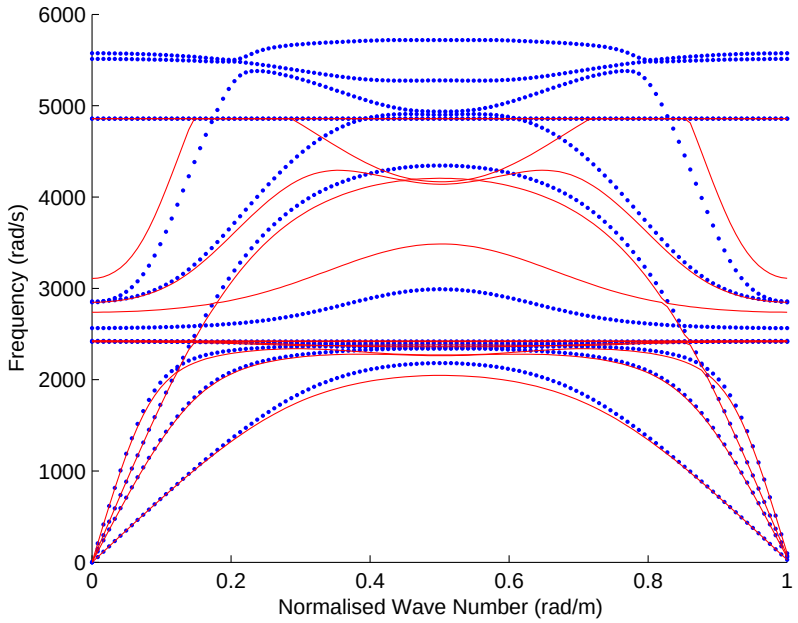

Figure 4.27: Comparisons of the dispersion curves for waves propagating along e_1^* when three struts, namely A, C, and F, are modified (blue dotted lines) and for waves propagating along e_1^* when two struts, namely A and F, are modified (red solid lines).

From Figure 4.27, the first significant difference is the frequency range at which the waves propagate when the number of modified struts are increased. When two struts are modified, the waves propagate between 39.81 and 4859 rad/s. However, when three struts are modified, the waves propagate at a higher frequency range, with the maximum frequency of propagation occurring at 5719 rad/s. The second significant difference is the change in dispersion curves and the band structure. There exists no complete band gap for waves propagating along e_1^* for both cases of modification. Similarly, the dispersion curves for waves propagating along the e_2^* directions of the current (three struts, namely A, C, and F, modified) non-symmetric lattice structure were compared with the dispersion curves for waves propagating along the e_2^* directions of the previous (two struts, namely A and F, modified) non-symmetric lattice structure. The dispersion curves of the current lattice structure were plotted with blue dotted lines, while the dispersion curves of the previous lattice structure (red solid line from Figure 4.26) were plotted with red solid lines.

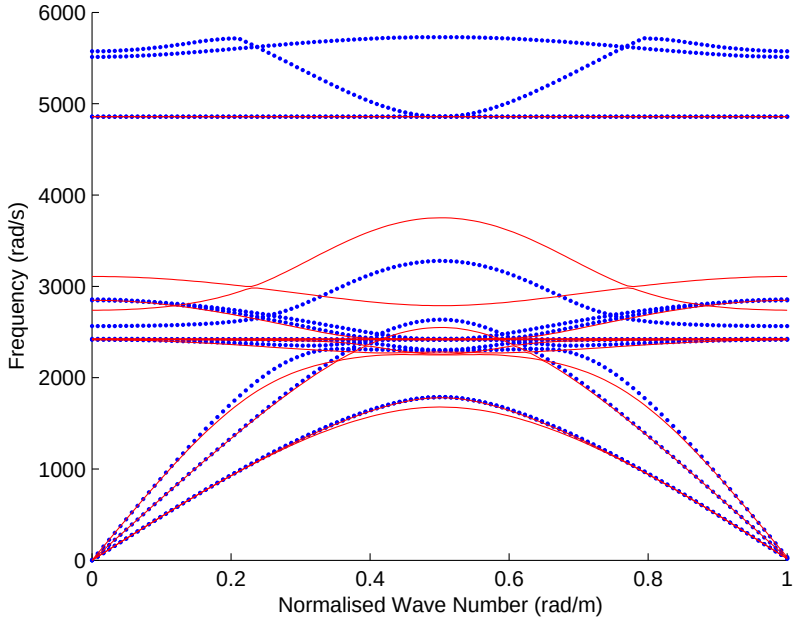

Figure 4.28: Comparisons of the dispersion curves for the waves propagating along e_2^* when three struts, namely A, C, and F, are modified (blue dotted lines) and for waves propagating along e_2^* when two struts, namely A and F, are modified (red solid lines).

Similar to the phenomenon that occurs for the dispersion curves of waves propagating along e_1^*, from Figure 4.28, the first significant difference is the frequency range at which the waves propagate when the number of modified struts are increased. When two struts are modified, the waves propagate between 39.81 and 4859 rad/s. However, when three struts are modified, the waves propagate at a higher frequency range, with the maximum frequency of propagation occurring at 5715 rad/s. The second significant difference is the change in dispersion curves and the band structure. There exist a complete band gap at the frequency range of 3751-4859 rad/s, when two struts are modified; however, when three struts are modified, a complete band gap occurs at the frequency range of 3279-4859 rad/s. The changes in the dispersion curves and the ranges at which waves propagate occurs due to the change in the global stiffness matrix. When an additional strut is modified to have Young's modulus multiplied by 10, the values of the parts of the global stiffness matrix corresponding to the nodes related to the modified struts are all increased by a factor of 10 times too. Increasing the number of modified struts, increases the parts of the global stiffness matrix at which the values are increased due to the modification. The same phenomenon occurs when the number of modified struts are increased to four struts, such as struts A, C, D, and F. Figure 4.29 illustrates the changes in the dispersion curves when the number of modified struts are increased from three struts to four struts. The top figure compares the dispersion curves for waves propagating along the e_1^* direction, while the bottom figure compares the dispersion curves for waves propagating along the e_2^* direction. The dispersion curves of the lattice structure with four modified struts are plotted with blue dotted lines, while the dispersion curves of the previous lattice structure with three modified struts are plotted with red straight lines in this figure. Similar to the phenomenon that occurs when the number of modified struts are increased from two to three, a different

band structure of the dispersion curves are obtained, together with increased frequency ranges at which the waves propagate. For waves propagating along e_1^*, when three struts are modified, the maximum frequency at which waves propagate occurs at 5719 rad/s. However, when four struts are modified, the maximum frequency at which the waves propagate occurs at 6708 rad/s. Similarly, for waves propagating along e_2^*, when three struts are modified, the maximum frequency at which the waves propagate occurs at 5715 rad/s. However, when four struts are modified, the maximum frequency at which the waves propagate occurs at 6487 rad/s. There exists no complete band gap for waves propagating along e_1^* for both cases of modification. For waves propagating along e_2^*, there exists a complete band gap at the frequency range of 3279 - 4859 rad/s, when three struts are modified. However, when four struts are modified, there exists no band gap.

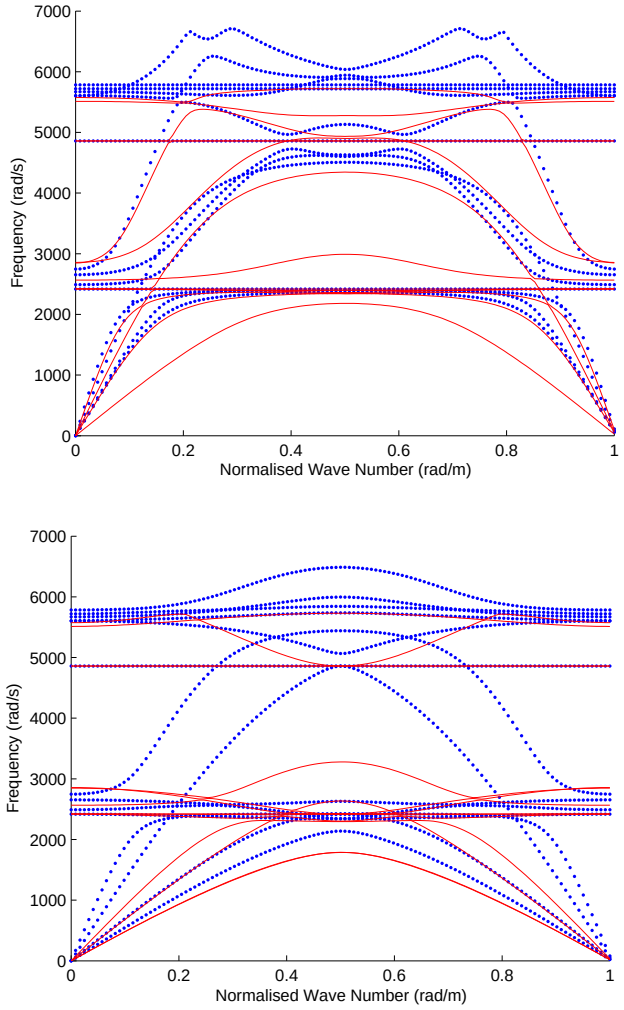

Figure 4.29: Comparisons of the dispersion curves for waves propagating along e_1^* when four, namely struts A, C, D, and F, were modified (blue dotted lines, top) and for waves propagating along e_1^* when three struts, namely A, C, and F, were modified (red solid lines, top), and another comparison of the dispersion curves for waves propagating along e_2^* when four struts, namely A, C, D, and F, were modified (blue dotted lines, bottom) and for waves propagating along e_2^* when three struts, namely A, C, and F, were modified (red solid lines, bottom).

A Further increase in the number of struts modified leads to the same phenomenon in the dispersion curves. A different band structure is obtained, where the waves of each dispersion branch are propagating at higher frequency ranges. When the number of modified struts is gradually increased, starting from one strut being modified, the frequency range at which the waves propagate gradually increase toward the frequency range at which waves propagate in a symmetric lattice structure (i.e. when all the struts are modified). As the band structure changes as the number of modified struts increases, a new band gap may be introduced in the new dispersion curves, or no band gap may exist for the new dispersion curves. Combining these two behaviours, all band gaps, which are present for non-symmetric lattice structures, always occur within the frequency ranges of the initial symmetric lattice structure (Figure 4.11) and the frequency ranges of the modified symmetric lattice structure (Figure 4.14).

4.6.6 Intuitive and Physical Understanding of the Dispersion Relations of a Non-Symmetric Lattice Structure

In this chapter, the dispersion relations of symmetric and non-symmetric lattice structures have been analyzed. In previous sections of this chapter, analyses of the dispersion curves of the symmetric and non-symmetric lattice structures were performed primarily based on a mathematical perspective. In this section, it is of interest to gain a physical understanding on the dispersion relations of the lattice structures with various structural configurations.

Dispersion Relations of Symmetric Lattice Structure

First, in Section 4.6.2, the dispersion curves of the symmetric lattice structure, with all struts modified, were analyzed. It was found that for symmetric lattice structures, an increase in the Young's modulus or a decrease in the density resulted in an increased frequency range at which the dispersion curves occur. On the other hand, it was also found that a decrease in the Young's modulus or a increase in the density resulted in a decreased frequency range at which the dispersion curves occur. A physical understanding of these results can be obtained by studying how waves propagate in different mediums. Wave propagation through a medium, in another perspective, is the transfer of energy from one point of the medium to another. If the medium is modified to have an increased Young's modulus, the medium becomes much stiffer and the atoms of the medium are then held more tightly to each other. As the atoms are tightly held together, the waves propagate through the medium at a much faster speed, leading the waves to propagate at a higher frequency. However, if the medium has a decreased Young's modulus, and therefore is less stiff, the atoms of the medium are held more widely apart from each other, which causes the waves to propagate at a slower speed, leading them to propagate at a lower frequency range.

On the other hand, if the density of the medium is increased, the size and mass of the atoms of the medium are increased. In order for waves to propagate through the heavier medium, more energy is required. Hence, when the density of the medium is increased, the waves propagate at a lower frequency. However, if the density of the medium is decreased, the size and mass of the atoms are decreased, thus allowing the waves to be able to propagate much easier than before, and allowing the waves to propagate at a higher frequency range.

Dispersion Relations of Non-Symmetric Lattice Structure: Impact of Modifying Different Combinations of Struts of the Lattice Structure

A second major analysis on the dispersion relations was made on the impact of applying modifications on different combinations of struts of the non-symmetric lattice structure, which was covered in Section 4.6.4. In that section, it was analyzed that as long as the total number of struts being modified are fixed, the dispersion curves of each of the different combinations of strut modification occur at the same frequency ranges with each other, even though the band structures are different from each other. A physical understanding of this dispersion relation can be obtained based on the analysis made above. If struts A and B are modified to have differing Young's modulus, in the context of the overall unit lattice cell, the overall structure is as stiff as when other combinations of two struts are modified to have the same differing Young's modulus values. Hence, waves would propagate at a similar frequency through the non-symmetric lattice structure, as long as same number of struts are modified to have increased Young's modulus values with the same modifications. Likewise, the frequency ranges at which the waves propagate for the dispersion curves are similar for various non-symmetric lattice structures with any combination of three struts being modified, while each of the dispersion curves would have a different band structure.

Dispersion Relations of Non-Symmetric Lattice Structure: Impact of Increasing the Number of Struts Being Modified

In Section 4.6.5, the impact of increasing the number of modified struts was analyzed. Throughout the analysis, it was found that gradually increasing the number of struts being modified, increases the frequency range at which the dispersion curves occur. For instance, the frequency range at which waves propagate when three struts are modified to have a higher Young's modulus, occurs at a higher frequency range than when only two struts are modified to have an increased Young's modulus. Likewise, the frequency range at which waves propagate when four struts are modified to have a higher Young's modulus, occurs at a higher frequency range than when three struts are modified to have an increased Young's modulus. As such, as more struts are modified for a non-symmetric lattice structure to gain an increased Young's modulus, the frequency range at which the waves propagate tends to occur at higher frequency. The physical reasoning behind this phenomena is also related to the reasoning made above. In the context of a unit lattice cell, if a greater number of struts are modified to have an increased Young's modulus, the overall lattice cell becomes stiffer. Hence, when waves are propagating through the lattice unit cell, as the atoms of the unit cell are more stiff and held more tightly close to each other, the waves will tend to propagate at a higher frequency. On the other hand, if more struts are modified to have a reduced Young's modulus, in the context of the overall unit cell, the unit cell is less stiff and the atoms are spread further apart from each other. As a result, when more struts are modified to have a decreased Young's modulus, the waves would propagate at a lower frequency. Similarly, as the number of struts being modified is increased, causing the structure to have an increased density for each strut, in the context of the overall unit cell, it would require more energy for the waves to propagate through, thereby causing waves to propagate at a lower frequency. Likewise, if the number of struts being modified is gradually increased to have a lower density, the overall unit cell would have a lower density, allowing the waves to propagate at a higher frequency.

4.6.7 Significance of the Asymmetric Dispersion Relations

The strength of non-symmetric lattice structures with asymmetric dispersion relations comes from the high flexibility they offer when designing and tailoring lattice structures and dispersion curves. First, consider a structure with waves propagating in multiple directions. For applications of the lattice structure as a noise absorber, in which the waves are propagating in all directions within the system, the symmetric lattice structure is required to satisfy the need for a band gap to be present at the desired frequency range, with a common band gap required for all waves propagating in all directions.

However, consider a system where waves are known to propagate in certain directions only, or a system where only the waves propagating in certain directions are of interest, such as a system with guided waves where waves are propagating in specific directions. A cylindrical water pipe is an example of a system with guided waves. Within the cylindrical pipeline, the acoustic wave propagates in a direction along the centerline of the pipe. If lattice structures are to be used for the applications with cylindrical pipeline, symmetric lattice structures give symmetric dispersion relations that give only one type of dispersion curve, which is applicable for waves propagating in all directions. However, by breaking the symmetry and giving asymmetric dispersion relations, many numbers of different dispersion curves with varying band structures can be generated, while it is only required to satisfy waves propagating in a specific direction, which is along the centerline of the cylindrical pipe. By increasing the number of struts being modified, more different choices of dispersion curves are generated. Furthermore, by changing the different combinations of struts to be modified, the possible dispersion curves to explore can be further increased. Therefore, while in symmetric dispersion relations, only single dispersion curves is provided to tailor around, the asymmetric relations provide much more choices of dispersion curves to tailor around, therefore providing more ways to design and optimize the lattice structure and its band gap. Also, asymmetric dispersion relations are easier to tailor as the dispersion relations of the waves propagating along unnecessary directions can be ignored.

Second, consider a system with waves propagating in multiple directions, in which the different band gaps are required for each of the waves propagating in each of the different directions. Achieving such a goal with a symmetric lattice structure is difficult as the symmetric lattice structure results in one symmetric dispersion curves. Hence, that one symmetric dispersion curve must have multiple band gaps, each appearing at the different desired frequency ranges that satisfy the requirement for each wave propagating in each of the different direction. However, if the dispersion relations are asymmetric, as the dispersion relations are different for different directions of wave propagation, and as there are many more different variations of asymmetric dispersion curves that can be studied, the asymmetric dispersion relations provide higher flexibility for achieving that goal.

4.6.8 Impact of Changing the Other Design Variables

Changing the Young's Modulus and the Density

In the previous sections, the thesis focused on the modification with the Young's modulus value of the struts being multiplied by 10. In this section, the impact of applying different modifications are discussed, such as applying different values of the Young's modulus or changed values of the density.

For a symmetric lattice structure, in which all the struts are modified with the same changes in the design variables, a change in the design variables of Young's modulus or the density simply applies a scaling effect to the dispersion curves while maintaining the same band structures. As discussed in Section 4.6.2, when the Young's modulus or the density of all the struts are modified, the dispersion curves of the modified symmetric lattice structure is simply scaled by the factor of $\sqrt{\frac{E}{\rho}}$. Hence, increasing the Young's modulus or decreasing the density of all the struts simply increases the scale of the dispersion curves, whereby the waves of the modified symmetric lattice structure propagate at an increased frequency range. On the other hand, decreasing the Young's modulus or increasing the density of all struts decreases the scale of the dispersion curves, whereby the waves of the modified symmetric lattice structure propagate at a reduced frequency range.

For non-symmetric lattice structures, in which only one or more, but not all of the struts are modified, a change in the Young's modulus or density no longer applies a scaling effect. As discussed in Section 4.6.3, when only part of the unit lattice cell is modified, the expressions for the mass and stiffness matrices are no longer related as a scalar factor. Hence, when Young's modulus or the density is changed as modifications for non-symmetric lattice structures, different dispersion curves and band structures are obtained. For waves propagating in different directions of the non-symmetric lattice structures, the symmetric/asymmetric relations on the resulting dispersion curves are related to the location at which the modifications are applied on the structure. Similar to the discussions in Section 4.6.3, when the density of the struts are changed as a modification, if the modifications applied on the lattice structure are geometrically symmetric with respect to each direction of wave propagation, symmetric dispersion relations between waves propagating along each direction are obtained; whereas if the modification applied on the lattice structure are not geometrically symmetric with respect to each direction of wave propagation, asymmetric dispersion relations are present. Likewise, as illustrated in Section 4.6.4, when different combinations of struts are modified to have changed values in density, different dispersion curves are generated.

The differences in dispersion relations when different design variables are modified can be observed when gradually increasing the number of struts modified. In Section 4.6.5, for the modifications with an increased Young's modulus, it was discussed that when the number of modified struts was gradually increased, starting from one strut being modified, the frequency range at which the waves propagate gradually increased toward the frequency range at which waves propagate in a symmetric lattice structure, i.e. a structure in which all the struts are modified. Based on the same relation, if Young's modulus of the modified struts is reduced instead, when the number of modified struts are gradually increased, starting from one strut being modified, the frequency range at which the waves propagate gradually decreases toward the frequency range at which waves propagate in a symmetric lattice structure. On the other hand, increasing the density of the modified struts for a symmetric lattice structure causes the dispersion curves to be scaled down by a factor of $\sqrt{\frac{E}{\rho}}$. Therefore, if the density is increased for the modified struts of non-symmetric lattice structures, when the number of modified struts are gradually increased, starting from one strut being modified, the frequency range at which the waves propagate will gradually decrease. Likewise, if the density is decreased for the modified struts of non-symmetric lattice structures, when the number of modified struts are gradually increased, starting from one strut being modified, the frequency range at which the waves propagate will gradually increase. Another difference

occurs when the dispersion curves are compared between the case when the Young's modulus is changed as a modification and when the density is changed as a modification. As discussed previously, the change in the Young's modulus or density in non-symmetric lattices no longer provides a scaling effect of the dispersion curve. Also, as a change in the Young's modulus changes the global stiffness matrix while a change in density changes the global mass matrix, the dispersion curves of the two types of modifications are different.

Changing the Radius to Length Ratio of the Lattice Structure

In this section, analyses were performed to understand the impact on the resulting dispersion curves when the radius to length ratio of the lattice strut is changed for all the struts of the lattice structure. The radius to length ratio of the lattice structure was modified to be 0.02, by increasing the length of the struts of the lattice structure. The dispersion curves of the modified symmetric tetrahedral lattice structure with a radius to length ratio of 0.02 are illustrated in Figure 4.30. The dispersion curves for waves propagating along e_1^* were plotted with blue dotted lines, while the dispersion curves for waves propagating along e_2^* were plotted with red solid lines. The dispersion curves were plotted for the first 14 dispersion branches.

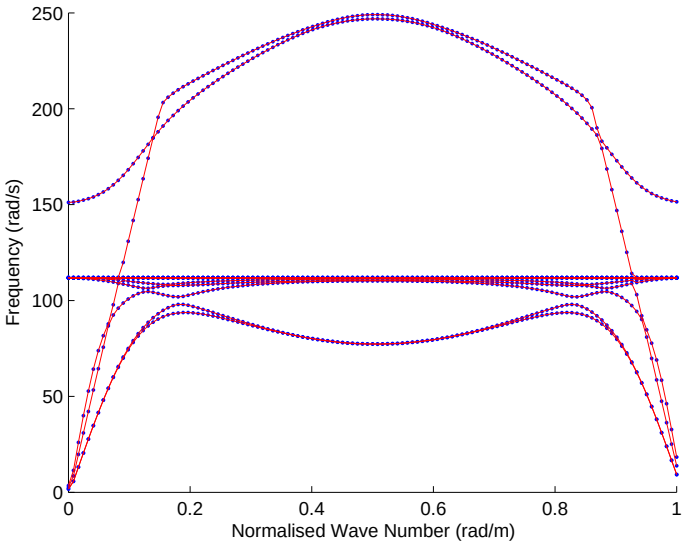

Figure 4.30: Dispersion curves of a symmetric tetrahedral lattice with r:l ratio of 0.02 for waves propagating along e_1^* (blue dotted lines) and for waves propagating along e_2^* (red solid lines).

As the figure illustrates, the band structure of the current dispersion curve is completely different from the band structure of the initial symmetric tetrahedral lattice structure with a radius to length ratio of 0.1. For the dispersion curves of the lattice structure with the radius to length ratio of 0.02, waves are propagating at much lower frequency ranges, with the maximum frequency of propagation occurring at 249.1 rad/s, compared to the waves propagating in the dispersion curves of the lattice structure with a radius to length ratio of 0.1, which implies that the waves of each dispersion branch of Figure 4.30 are propagating at reduced phase velocity compared to the corresponding waves of the dispersion branches in Figure 4.11. This significant change in the dispersion curves and the band structures can be explained

by re-visiting the energy equations involving the mass matrix and the stiffness matrix.

$$m_{ij} = \int_0^L [A\rho(a_i a_j + b_i b_j + c_i c_j) + I_y \rho e_i e_j + I_z \rho f_i f_j + (I_y + I_z)\rho d_i d_j]\, dx \tag{4.44}$$

$$k_{ij} = \int_0^L [\lambda(A a_i' a_j' + I_y e_i' e_j' + I_z f_i' f_j') + 2G(A a_i' a_j' + I_y e_i' e_j' + I_z f_i' f_j') + \kappa GA((b_i' - f_i)(b_j' - f_j) + (c_i' + e_i)(c_j' + e_j)) + \kappa G(I_z + I_y)(d_i' d_j')]dx \tag{4.45}$$

When a different radius to length ratio is applied, the changed radius and length of the struts both impact on multiple variables involved in the mass and stiffness matrices of the struts. Change in the variables, such as the area of the cross section of the strut element, the second moment of the area, and the length of the strut element causes significant differences in the resulting mass and stiffness matrices compared to the initial matrices. Also, as the changed matrices are not in a scalar relation with the initial matrices, a different band structure is generated.

Wave Propagation Through Pyramidal Lattice Structures

In this section, analyses were performed to understand the impact on the resulting dispersion curves when waves are propagating through different unit cell geometries. The pyramidal lattice structure was experimented on, where the dispersion curves were measured for waves propagating along e_1^* and e_2^*. The resulting dispersion curves are plotted in Figure 4.31. The dispersion curves for waves propagating along e_1^* were plotted with blue dotted lines, while the dispersion curves for waves propagating along e_2^* were plotted with red solid lines. The dispersion curves were plotted for the first 14 dispersion branches. First, the dispersion curves for the initial symmetric pyramidal lattice structure with a radius to length ratio of 0.1 were plotted. The band gap appears in the frequency range between 2424 and 2957 rad/s.

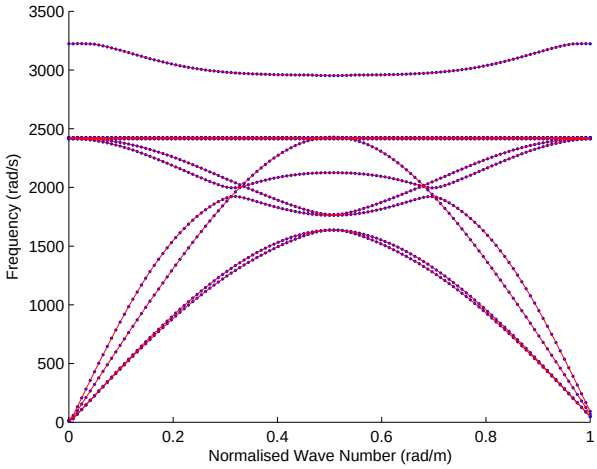

Figure 4.31: Dispersion curves of a symmetric pyramidal lattice with a r:l ratio of 0.1 for waves propagating along e_1^* (blue dotted lines) and for waves propagating along e_2^* (red solid lines).

Next, the dispersion curves for a symmetric pyramidal lattice structure with a radius to length ratio of 0.02 were plotted for waves propagating along e_1^* and e_2^*. The dispersion curves for waves propagating along e_1^* were plotted with blue dotted lines, while the dispersion curves for waves propagating along e_2^* were plotted with red solid lines. The dispersion curves were plotted for the first 14 dispersion branches, and it could be seen that there exists no complete band gap within the first 14 dispersion branches (Figure 4.32).

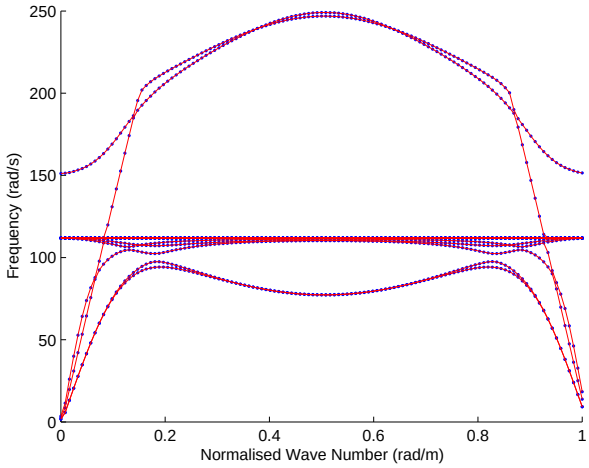

Figure 4.32: Dispersion curves of a symmetric pyramidal lattice with a r:l ratio of 0.02 for waves propagating along e_1^* (blue dotted lines) and for waves propagating along e_2^* (red solid lines).

When the wave propagation behaviour of the waves along e_1^* and e_2^* were analyzed, the resulting dispersion curves of the pyramidal lattice structures can be seen to be very similar to the dispersion curves of the tetrahedral lattice structures. While the band structures illustrate minor insignificant differences in small regions of the dispersion curves, the same behaviours, which were analyzed and discussed in the previous sections for wave propagation in the tetrahedral lattice structures, were also observed for the waves propagating in the pyramidal lattice structures. Hence, the analysis and discussions outlined above for symmetric and non-symmetric tetrahedral lattice structures can also be applied for lattice structures with different unit cell geometries.

Chapter 5

Conclusion and Future Recommendations

5.1 Conclusion

Through the application of the finite element analysis, wave propagation behaviour through symmetric and non-symmetric 3D lattice structures were analyzed. The analysis was performed on the lattice structures of two different geometries: tetrahedral and pyramidal lattice structures. The symmetric lattice structure refers to a structure in which all struts of the lattice have the same design variables, while the non-symmetric lattice structure refers to a structure in which the struts have modified design variables. The eigenfrequencies to plot the dispersions curves were obtained by solving the eigenvalue problem, with the input wave vectors limited to the waves propagating along the e_1^* and e_2^* directions, in order to compare the dispersion relations of waves propagating along the e_1^* and e_2^* directions through symmetric and non-symmetric lattice structures.

First, two symmetric lattice structures with a tetrahedral lattice structure were studied: initial symmetric lattice structure and a modified symmetric structure. When the Young's modulus or density of all the struts was changed, while the other design variables were fixed to stay the same, the resulting dispersion curves were simply the scaled dispersion curves of the initial symmetric lattice structure by a factor of $\sqrt{\frac{E}{\rho}}$. This was explained by analyzing how the design variables impact on the mass matrix and the stiffness matrix of the eigenvalue problem. When only the Young's modulus and/or density was changed, the mass and stiffness matrices of the initial and modified symmetric lattice structures remained constant, and were simply scaled based on the ratio of the changed values of the Young's modulus and density. Therefore, when the dispersion curve of the initial symmetric lattice structure were obtained, the dispersion curves after the change in the Young's modulus and/or density could be fully predicted. However, this scalar relationship did not apply when other design variables, such as the radius or length of the overall struts, were changed. The change in the other design variables impacted the mass matrix and the stiffness matrix heavily. As the change in the other design variables led to entirely different mass and stiffness matrices, the resulting dispersion curves were expected to provide different band structures.

Second, the non-symmetric lattice structures were studied. The effect of the change in design variables

were analyzed when only one or more struts was modified rather than modifying the design variables for all the struts. Unlike the behaviours in symmetric lattice structures, a change in the Young's modulus or density for non-symmetric lattice structures no longer performed as a tool for scaling the dispersion curves, since the stiffness and mass matrices of the non-symmetric lattice structure could no longer be expressed as the scalar factor of the initial symmetric lattice structure. Therefore, for non-symmetric lattice structures, when any design variable is changed, new band structures of the dispersion curves can be expected.

The analysis of the non-symmetric lattice structure with waves propagating along e_1^* and e_2^*, showed three distinct relations. First, when the modifications applied on the struts with respect to the waves propagating along e_1^* direction, was applied on the struts at geometrically symmetric location with respect to the waves propagating along e_2^* directions instead, the resulting dispersion relations between the waves propagating along e_1^* and e_2^* were symmetric, in which the dispersion curves of waves propagating along e_1^* and e_2^* of the same non-symmetric lattice structure were the same. On the other hand, if the modifications applied on the struts are not geometrically symmetric with respect to each direction of the wave propagation, the resulting dispersion relations between the waves propagating in each direction were asymmetric, in which the dispersion curves of waves propagating along e_1^* and e_2^* of the same non-symmetric lattice structure were different. Second, when different combinations of modifications were applied, the resulting dispersion curves showed a different band structure. When the total number of struts being modified was kept constant, and only different combinations of struts were modified, the frequency ranges at which waves propagated along e_1^* and e_2^* of the non-symmetric lattice structure remained relatively close to each other. Third, starting from a non-symmetric lattice structure with only one modified strut, when the number of modified struts was gradually increased, the resulting dispersion curves showed a gradual change in the frequency ranges at which the waves propagated. When the modification increased the Young's modulus or decreased the density of the struts, as the number of modified struts was gradually increased, the resulting dispersion curves showed a gradual increase in the frequency ranges at which the waves propagated, in fact toward the frequency ranges at which the waves would propagate through a symmetric lattice structure with all the struts modified. When the modification decreased the Young's modulus or increased the density of the struts, as the number of modified struts was gradually increased, the resulting dispersion curves showed a gradual decrease in the frequency ranges at which the waves propagated, in fact toward the frequency ranges at which waves would propagate through a symmetric lattice structure with all the struts modified. Moreover, as the band structure changes as the number of modified struts increases, a new band gap may be introduced in the new dispersion curves, or no band gap may exist for the new dispersion curves. Combining these two behaviours, all the band gaps present for non-symmetric lattice structures, always occur within the frequency ranges of the initial (not-modified) symmetric lattice structure and in the frequency ranges of modified symmetric lattice structures.

Concluding the analysis, for symmetric lattice structures, a change in the Young's modulus or density performs as a powerful tool for scaling the dispersion curves and its band gap, whereby both the location of the band gap and the resulting band structure of the dispersion curves are predictable. While this scaling effect in symmetric lattice structures seem powerful for optimizing the size and location of the band gap, limitations in the changes in the design variables could be expected due to the require-

ments of the structural properties of the lattice structure. For example, in the application of the lattice structure in aerospace industries, a structure with a high stiffness and low density would be preferred. To achieve these ideal structural properties, the amount that the Young's modulus or density that could be modified is likely to be limited. For instance, when a structure has a band gap at a high frequency range, and the band gap is required to be at a lower frequency range, the change in band gap location can be performed by reducing the Young's modulus or by increasing the density in a symmetric lattice structure, but at the risk of turning the structural properties to be less than ideal. Another weakness of the symmetric lattice structure comes from the total number of dispersion curves available per each design of the lattice structure. The symmetric lattice structures yield one dispersion curve, which is symmetric for waves propagating in different directions. Therefore, the number of dispersion curves to tailor is highly limited for the symmetric lattice structures. On the other hand, the non-symmetric lattice structures with asymmetric dispersion relations show strength in terms of its high flexibility when designing and tailoring the lattice structures and the dispersion curves. The asymmetric dispersion relations provide large numbers of different dispersion curves with varying band structures, in which each dispersion curve is unique for each different direction of wave propagation. By increasing the number of struts being modified, more unique choices of dispersion curves are generated. Furthermore, by applying different combinations of struts to be modified, the possible dispersion curves to explore are further increased. Therefore, the asymmetric relations provide a large number of dispersion curves to tailor around, providing more options to design and optimize the lattice structure and its band gap. Also, asymmetric dispersion relations demonstrate great strength in terms of their flexibility when tailoring the dispersion curves, as the dispersion relations of the waves propagating along unnecessary directions can be ignored.

5.2 Future Recommendations

5.2.1 Multi-Tetrahedral/Pyramidal Non-Symmetric Unit Cell

The present thesis has focused on the analysis of the lattice structure, in which the unit lattice cell was limited to a single tetrahedral or pyramidal structure. However, clusters of tetrahedral or pyramidal structures can be defined as the single unit cell by making the structure non-symmetric. Figure 5.1 illustrates a $3 \times 3 \times 3$ pyramidal lattice structure as a single unit cell, where the unit cell is defined as non-symmetric by having one of the pyramidal at the centre (in red), making it different to the other remaining pyramidal structures. Differences between the two types of pyramidal structures can be made by applying different design variables for each type of pyramidal structure, or by applying differences in the structure geometry by adding additional supporting struts in the pyramidal structure, as illustrated in Figure 5.2.

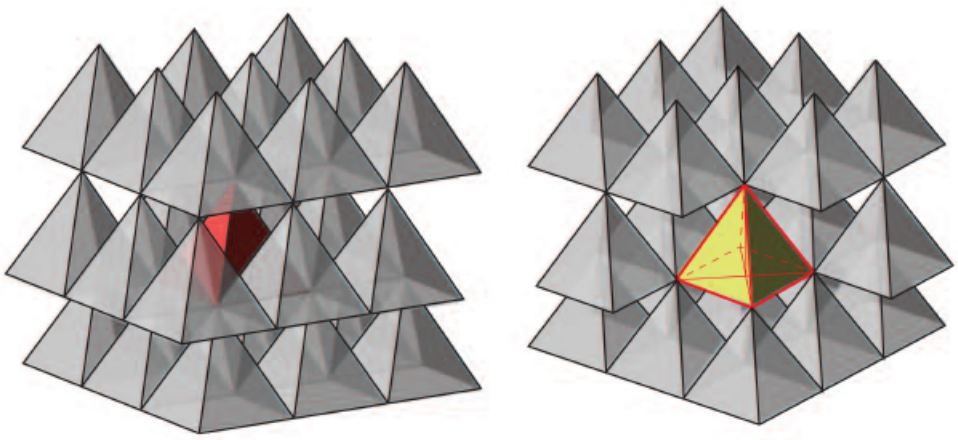

Figure 5.1: Illustration of a non-symmetric unit cell with multiple pyramidal structures.

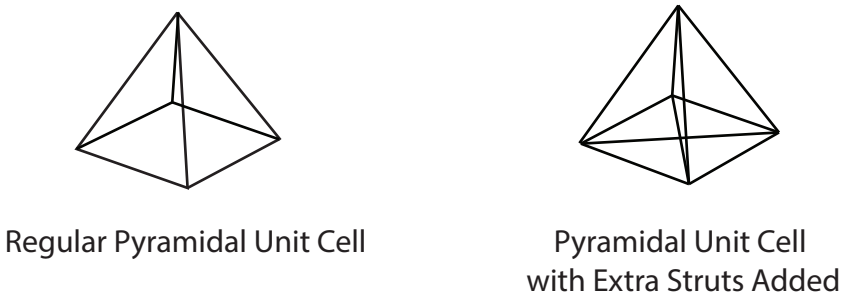

Figure 5.2: Illustration of a normal pyramidal structure and a modified pyramidal structure with extra supporting struts.

More than one pyramidal structure can be modified, and also, the location of the modified pyramidal structures can vary. The analysis of the multi-pyramidal lattice structure can further be extended by studying the difference in wave propagation behaviour, when the modified pyramidal structures are skewed to one side of the unit lattice cell, as illustrated in Figure 5.3.

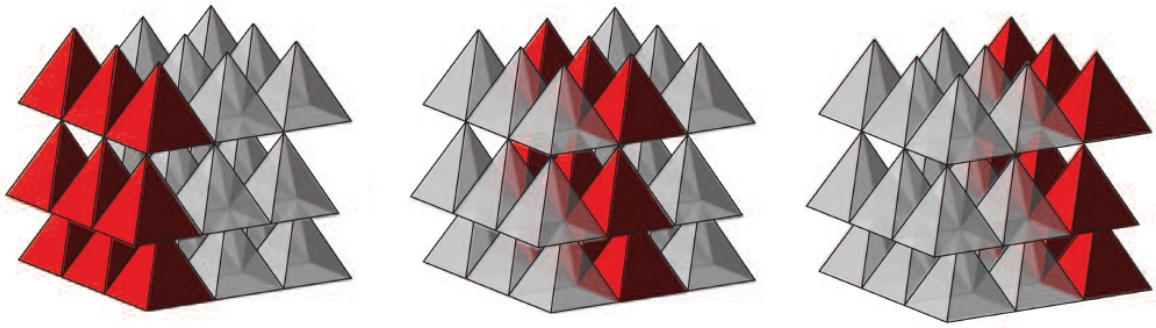

Figure 5.3: Illustration of a skewed modification of a multi-pyramidal unit cell.

5.2.2 Shape Shifting Lattice Structure

The introduction of the multi-tetrahedral or multi-pyramidal unit cell opens up the route to other potential studies on the lattice structure, in which the lattice structure could handle two different band gaps. First, a multi-tetrahedral lattice unit cell with four tetrahedral structures, in which the struts of the tetrahedral structures have a radius to length ratio of 0.1, can be considered, as illustrated in Figure 5.4. The multi-tetrahedral unit cell can be turned into non-symmetric by applying a different material for some struts. For example, in Figure 5.4, struts in orange colour are made out of polymer, while the rest of the struts in light blue are made out of wax. If the structure goes through a procedure that could melt and eliminate the struts made of wax completely without deforming or damaging the struts made of polymer, the multi-tetrahedral unit cell becomes a unit cell with single tetrahedral structure with a radius to length ratio of 0.05.

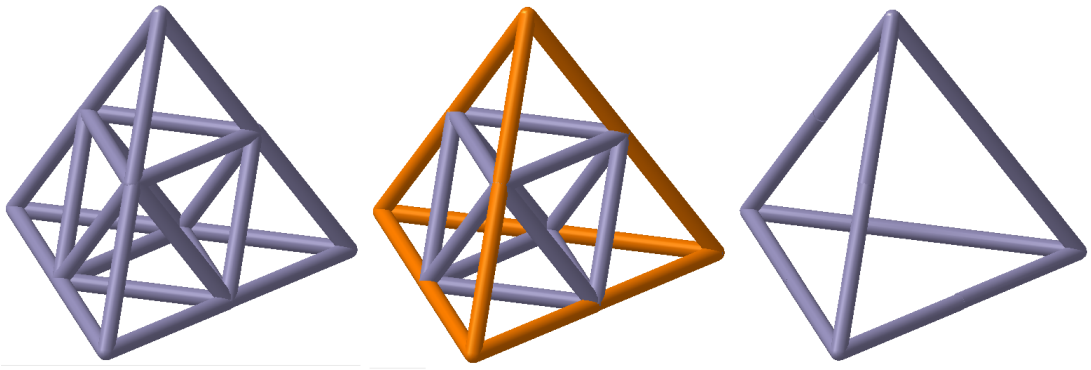

Figure 5.4: Illustration of a non-symmetric multi-tetrahedral unit cell (left), a non-symmetric multi-tetrahedral unit cell with two different materials (middle), and after the struts in one type of material are eliminated (right).

Therefore, if there exists such a procedure that could eliminate struts made out of one type of material, while not deforming the geometries or damaging the material properties of the strut made of the other material, the unit cell of the lattice structure could change its shape through the procedure. Assuming that a multi-tetrahedral unit cell would provide dispersion curves with unique band structure and band gap phenomena, and that a tetrahedral unit cell with a radius to length ratio of 0.05 would provide a different dispersion curves and band gap, the lattice structure could accommodate two different band gaps in changing environment conditions.

5.2.3 Lattice Structure as the Core of Sandwich Panel

The last potential future recommendation is the application of a lattice structure as the core of a sandwich panel. In this thesis, the analysis was focused on the wave propagation behaviour through the lattice structures. However, when lattice structures are applied as the core of a sandwich panel, the resulting structure may provide different wave propagation behaviour due to the introduction of top and bottom panels.

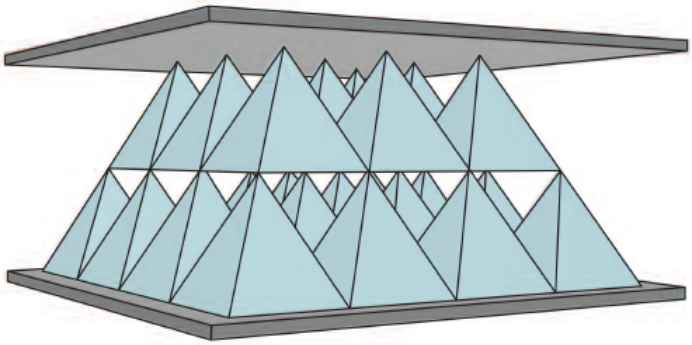

Figure 5.5: Illustration of a pyramidal lattice structure as the core of a sandwich panel.

Bibliography

[1] M. Arya and C.A. Steeves. Bandgaps in Octet Truss Lattices. *Canadian Congress of Applied Mechanics*, 1 of 2:471–474, 2011.

[2] Manan Arya and Craig A Steeves. Wave Propagation in Three-Dimensional Periodic Lattices. Technical report, 2011.

[3] A. Bazoune, Y.a. Khulief, and N.G. Stephen. Shape Functions of Three-Dimensional Timoshenko Beam Element. *Journal of Sound and Vibration*, 259(2):473–480, January 2003.

[4] O. O. Bendiksen. Localization phenomena in structural dynamics. *Chaos, solitons and fractals*, 11:1621–1660, 2000.

[5] R.M. Christensen. Mechanics of cellular and other low-density materials. *International Journal of Solids and Structures*, 37(1-2):93–104, 2000.

[6] John Chu. *Topics in Designing Low Thermal Expansion Lattices at the Microscale*. PhD thesis, 2011.

[7] Nastase-dan Ciobota. Standard Tessellation Language in Rapid Prototyping Technology. *The Science Bulletin of VALAHIA University*, 7(7):81–85, 2012.

[8] V.S. Deshpande, N.A. Fleck, and M.F. Ashby. Effective properties of the octet-truss lattice material. *Journal of the Mechanics and Physics of Solids*, 49:1747–1769, 2001.

[9] E. N. Economou and M. M. Sigalas. Classical wave propagation in periodic structures: Cermet versus network topology. *Physical Review B*, 48(18):13434–13438, 1993.

[10] Henri P Gavin. Structural Element Stiffness, Mass, and Damping Matrices. Technical report, 2014.

[11] H Gleiter. Nanostructured Materials: Basic Concepts and Microstructure. *Acta Materialia*, 48:1–29, 2000.

[12] Dirk Hundertmark. *A short introduction to Anderson localization*. PhD thesis, 2007.

[13] R.G. Hutchinson and N.A. Fleck. The structural performance of the periodic truss. *Journal of the Mechanics and Physics of Solids*, 54(4):756–782, April 2006.

[14] K.S Kumar, H Van Swygenhoven, and S Suresh. Mechanical behavior of nanocrystalline metals and alloys. *Acta Materialia*, 51(19):5743–5774, November 2003.

[15] M.S. Kushwaha, P. Halevi, L Dobrzynski, and B Djafari-Rouhani. Theory of acoustic band structure of periodic elastic composites. *Physical review. B, Condensed matter*, 49(4):2313–2322, January 1994.

[16] Yunhua Luo. An Efficient 3D Timoshenko Beam Element Homogeneous Euler-Lagrangian equations governing 3D Timoshenko beam. 1(3):95–106, 2008.

[17] Giorgio Mantica. Wave propagation in almost-periodic structures, 1997.

[18] D.M. Mead. Wave Propagation in Continuous Periodic Structures: Research Contributions From Southampton, 19641995. *Journal of Sound and Vibration*, 190(3):495–524, February 1996.

[19] M.A. Meyers, A. Mishra, and D.J. Benson. Mechanical properties of nanocrystalline materials. *Progress in Materials Science*, 51(4):427–556, May 2006.

[20] Gisli Sigurbjorn Ottarsson. DYNAMIC MODELING AND VIBRATION ANALYSIS OF MISTUNED BLADED DISKS Gísli Sigurbjörn Óttarsson. Technical report, 1994.

[21] J. Pearson. Solid State Physics, 2008.

[22] N.C. Perkins and C.D. Mote. Comments on curve veering in eigenvalue problems. *Journal of Sound and Vibration*, 106(3):451–463, 1986.

[23] A. Srikantha Phani, J. Woodhouse, and N.A. Fleck. Wave propagation in two-dimensional periodic lattices. *The Journal of the Acoustical Society of America*, 119(4):1995, 2006.

[24] Michel Piche Pierre R. Villeneuve. Photonic band gaps in two-dimensional square and hexagonal lattices. *The American Physical Society*, 46(8):4969–4972, 1992.

[25] Yair Shapira. *Solving PDEs in C ++*. Technion-Israel Institute of Technology, 2006.

[26] Ole Sigmund and Jakob Søndergaard Jensen. Systematic design of phononic band-gap materials and structures by topology optimization. *Philosophical transactions. Series A, Mathematical, physical, and engineering sciences*, 361(1806):1001–1019, 2003.

[27] A. Vigliotti and D. Pasini. Stiffness and strength of tridimensional periodic lattices. *Computer Methods in Applied Mechanics and Engineering*, 229-232:27–43, July 2012.

[28] N. Wicks and J.W. Hutchinson. Optimal truss plates. *International Journal of Solids and Structures*, 38(30-31):5165–5183, July 2001.

[29] C.H. Hodges Woodhouse and J. Vibration isolation from irregularity in a nearly periodic structure. *J. Accoust. Soc. AM*, 74(September), 1983.

[30] E. N. Economou Zdetsis and A. Classical wave propagation in periodic structures. *Rapid Communications*, 40(2):3–8, 1989.